



# **Stability and Accuracy of Electromagnetic Transient Simulation Algorithms**

By

Huanfeng Zhao

A Thesis submitted to the Faculty of Graduate Studies of  
The University of Manitoba  
in partial fulfillment of the requirements for the degree of

**Doctor of Philosophy**

Department of Electrical and Computer Engineering  
The University of Manitoba  
Winnipeg, Manitoba, Canada

Copyright © 2020

## **Abstract**

The main topic of this Ph.D. program is focus on the numerical stability and accuracy of Electromagnetic transient simulations.

In the first part of this thesis, novel techniques are developed to evaluate the stability.

Firstly, in order to adapt the existing stability analysis techniques for analyzing the stability of companion circuit based electromagnetic transient simulation, we prove the equivalency of state space equations models and electromagnetic companion circuit methods. Therefore, the stability conclusion for state space equations based simulation could be directly used for companion circuit model based simulation.

After that, a novel technique is developed by applying Common Quadratic Lyapunov Function theory to analysis the numerical stability of lumped strictly passive switched system simulations. Based on the proposed method, it allows us to determine the stability of numerical algorithms in lumped strictly passive switched system simulations. This method is then extended to analyze the stability of simulations that use CDA or interpolation which are widely used approaches in modern simulators.

In the second part, we developed a novel technique to assess the accuracy of electromagnetic transient (EMT) simulations. The proposed method globally quantifies the simulation accuracy and is convenient to apply to large systems without explicitly forming the state space equations. It also permits the accuracy analysis of networks with distributed component such as frequency dependent transmission lines.

**Index Terms:** stability; accuracy; equivalency; switched system;

## **Acknowledgements**

It is my great honor and pleasure to have had Prof. Aniruddha Gole as my supervisor during this 6 years' journey. Besides his consistent and kind support to my study, Prof. Gole also encouraged me to become an “interdisciplinary” student. Thanks to his support, I have had the opportunities of interacting with many professors and researches in various research fields (e.g., Prof. Peter Blunden, Prof. Michael Gericke working on physics, Prof. Witold Kinsner working on signal processing, Prof. Douglas Thomson, working on bio-electronics, Prof. Akihiro Ametani, Prof. Joe LoVetri and Prof. Ian Jeffrey, working on electromagnetic theory). This experience helped me build a comprehensive background, which I benefited a lot in my later research carrier. Prof. Gole also supported me to attend international conferences, which significantly broadened my academic view. In my whole program, Prof. Gole is not only a great supervisor, but also a good friend.

I would like to sincerely appreciate my thesis committee member Prof. Yi Zhang and Prof. Jason Morrison. As an industry leader in simulation, Prof. Yi Zhang gave extensive support and guidance to my study. He also provided me with a great opportunity to closely working with experienced industry experts. I feel so lucky to have Prof. Jason Morrison in my committee. Although he is a professor from biosystems (not electrical engineering), he is a great expert in mathematics and we had lots of valuable discussions on my research from mathematical point of view. Besides, his reviewing of thesis is extremely careful and I really appreciate his comments on improving the quality of this thesis.

I would like to thank Prof. Neville Watson for his time and attention to review my thesis as an external examiner.

I would like to thank Dr. Shengtao Fan. In my Ph.D. program, Dr. Fan closely worked together with me and provided extensive support for my academic research.

I would like to thank Dr. Hui Ding, Dr. Yi Qi, Dr. Yizhong Hu, Dr. Mukesh Das, Dr. Rohitha Jayasinghe, Dr. Jeewantha De Silva, Mr. John Liu. I feel so fortunate to have the opportunity to work with those experienced experts in the industry.

I would like to thank Prof. Chengyong Zhao. Prof. Zhao introduced me to Prof. Gole to start this wonderful journey.

I would like to thank my research lab classmates, including visiting scholars Chengyu Li, Tan Li, etc. The time spent with them is really great, and I sincerely appreciate their help and friendship.

In the end, I would like to sincerely appreciate my family, including my wife Yanan Ren, parents, inlaws, uncle and aunt, kid Victoria. I could not finish this program without their consistent support and encouragement.

Huanfeng Zhao

## List of Tables

Table 1-1 Origin of Transients and Frequency Range in Power Systems .....	9
Table 3-1 Eigenvalues for Each Switching State in Example 1 .....	35
Table 3-2 Eigenvalues for Each Switching State When Trapezoidal Method is Applied .....	38
Table 3-3 Eigenvalues for Each Switching State in Example 2 .....	39
Table 3-4 Simulation System Parameters .....	45
Table 5-1 Frequency Dependent Model Parameters.....	81



Figure 5-7 Network and transmission line configuration .....	81
Figure 5-8 Simulation accuracy spectrum with $\Delta t = 10 \mu s$ .....	82
Figure 5-9 Impact of fitting error on simulation ( $\Delta t = 10 \mu s$ ).....	82
Figure 5-10 Simulation accuracy spectrum with 2% fitting error and $\Delta t = 10 \mu s$ ..	83
Figure 5-11 EMT simulation verification with different $\Delta t$ .....	84
Figure 5-12 Topology of studied system .....	85
Figure 5-13 Eigenvalue distribution .....	85
Figure 5-14 Simulation accuracy spectrum .....	86
Figure 5-15 Simulation validation .....	87
Figure C-1 Network showing boundary and internal buses.....	104
Figure C-2 Simulation Accuracy Spectrum .....	105
Figure C-3 Simulation of node Ni1 voltage with 912 Hz Excitation .....	106

## List of Abbreviations

EMT	Electromagnetic transient
LTI	linear time-invariant
BIBO	bounded-input-bounded-output
BE	Backward Euler
FE	Forward Euler
CDA	Critical Damping Adjustment
dc	direct current
ac	alternating current
HVdc	high voltage direct current
TSA	transient stability analysis
FDNE	Frequency Dependent Network Equivalent
DSE	descriptor state space equations
SVE	state variable equations
SV	state variable
MNA	Modified nodal analysis
LSPSC	lumped strictly passive switched circuits
CQLF	common quadratic Lyapunov function
FACTS	flexible alternating current transmission system
RLCM	resistor, inductor, capacitor, mutual inductor
SI	switched inductors

# Contents

Abstract .....	II
Acknowledgements.....	III
List of Tables .....	V
List of Figures .....	VI
List of Abbreviations .....	VIII
1 Introduction .....	1
1.1 Background.....	1
1.2 Formulation Approaches for Electromagnetic Transient (EMT) Digital Simulation .	1
1.2.1 State Space Equations Based Simulation of Power Systems .....	1
1.2.2 Companion Circuit Based Simulation of Power Systems .....	2
1.2.3 Relationship of Two Methods .....	3
1.3 Numerical Stability of Electromagnetic Transient (EMT) Digital Simulation with Switches and Non-linear Inductors .....	4
1.4 Special Techniques for Accurate Simulation of Power Electronic Systems .....	5
1.4.1 Locating the Switching Instant .....	5
1.4.2 Re-initialization after Switching Operation.....	6
1.4.3 Numerical Oscillation Suppression .....	7
1.4.4 Re-synchronizing to the Original Time step Grid .....	8
1.5 Evaluating the Numerical Accuracy of Power System Simulation .....	9
1.7 Thesis Contributions.....	10
1.8 Thesis Outline .....	11
2 Equivalency of State Space Models and EMT Companion Circuit Models .....	12
2.1 Motivation .....	12
2.2 Approach for Establishing the Equivalency of State Space and Dommel’s EMT Companion Circuit methods .....	13
2.3 Generation of Descriptor State Space Equations by Modified Nodal Analysis.....	13
2.3.1 Description of the Circuit by a Node Incidence Matrix .....	14
2.3.2 Generation of Descriptor State Space Equations.....	15
2.4 Update Equation Derived from Descriptor State Equations.....	17
2.4.1 Discretization of Descriptor State Equations.....	17

2.4.2 Derivation of Update Equation by Row Expansion .....	17
2.5 Update Equation in EMT Type Simulation .....	19
2.6 Comparison of Update Equations from Descriptor State Equations and Companion Circuit Based Method.....	21
2.6 Chapter Summary.....	24
3 Stability of Algorithms for Electro-Magnetic-Transient Simulation of Networks with Switches and Non-linear Inductors.....	25
3.1 Energy Function Based Stability Analysis .....	26
3.1.1 Energy Function of Lumped Strictly Passive Switched Circuit (LSPSC) System .....	27
3.1.2 System Properties When Each State Is Strictly Passive .....	28
3.1.3 Proof of Stability of the Real-World (physical) LSPSC.....	29
3.2 Stability of Numerical Algorithms in LSPSC System Simulations .....	29
3.2.1 Global Stability of Numerical Algorithms in a Switched System (Discrete Time Lyapunov Theory) .....	30
3.2.2 Energy Variation in Each Switching State with Different Numerical Integration Algorithms .....	31
3.2.2.1 Stability of Algorithm for Forward Euler Integration.....	31
3.2.2.2 Stability of Algorithm for Backward Euler Integration .....	32
3.2.2.3 Stability of Algorithm for Trapezoidal Integration.....	32
3.2.3 The Stability of the Non-autonomous Case.....	33
3.3 General Stability of Numerical Algorithms in Switched System Simulation .....	34
3.3.1 Example 1 (simulation with Trapezoidal method) .....	34
3.3.1.1 Numerical Stability of Permanent Switching States .....	35
3.3.1.2 Stability with Periodic State Transitions.....	36
3.3.2 Example 2 (Simulation with Backward Euler Method) .....	39
3.3.3 Discussion.....	40
3.4 Stability of Simulations of Non-linear Resistors and Inductors .....	41
3.4.1 Stability of Simulation of Non-linear Resistors .....	41
3.4.2 Stability of Simulation of Non-linear Inductors .....	42
3.4.2.1 Theoretical Analysis .....	43

3.4.2.2 Case Study .....	44
3.5 Chapter Conclusion .....	48
4 Stability Evaluation of Interpolation, Extrapolation, and Numerical Oscillation Damping Methods Applied in EMT Simulation of Power Networks with Switching Transients.....	50
4.1 Energy Function Based Stability Analysis .....	51
4.1.1 State-Space Model of Network with Switches .....	51
4.1.2 Common Quadratic Lyapunov Function Theory.....	52
4.1.3 Stability of Numerical Simulation Algorithms.....	52
4.2 Stability of simulation when interpolation is used to locate the switching instant	53
4.2.1 Impact on Simulation Stability with Interpolation Technique Used for Locating the Switching Event.....	53
4.2.2 Locating the Switching Instant .....	54
4.2.3 Additional Interpolation for Synchronizing to Original Time Grid .....	57
4.3 Stability of Numerical Oscillation Suppression Strategy .....	57
4.3.1 Stability of Critical Damping Adjustment (CDA).....	58
4.3.2 Stability of Interpolation.....	58
4.4 Stability of Re-Initialization procedure .....	59
4.4.1 The Discontinuity of Derivative Problem .....	59
4.4.2 Techniques for Re-initialization .....	60
4.5 Application to Other Methods for Re-synchronizing to Original Time Grid .....	61
4.5.1 Flexible Integration for Readjustment in Simulation of Transients (FIRST)...	61
4.5.2 Extrapolation .....	63
4.5.3 Verification by Simulation .....	63
4.6 Chapter Conclusions.....	66
5. Accuracy Evaluation of Electromagnetic Transients Simulation .....	68
5.1 Previous Approaches for Accuracy Evaluation and their Limitations .....	68
5.1.1 Component Level Accuracy Evaluation.....	68
5.1.2 Limitation of Component Level Accuracy Evaluation.....	69
5.2 Proposed Methods for Accuracy Evaluation of EMT Simulation .....	70
5.2.1 Theoretical Foundation of Simulation Accuracy Evaluation [43].....	70
5.2.2 Method I: Global Evaluation of Simulation Accuracy .....	71

5.2.3 Challenge for Practical Application .....	72
5.3 Method 2: Simulation Accuracy Considering Driving Port Admittances .....	73
5.3.1 The Equivalent Admittance Matrix from Boundary Ports .....	73
5.3.2 Bi-linear Transformation .....	74
5.3.3 Simulation Accuracy Spectrum .....	75
5.3.4 Advantage of the Proposed Index.....	76
5.4 Consideration of Distributed Parameter Elements.....	77
5.4.1 Transmission Line Formulation.....	77
5.4.2 Discretized Model in EMT Type Simulation .....	78
5.5 Application of Proposed Method .....	80
5.5.1 System with a Distributed Parameter Transmission Line .....	80
5.5.2 Accuracy of EMT Simulation of IEEE 39 BUS System .....	84
5.6 Chapter Summary.....	87
6 Concluding Remarks and Future Work .....	89
6.1 Summary of Results.....	89
6.2 Publications Resulting from the Thesis .....	90
6.3 Future Work .....	91
References .....	93
Appendix A – Matrix commutation relation proof .....	97
Appendix B – Stability of Instantaneous Solution Interpolation .....	101
Appendix C – Modified admittance approach for simulation accuracy evaluation .....	104

# 1 Introduction

## 1.1 Background

Electromagnetic transient (EMT) digital simulation tools such as ATP, EMTP, PSCAD/EMTDC, RTDS, etc. are widely used in power system applications [1, 2]. These digital tools model the network in very high detail and provide the most accurate simulation results over a wide frequency range, as compared with more approximate modelling tools such as transient stability programs [1].

One important necessary property for the simulation is that a stable real-world system should have a stable simulation (i.e., one that has bounded output for bounded excitation). Additionally, the simulation result is expected to reflect the real world dynamic phenomenon with minimum computation cost.

In this thesis, we study the numerical stability and accuracy of such simulations, hoping to help developing new simulation techniques for a more robust and efficient property.

## 1.2 Formulation Approaches for Electromagnetic Transient (EMT) Digital Simulation

There exist two main formulation methods for Electromagnetic Transient Simulation of lumped circuit networks: state space equations and the companion circuit based nodal analysis approach introduced by Dommel [1, 2].

### 1.2.1 State Space Equations Based Simulation of Power Systems

Graph theory based methods which subdivide the graph of the circuit into a tree and a cotree are one previously used systematic approach for deriving the state space equations [3]. Such a method provides a set of linearly independent differential equations of the form:

$$\dot{\mathbf{x}} = \mathbf{A} \cdot \mathbf{x} + \mathbf{B}\mathbf{u} \quad (1.1)$$

where  $\mathbf{x}$  and  $\mathbf{u}$  are the state and input vector. Matrix  $\mathbf{A}$  represents the system matrix and  $\mathbf{B}$  denotes the input matrix.

However, as pointed out in [4, 5], a drawback of this approach is that the time and computational effort for generating state space equations is excessive and impractical when applied to large networks. Therefore, this method is used primarily for theoretical analysis of small circuits.

Alternative approaches such as the transform method [6, 7] were developed which made it easier to generate the state equations for large networks. In the transform method [7], capacitor charges and inductor fluxes are selected as state variables. This yields equations in the form of  $\mathbf{M} \cdot \dot{\mathbf{x}} = \mathbf{A} \cdot \mathbf{x} + \mathbf{B}\mathbf{u}$  where  $\mathbf{M}$  may be singular. Gaussian elimination can then be applied to convert the equation set to linearly independent true SV equations.

After the state space equations are formulated, the system can be simulated in the time domain by using a suitable method. Additionally, eigenvalues of the system matrix  $\mathbf{A}$  can yield important information about the system, such as its stability margin, time constants and oscillation modes.

### 1.2.2 Companion Circuit Based Simulation of Power Systems

On the other hand, the popular approach [1] for EMT type simulation is to convert all energy storage elements, e.g., inductors and capacitors into their companion circuit form using a suitable integration method, typically the Trapezoidal rule. The companion circuit form generates a conductance in parallel with a history current source. For instance, the differential equation of the voltage current relation for an inductor is:

$$L \frac{di_L(t)}{dt} = v_L(t) \quad (1.2)$$

Applying Trapezoidal method gives:

$$i_L(t) = \frac{\Delta t}{2 \cdot L} \cdot v_L(t) + [i_L(t - \Delta t) + \frac{\Delta t}{2 \cdot L} \cdot v_L(t - \Delta t)] \quad (1.3)$$

Which is corresponding to a circuit as shown in Fig. 1-1 with the format:

$$i_L(t) = g_L \cdot v_L(t) + I_L(t - \Delta t) \quad (1.4)$$

Where:

$$g_L = \frac{\Delta t}{2 \cdot L}, I_L(t - \Delta t) = i_L(t - \Delta t) + \frac{\Delta t}{2 \cdot L} \cdot v_L(t - \Delta t)$$

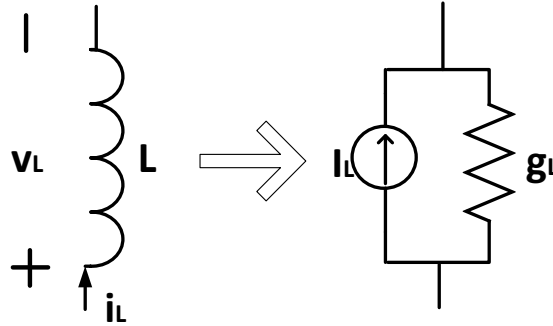


Figure 1-1 Equivalent circuit for inductor valid during a time step

Using nodal analysis, the admittance matrix corresponding to the connected set of companion elements can be assembled [1, 8] and the voltages in each time step determined by solving the set of nodal equations. This method is widely used for large circuit simulations because it is straightforward to apply. However, [3] claims that the network time constants and oscillation frequencies can not directly be extracted, which is significant for stability analysis and simulation time step selection.

### 1.2.3 Relationship of Two Methods

In the famous EMTP theory book [1], Prof. Hermann Dommel makes the comment “...the author has never proved it, but suspects the answer [i.e., the two methods] are identical for an arbitrary circuit”.

Equations relating nodal equations and state space equations were presented in [9] to reconstruct the eigenvalues from the EMTP simulations. This method finds the eigenvalues in the discrete time domain in advance and maps them back to the continuous time domain according to the applied numerical algorithms. However, due to the fact that the state space equations are recovered from an EMT companion circuit, an implicit assumption is made

that the nodal analysis method is theoretically identical to directly applying the Trapezoidal method to state space equations.

In this thesis, we prove that Prof. Dommel's suspicions are correct and that the two approaches are exactly equivalent.

### **1.3 Numerical Stability of Electromagnetic Transient (EMT) Digital Simulation with Switches and Non-linear Inductors**

(This summary was published in IEEE Transactions on Power Delivery [10])

Typically, these Electromagnetic transient (EMT) digital simulation tools utilize the Trapezoidal rule for numerical integration. This algorithm is known as A-stable algorithm which will always result in *stable* simulations of *stable linear time-invariant* (LTI) real-world systems [11], regardless of the time step used. However, the type of simulations being carried out today include systems with a large number of switching devices, such as HVDC converters and non-linear elements such as saturating inductors and transformers. However, it is nevertheless a common experience that EMT type simulation usually generates good results for systems with switches such as power electronic systems. Therefore, one unexplored area is the theory to support this observed experience.

Some publications have discussed the stability of actual switched systems [12-16], but little has been done to analyze the stability of the simulations of such systems. Consider a system with linear elements and  $s$  switches. Each of the  $2^s$  switching state combinations individually is a linear circuit, and would result in a stable simulation if no switch operated and the system remained in that configuration. However [17] shows that even though every switching state is individually stable, it does not imply that the system is stable, under arbitrary operation of the switches. In reference [16], an example is provided to show that a real-world switched system can still be unstable even if every switching state is stable and strictly passive.

Regarding to the stability of the simulations of such systems, earlier research has focused on the stability of simulation of linear lumped energy storage components such as inductors and capacitors [11-13]. But, it does not consider system stability when non-linear

elements are present, nor does it discuss the stability of networks in which such elements are connected by switches that turn on and off.

A contribution of this thesis is to investigate the bounded-input-bounded-output (BIBO) stability of the simulations of such systems. Based on the proposed method, we are hoping to set up a theory to determine the stability of numerical algorithms in EMT type simulations of Lumped Strictly Passive Switched Circuits.

## **1.4 Special Techniques for Accurate Simulation of Power Electronic Systems**

For accurate representation of the switching in Electromagnetic transient simulations, several factors must be considered as listed below.

### **1.4.1 Locating the Switching Instant**

Firstly, the switching operation does not typically coincide with the time step grid. For example, while simulating a diode, the zero current at which the device turns off may occur between time steps. Forcing the switching to coincide with a time step in such cases results in additional transients due to current chopping or non-characteristic harmonics [18, 19]. One practical solution in many commercial EMT solvers (e.g., NETOMAC, PSCAD, etc.) is to use linear interpolation to locate the exact switching instant. From the start to the end of a time step, the currents and voltages can be presumed to vary linearly. For instance, consider the diode turn-off problem shown in Fig. 1-2, where the current crosses zero within the interval  $[0, \Delta t]$ , at time  $\delta t$ . The algorithm determines that the crossing must lie in  $[0, \Delta t]$  because the current at  $\Delta t$  is negative. Subsequently, linear interpolation is applied to determine the zero crossing of the current to be at  $\delta t$  as shown in Fig. 1-2. The tentative time step solution at  $\Delta t$  is disregarded in the simulation, and the interpolated solution at  $\delta t$  is retained as the “true” solution. However, this creates the problem, that the next simulation point using the same time step would be  $\Delta t + \delta t$ , which is not in the original time grid. Other ways to improve the interpolation accuracy can be found in reference [11],

where a two stage interpolation method is proposed which improves the accuracy of interpolation to second order.

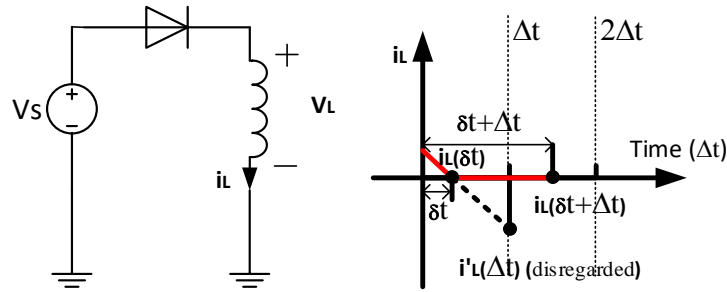


Figure 1-2 Interpolation example

#### 1.4.2 Re-initialization after Switching Operation

Consider the simulation of an inductor in series with a diode as shown in Fig. 1-2. Let us ignore interpolation for the time being and assume that the current goes to zero precisely at time  $\Delta t$ . The theoretical variation of inductor voltage is shown in the Fig. 1-3. Although the current is continuous during the switching operation, the voltage is not. Actually, there are two inductor voltages as shown in Fig. 1-3, one,  $v_L(t_-)$ , just before and the other  $v_L(t_+)$  just after the switch operation. The calculation of the history current source by the Trapezoidal method requires a knowledge of the inductor voltage and current in the previous time step. Only one of these,  $v_L(t_+)$  yields the correct history term for calculating the solution at  $t = 2\Delta t$ . However, the companion circuit method in EMT solvers cannot directly give  $v_L(t_+)$ , as  $v_L(t_-)$  is the last calculated voltage value.

Three methods have been proposed to address this issue [7]. The first, used in programs such as NETOMAC applies one half time step Backward Euler (BE) after the switching operation. In BE, the history current (for an inductor) is just the current in the previous time step, i.e.,  $i_L(t_-)$ . As voltage is not even involved, the problem of using the incorrect voltage is avoided entirely. The calculated new voltage is a good approximation of  $v_L(t_+)$  and is used in the calculation of the history current for the new time step solution.

Programs such as XTAP [20] use the 2s-Dirk method, which has the same order of accuracy as the Trapezoidal method [11]. Just like BE, 2S-Dirk only considers the previous time step current for the history term of an inductor and avoids the problem of using the incorrect voltage.

The third method, labelled “instantaneous solution method” [21], also recalculates an approximate history term after switching (e.g.  $v_L(t_+)$  and  $i_L(t_+)$ ) using the post-switching admittance matrix, and has been implemented in programs such as PSCAD. It is seen to reduce spurious losses associated with a straightforward implementation of interpolation.

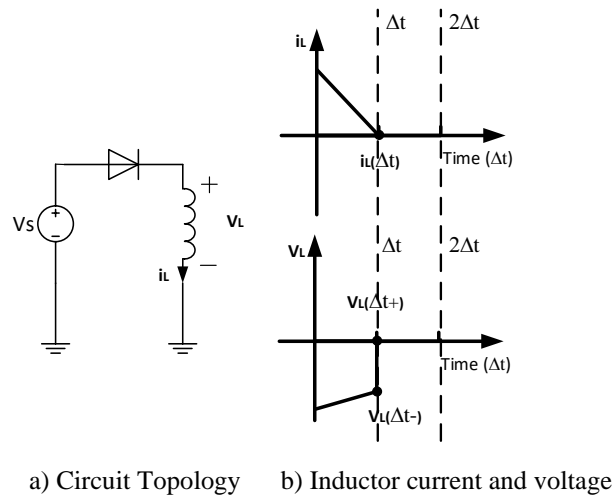


Figure 1-3 Discontinuity example

### 1.4.3 Numerical Oscillation Suppression

Although the Trapezoidal method is the most accurate single stage method which is A-stable, it results in a spurious numerical oscillation known as “chatter” when the switch’s off resistance is large [19, 22]. Several methods exist to remove chatter, such as the use of artificial snubber circuits across switches [1, 7], interpolation [19], position dependent control of the integration method [23], by applying two half-time step BE steps (referred to as Critical Damping Adjustment or CDA) [22, 24] or using an inherently L-stable method such as 2s-Dirk [25].

### 1.4.4 Re-synchronizing to the Original Time step Grid

A straightforward application of interpolation or half-step BE derails the simulation from the original time grid, as the new time grid would now be  $\delta t + \Delta t, \delta t + 2\Delta t \dots$  etc. (as shown in Fig. 1-2). An additional linear interpolation step can be applied to re-synchronize with original time grid [19].

The 4-steps discussed above are summarized in the flow chart of Fig. 1-4.

This thesis discusses the numerical stability of these special techniques. We hope to verify the stability of the existing methods and also to help the digital simulator designer to develop robust and better techniques for treating switching operation phenomenon.

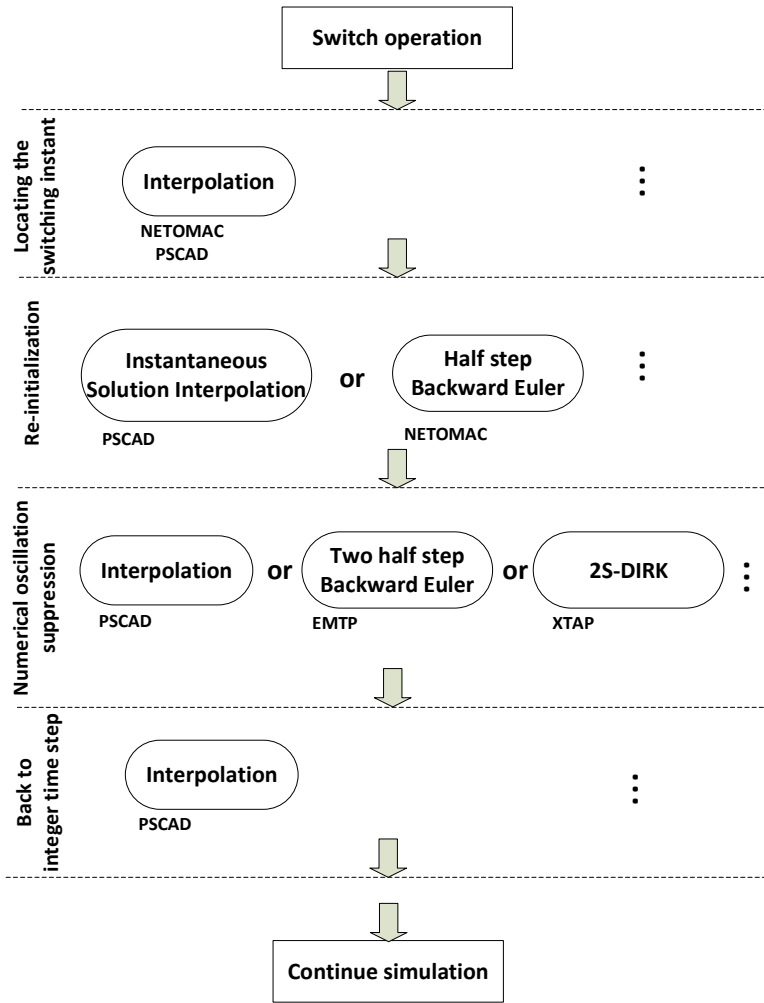


Figure 1-4 Flow chart of procedures for accurately representing switching

## 1.5 Evaluating the Numerical Accuracy of Power System Simulation

In power system analysis, the frequency range of interest can typically varies from DC (0 Hz) to 50 MHz depending on specific electrical transient phenomenon as shown in Table 1-1 [26]. In order to study the transient phenomenon, electro-magnetic transient (EMT) simulation tools are widely used in modern power system analysis.

Since EMT type simulation usually covers a wide frequency band, one important topic is how to quantify the accuracy of such simulations. For instance, in order to accurately study the effect of lightning surges on power networks, the simulation must provide an accurate result in the frequency range from 10k Hz to 3 MHz. Since the numerical accuracy in EMT type simulation is influenced by factors such as the simulation time step, numerical algorithms, distributed elements, non-linear components, etc., systematically qualifying the numerical accuracy by considering most of the significant factors remains an important concern. This will be addressed in the thesis.

Table 1-1 Origin of Transients and Frequency Range in Power Systems

<i>Origin</i>	<i>Frequency Range</i>
<i>Transformer energization Ferro resonance</i>	<i>0.1 Hz-1000Hz</i>
<i>Load Rejection</i>	<i>0.1 Hz-3000Hz</i>
<i>Lightning Surges</i>	<i>10 kHz-3MHz.</i>
<i>Disconnecter Switching and faults in GIS</i>	<i>100 kHz-50MHz</i>

In reference [22], the numerical accuracy is analyzed for each dynamic element (i.e. capacitor and inductor). The mapping from discrete to continuous frequency domain is used to compare the simulation result with theoretical result in frequency domain. However, this technique does not actually demonstrate the simulation accuracy of the system as a whole. In reference [11], the numerical accuracy is mathematically analyzed based on truncation error. The numerical accuracy for each switching state and propagation error is analyzed. However, the influence of distributed elements like transmission lines is still not considered. Besides, modern simulation programs sometimes locally change the integration method for select components, for example, to suppress the numerical

oscillation in power electronic simulations [23]. Such factors also significantly influence the accuracy of simulation and still have not been included in the existing accuracy evaluation method. In this thesis, a new method is developed to evaluate the accuracy of the simulation, which rather than consider each element separately investigates accuracy at driving ports for the entire network. It is hoped that this could aid the user in implementing an accurate EMT simulation with minimum computation cost.

## **1.7 Thesis Contributions**

This research primarily focus on investigating the stability and accuracy of Electromagnetic transient simulations for modern power systems. The following major contributions will result from this research:

1. In Chapter 2, In order to adapt the existing stability analysis techniques for analyzing the stability of companion circuit based electromagnetic transient simulation, we firstly prove the equivalency of state space equations models and electromagnetic companion circuit methods. Therefore, stability analysis using state space equations could be directly applied for the more commonly used companion circuit model based simulation.
2. A novel technique is developed by applying Common Quadratic Lyapunov Function theory to analyze the numerical stability of lumped strictly passive switched system simulations is developed in Chapter 3. This method allows one to determine the stability of numerical algorithms in lumped strictly passive switched system simulations.
3. The use of interpolation or CDA steps essentially modifies the integration method at the instant of switching, and so the conclusions of Chapter 3 no longer directly apply. This gap is addressed in Chapter 4 by extending the stability analysis to simulations that use CDA or interpolation which are widely used approaches in modern simulators.
4. A novel technique to assess the accuracy of electro-magnetic transient (EMT) simulations is developed in Chapter 5. The proposed method globally quantifies the

simulation accuracy and is convenient to apply to large systems without explicitly forming the state space equations. It also permits the accuracy analysis of networks with distributed component such as frequency dependent transmission lines.

## **1.8 Thesis Outline**

- In Chapter 2, the equivalency of state space equations models and electromagnetic companion circuit methods is proved, which is required for extending the state-space based stability analysis to EMT simulation.
- Chapter 3 investigates the stability of numerical algorithms in lumped strictly passive switched circuit simulations.
- Chapter 4 analyzes the numerical stability of Interpolation, Extrapolation, and Numerical Oscillation Damping Methods applied in EMT simulation of power networks with switching transients.
- Chapter 5 proposes a new method to globally evaluate the simulation accuracy of a practical power network.
- Thesis conclusions are summarized in Chapter 6 and several potential future research are given.

## 2 Equivalency of State Space Models and EMT Companion Circuit Models

This chapter demonstrates the equivalence of the state space models and the EMT companion circuit method. The author's work is the first time such equivalence has been proved [27] although it has been speculated to be so by others [1].

### 2.1 Motivation

There exist two main methods to simulate lumped circuit networks: state space equations and the companion circuit based nodal analysis approach introduced by Dommel [1]. For the state space equations based method, the eigenvalues of the system matrix are directly available which can yield important information about the system, such as its stability, time constants and oscillation modes. However, one drawback of this approach as pointed by [5] is that the time and computational effort for generating state space equations is excessive and impractical when applied to large networks. Therefore, this method is used primarily for theoretical analysis of small circuits.

On the other hand, as presented in section 1.2.2, the popular approach for EMT type simulation is to convert all energy storage elements, e.g., inductors and capacitors into their companion circuit form [1]. Due to its convenience, this method is widely used for large circuit simulations. However, the network time constants and oscillation frequencies can not directly be extracted, which is significant for stability analysis and simulation time step selection.

In the field of control systems, stability analysis is conducted using the state space equation form. On the other hand, most modern power system digital simulation is based on the companion circuit method. In order to use the existing stability analysis technique to study the numerical stability of integration algorithms in modern power system simulations, a gap that must be filled is to prove that these two methods are completely equivalent. In the famous EMTP theory book [1], Prof. Hermann Dommel, considered the

father of power systems transients simulation, makes the comment “...*the author has never proved it, but suspects the answer* [i.e., the two methods] *are identical for an arbitrary circuit*”. In this chapter we will prove that Prof. Dommel’s suspicions were correct and that the two approaches are exactly equivalent.

## **2.2 Approach for Establishing the Equivalency of State Space and Dommel’s EMT Companion Circuit methods**

Firstly, descriptor state space equations (DSEs) are used to show the equivalence between the state space and companion circuit nodal analysis (traditional EMT approach by Dommel [1]) approaches. DSEs are formed by Modified Nodal Analysis, which usually has more state variables (because linearly dependency is not always eliminated) than the standard state space equations. Secondly, Chua [6, 28] has shown a generic approach for transforming the DSE to a standard state variable form. Galvão et al [29] also point out that the transfer function obtained by DSEs is identical to the transfer function from the standard state space equations, and the standard state space equations corresponding to DSEs can be consequently obtained by a minimum realization of its transfer function. Once we prove the first step, the equivalence of Dommel’s approach with DSE is established. Then relying on the work of Chua et al and Galvão, the equivalence of DSE with traditional SE immediately follows. Hence, the equivalence between classical state variable equations (SVE) and Dommel’s EMT approach is established.

## **2.3 Generation of Descriptor State Space Equations by Modified Nodal Analysis**

In this section, the descriptor state space equations (DSE) can be generated based on Kirchhoff’s laws using modified nodal analysis. The admittance matrix and history current source terms used by EMT type simulations are reviewed, which will be used to show the equivalence with DSEs in the next section.

### 2.3.1 Description of the Circuit by a Node Incidence Matrix

In lumped circuits, the electrical behavior of the network is completely described by Kirchhoff's laws. This can be shortly summarized as below:

Assuming branch currents  $i_1 \cdots i_l$  entering any node  $n$  in the circuit, Kirchhoff's current law (KCL) gives  $\sum_{k=1}^l i_{nk} = 0$ . Similarly, for a loop  $p$  composed of  $m$  branches with voltages  $v_1 \cdots v_m$ , Kirchhoff's voltage law (KVL) states that  $\sum_{i=1}^m v_{pi} = 0$ .

For a practical circuit, there are usually many nodes and loops. In order to form the standard state space equations with a non-singular system matrix, the circuit is partitioned into a normal tree and normal co-tree to systematically generate the state space equations [3]. This is achieved by including as many of the capacitor elements in tree branches and as many as possible inductor branches in the co-tree, and then using these capacitor voltages and inductor currents as the state variables. Partitioning the circuit's branches into the normal tree and co-tree establishes the "fundamental loops" (those formed by including exactly one tree branch with all other branches in the loop being co-tree branches) and "fundamental cut-sets" (formed by exactly one co-tree branch and other tree branches). The state equations are then found by applying KVL to the fundamental loop equations and KCL to the fundamental cut-set equations. However, such a procedure is impractical for very large circuits because of the excessive computation time to formulate the state space equations [5]. As an alternative, the MNA method, which is widely used in computer aided design [30] can be used. The MNA equations can be easily generated from the circuit netlist but in the form of descriptor state space equations, which are also sometimes called Differential-algebraic equations (DAEs). Unlike normal state variables, the descriptor variables can be linearly dependent.

Consider a circuit with  $n$  nodes (excluding the datum or ground node) and  $b$  branches. We define an orientation for each branch, i.e. one node is set to be the "start" node while the other is the "end" node. The node incidence matrix with elements as shown below relates the nodes to the branches [3]. Note that this matrix can be directly formed based on the circuit netlist, which is the same information used for EMT type simulations:

$$a_{ij} = \begin{cases} 1, & \text{if branch } j \text{ has start node } i \\ -1, & \text{if branch } j \text{ has end node } i \\ 0, & \text{otherwise} \end{cases} \quad (2.1)$$

Consequently, collecting all branch currents into one vector:

$$\mathbf{i} = [i_1 \quad \cdots \quad i_b]^T$$

The KCL equations are directly represented as below:

$$\mathbf{A} \cdot \mathbf{i} = 0 \quad (2.2)$$

where  $\mathbf{A}$  is the incidence matrix:

$$\mathbf{A} = \begin{pmatrix} a_{11} & \cdots & a_{1b} \\ \vdots & \ddots & \vdots \\ a_{n1} & \cdots & a_{nb} \end{pmatrix}$$

Using vector  $\mathbf{e}$  and  $\mathbf{v}$  to represent node voltage and branch voltage, the node incidence matrix also represents the mapping from node to branch voltage as below:

$$\mathbf{v} = \mathbf{A}^T \cdot \mathbf{e} \quad (2.3)$$

### 2.3.2 Generation of Descriptor State Space Equations

Assume there are  $n_C$  capacitors,  $n_L$  inductors,  $n_R$  resistors and  $n_I$  current sources. Ordering all the columns in matrix  $\mathbf{A}$  in the sequence of capacitor, inductor, resistor, current source branches, i.e.,  $\mathbf{A} = (\mathbf{A}_C, \mathbf{A}_L, \mathbf{A}_R, \mathbf{A}_I)$ , equation (2.3) can be rewritten as below:

$$\begin{pmatrix} \mathbf{v}_C \\ \mathbf{v}_L \\ \mathbf{v}_R \\ \mathbf{v}_I \end{pmatrix} = \begin{pmatrix} \mathbf{A}_C^T \\ \mathbf{A}_L^T \\ \mathbf{A}_R^T \\ \mathbf{A}_I^T \end{pmatrix} \cdot \mathbf{e} \quad (2.4)$$

Where  $\mathbf{v}_C$ ,  $\mathbf{v}_L$ ,  $\mathbf{v}_R$ ,  $\mathbf{v}_I$  denote capacitor, inductor, resistor and current source branch voltage vector respectively.

Consequently, substituting matrix  $\mathbf{A} = (\mathbf{A}_C, \mathbf{A}_L, \mathbf{A}_R, \mathbf{A}_I)$  to equation (2.2) gives:

$$\mathbf{A}_C \cdot \mathbf{i}_C + \mathbf{A}_L \cdot \mathbf{i}_L + \mathbf{A}_R \cdot \mathbf{i}_R + \mathbf{A}_I \cdot \mathbf{i}_I = \mathbf{0} \quad (2.5)$$

Substituting the RLC elements relation and equation (2.4) to (2.5) gives:

$$\begin{aligned}
& \begin{pmatrix} \mathbf{A}_c \cdot \mathbf{C} \cdot \mathbf{A}_c^T & \mathbf{0} \\ \mathbf{0} & \mathbf{L} \end{pmatrix} \cdot \frac{d}{dt} \begin{pmatrix} \mathbf{e} \\ \mathbf{i}_L \end{pmatrix} \\
& = - \begin{pmatrix} \mathbf{A}_R \cdot \mathbf{G} \cdot \mathbf{A}_R^T & \mathbf{A}_L \\ -\mathbf{A}_L^T & \mathbf{0} \end{pmatrix} \cdot \begin{pmatrix} \mathbf{e} \\ \mathbf{i}_L \end{pmatrix} - \begin{pmatrix} \mathbf{A}_I \\ \mathbf{0} \end{pmatrix} \cdot \mathbf{i}_I
\end{aligned} \tag{2.6}$$

where  $\mathbf{c}$ ,  $\mathbf{g}$ , and  $\mathbf{L}$  are diagonal matrixes containing all the capacitance, admittance and inductance values respectively. With  $\mathbf{C}' = \mathbf{A}_c \cdot \mathbf{C} \cdot \mathbf{A}_c^T$  and  $\mathbf{G}' = \mathbf{A}_R \cdot \mathbf{G} \cdot \mathbf{A}_R^T$  (2.6) becomes (2.7):

$$\begin{pmatrix} \mathbf{C}' & \mathbf{0} \\ \mathbf{0} & \mathbf{L} \end{pmatrix} \cdot \frac{d}{dt} \begin{pmatrix} \mathbf{e} \\ \mathbf{i}_L \end{pmatrix} = - \begin{pmatrix} \mathbf{G}' & \mathbf{A}_L \\ -\mathbf{A}_L^T & \mathbf{0} \end{pmatrix} \cdot \begin{pmatrix} \mathbf{e} \\ \mathbf{i}_L \end{pmatrix} - \begin{pmatrix} \mathbf{A}_I \\ \mathbf{0} \end{pmatrix} \cdot \mathbf{i}_I \tag{2.7}$$

which is in the form:

$$\mathbf{E} \cdot \dot{\mathbf{x}} = -\mathbf{A} \cdot \mathbf{x} + \mathbf{B}\mathbf{u} \tag{2.8}$$

Equation (2.8) is known as a descriptor state space equation [31].

In standard state space equations of the form (1.1) the state variables are the linearly independent capacitor branch voltages and linearly independent inductor branch currents (if inductor cut-sets or capacitor loops exists, not all inductor currents and capacitor voltages are SVs). These are a minimal set and are linearly independent. In DSEs, all node voltages  $\mathbf{e}$  and inductor branch currents are the descriptor state variables (which can be linearly dependent). It is also valuable to note that descriptor state variables are not standard state variables. State variables are always linearly independent, whereas descriptor variables may not be. Descriptor variables, however, do share one property in common with state variables in that any future state of the system at a time  $t$ , can be uniquely determined from the input over the interval  $[t_o, t]$  and the values of the descriptor variables at time  $t_o$ .

Consequently, the matrix  $\mathbf{E}$  may be singular and thus non-invertible. If it was invertible, (2.8) could directly be transformed to (1.1) by inverting  $\mathbf{E}$ . Reference [6, 28] describe methods to transform (2.8) to standard state variable, and eigenvalues of  $\mathbf{A}$  are the same as the generalized eigenvalues [32] of (2.8). As a results, (2.8) and (1.1) represent the same physical system and embody the same information. It is also valuable to notice that alternative formulations such as the transform method [7] also generate an equation form such as  $\mathbf{E} \dot{\mathbf{x}} = \mathbf{M} \cdot \mathbf{x} + \mathbf{B}\mathbf{u}$  except that elements of  $\mathbf{x}$  are capacitor charges

and inductor fluxes. Using Gaussian elimination, the equation set can also be transformed to a true state variable form of the type  $\dot{\mathbf{x}} = \mathbf{A} \cdot \mathbf{x} + \mathbf{B}\mathbf{u}$ .

## 2.4 Update Equation Derived from Descriptor State Equations

In a simulation, the DSEs can be used to calculate the values of the Descriptor variables in the next time step, i.e., the “updates” from those in the current time step. This section derives the update equations used for determining the new node voltages based on the descriptor state space and shows that it is identical to the update equation for EMT type companion matrix.

### 2.4.1 Discretization of Descriptor State Equations

Directly applying the Trapezoidal method to equations (2.8) gives:

$$\mathbf{E} \cdot \mathbf{x}(t) = \mathbf{E} \cdot \mathbf{x}(t - \Delta t) + \frac{-\mathbf{A} \cdot \Delta t}{2} \cdot (\mathbf{x}(t) + \mathbf{x}(t - \Delta t)) + \frac{\mathbf{B} \cdot \Delta t}{2} (\mathbf{u}(t) + \mathbf{u}(t - \Delta t)) \quad (2.9)$$

Substituting equation (2.7) gives:

$$\begin{aligned} \begin{pmatrix} \mathbf{C}' & \mathbf{0} \\ \mathbf{0} & \mathbf{L} \end{pmatrix} \cdot \begin{pmatrix} \mathbf{e}(t) \\ \mathbf{i}_L(t) \end{pmatrix} &= \begin{pmatrix} \mathbf{C}' & \mathbf{0} \\ \mathbf{0} & \mathbf{L} \end{pmatrix} \cdot \begin{pmatrix} \mathbf{e}(t - \Delta t) \\ \mathbf{i}_L(t - \Delta t) \end{pmatrix} + \\ \frac{\Delta t}{2} \cdot - \begin{pmatrix} \mathbf{G}' & \mathbf{A}_L \\ -\mathbf{A}_L^T & \mathbf{0} \end{pmatrix} \cdot \left( \begin{pmatrix} \mathbf{e}(t) \\ \mathbf{i}_L(t) \end{pmatrix} + \begin{pmatrix} \mathbf{e}(t - \Delta t) \\ \mathbf{i}_L(t - \Delta t) \end{pmatrix} \right) \\ + \frac{\Delta t}{2} \cdot - \begin{pmatrix} \mathbf{A}_I \\ \mathbf{0} \end{pmatrix} \cdot (\mathbf{i}_I(t - \Delta t) + \mathbf{i}_I(t)) \end{aligned} \quad (2.10)$$

### 2.4.2 Derivation of Update Equation by Row Expansion

Simplifying first row of equation (2.10) gives:

$$\begin{aligned} \frac{2\mathbf{C}'}{\Delta t} \cdot \mathbf{e}(t) &= \frac{2\mathbf{C}'}{\Delta t} \cdot \mathbf{e}(t - \Delta t) - (\mathbf{G}' \quad \mathbf{A}_L) \\ &\cdot \left( \begin{pmatrix} \mathbf{e}(t - \Delta t) \\ \mathbf{i}_L(t - \Delta t) \end{pmatrix} + \begin{pmatrix} \mathbf{e}(t) \\ \mathbf{i}_L(t) \end{pmatrix} \right) + \mathbf{I}_s \end{aligned} \quad (2.11)$$

where  $\mathbf{I}_s = -\begin{pmatrix} \mathbf{A}_I \\ \mathbf{0} \end{pmatrix} \cdot (\mathbf{i}_I(t) + \mathbf{i}_I(t - \Delta t))$ .

Using KCL, we have  $-(\mathbf{G}' \quad \mathbf{A}_L) \cdot \begin{pmatrix} \mathbf{e}(t - \Delta t) \\ \mathbf{i}_L(t - \Delta t) \end{pmatrix} = \mathbf{A}_c \cdot \mathbf{i}_c(t - \Delta t) + \mathbf{A}_I \cdot \mathbf{i}_I(t - \Delta t)$ .

Therefore:

$$\begin{aligned} \frac{2\mathbf{C}'}{\Delta t} \cdot \mathbf{e}(t) &= -(\mathbf{G}' \quad \mathbf{A}_L) \cdot \begin{pmatrix} \mathbf{e}(t) \\ \mathbf{i}_L(t) \end{pmatrix} + \left( \frac{2\mathbf{C}'}{\Delta t} \cdot \mathbf{e}(t - \Delta t) + \mathbf{A}_c \cdot \right. \\ &\quad \left. \mathbf{i}_c(t - \Delta t) - \mathbf{A}_I \cdot \mathbf{i}_I(t) \right) \end{aligned} \quad (2.12)$$

Since:

$$\begin{aligned} \frac{2\mathbf{C}'}{\Delta t} \cdot \mathbf{e}(t - \Delta t) &= \mathbf{A}_c \cdot \mathbf{g}_c \cdot \mathbf{A}_c^T \cdot \mathbf{e}(t - \Delta t) \\ &= \mathbf{A}_c \cdot \mathbf{g}_c \cdot \mathbf{v}_c(t - \Delta t) \end{aligned} \quad (2.13)$$

Expanding equation (2.12) gives:

$$\begin{aligned} &\left( \frac{2\mathbf{C}'}{\Delta t} + \mathbf{G}' \right) \cdot \mathbf{e}(t) \\ &= -\mathbf{A}_L \cdot \mathbf{i}_L(t) + \mathbf{A}_c \cdot \mathbf{g}_c \cdot \mathbf{v}_c(t - \Delta t) + \mathbf{A}_c \cdot \mathbf{i}_c(t - \Delta t) - \mathbf{A}_I \cdot \mathbf{i}_I(t) \\ &= -\mathbf{A}_L \cdot \mathbf{i}_L(t) - \mathbf{A}_I \cdot \mathbf{i}_I(t) - \mathbf{A}_C \cdot \mathbf{I}_C(t - \Delta t) \end{aligned} \quad (2.14)$$

Similarly, expanding and simplifying the second row of equation (2.10) gives:

$$\begin{aligned} \mathbf{i}_L(t) &= \mathbf{i}_L(t - \Delta t) - \frac{\Delta t}{2} \cdot (-\mathbf{L}^{-1} \cdot \mathbf{A}_L^T \quad \mathbf{0}) \\ &\quad \cdot \begin{pmatrix} \mathbf{e}(t - \Delta t) \\ \mathbf{i}_L(t - \Delta t) \end{pmatrix} + \begin{pmatrix} \mathbf{e}(t) \\ \mathbf{i}_L(t) \end{pmatrix} \end{aligned} \quad (2.15)$$

where the bold  $\mathbf{0}$  represents zero matrix.

This can also be represented as:

$$\mathbf{i}_L(t) = \mathbf{I}_L(t - \Delta t) + \frac{\Delta t}{2} \cdot \mathbf{L}^{-1} \cdot \mathbf{A}_L^T \cdot \mathbf{e}(t) \quad (2.16)$$

In direct numerical integration of DSEs, the descriptor variables include all node voltage and inductor currents. On the other hand, EMT simulation approaches using companion circuits and nodal analysis, only update node voltages. Hence to obtain the node voltage updates from DSEs, we need to eliminate inductor current term. This can be done by substituting equation (2.16) to the first row expansion (2.14) as below:

$$\begin{aligned}
& \left( \frac{2\mathbf{C}'}{\Delta t} + \mathbf{G}' + \mathbf{A}_L \cdot \frac{\Delta t}{2} \cdot \mathbf{L}^{-1} \cdot \mathbf{A}_L^T \right) \cdot \mathbf{e}(t) \\
& = -\mathbf{A}_I \cdot \mathbf{i}_I(t) - \mathbf{A}_L \cdot \mathbf{I}_L(t - \Delta t) - \mathbf{A}_C \cdot \mathbf{I}_C(t - \Delta t)
\end{aligned} \tag{2.17}$$

Which is in the form of:

$$\mathbf{Y} \cdot \mathbf{e}(t) = \mathbf{I}_{his}(t - \Delta t) + \mathbf{I}_s(t)$$

## 2.5 Update Equation in EMT Type Simulation

The EMT algorithm is a systematic approach to obtaining update values for node voltages based on the input current sources and past history of inductor and capacitor currents and voltages. All inductor and capacitor branches are first discretized into a companion circuit consisting of a conductance and a history current source as shown in Fig. 2-1 [1].

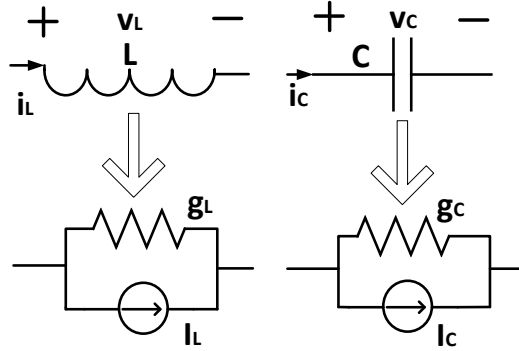


Figure 2-1 Companion circuit model for inductor and capacitor

For the  $j$ th inductor or  $k$ th capacitor

$$\begin{aligned}
i_c^{(k)}(t) &= g_c^{(k)} \cdot v_c^{(k)}(t) + I_c^{(k)}(t - \Delta t) \\
i_L^{(j)}(t) &= g_L^{(j)} \cdot v_L^{(j)}(t) + I_L^{(j)}(t - \Delta t)
\end{aligned} \tag{2.18}$$

The entire set of companion circuit branch equations (with  $n_c$  capacitors and  $n_L$  inductors) then become as in:

$$\begin{pmatrix} i_c^{(1)}(t) \\ \vdots \\ i_c^{(n_c)}(t) \end{pmatrix} = \begin{pmatrix} g_c^{(1)} & \dots & 0 \\ \vdots & \ddots & \vdots \\ 0 & \dots & g_c^{(n_c)} \end{pmatrix} \cdot \begin{pmatrix} v_c^{(1)}(t) \\ \vdots \\ v_c^{(n_c)}(t) \end{pmatrix} + \begin{pmatrix} I_c^{(1)}(t - \Delta t) \\ \vdots \\ I_c^{(n_c)}(t - \Delta t) \end{pmatrix}$$

And

$$\begin{pmatrix} i^{(1)}_L(t) \\ \vdots \\ i^{(n_L)}_L(t) \end{pmatrix} = \begin{pmatrix} g_L^{(1)} & \dots & 0 \\ \vdots & \ddots & \vdots \\ 0 & \dots & g_L^{(n_L)} \end{pmatrix} \cdot \begin{pmatrix} v^{(1)}_L(t) \\ \vdots \\ v^{(n_L)}_L(t) \end{pmatrix} + \begin{pmatrix} I^{(1)}_L(t - \Delta t) \\ \vdots \\ I^{(n_L)}_L(t - \Delta t) \end{pmatrix}$$

which can be written in matrix and vector form as below:

$$\begin{aligned} \mathbf{i}_c(t) &= \mathbf{g}_c \cdot \mathbf{v}_c(t) + \mathbf{I}_c(t - \Delta t) \\ \mathbf{i}_L(t) &= \mathbf{g}_L \cdot \mathbf{v}_L(t) + \mathbf{I}_L(t - \Delta t) \end{aligned} \quad (2.19)$$

Where  $\mathbf{g}_c$  and  $\mathbf{g}_L$  are diagonal matrixes containing all the equivalent inductor and capacitor admittance respectively,  $\mathbf{i}_c$ ,  $\mathbf{v}_c$ ,  $\mathbf{i}_L$ ,  $\mathbf{v}_L$  are column vectors which represent capacitor and inductor branch currents and voltages. Their elements are arranged corresponding to matrix  $\mathbf{g}_c$  and  $\mathbf{g}_L$ .  $\mathbf{I}_c, \mathbf{I}_L$  are history current source vectors:

$$\begin{aligned} \mathbf{I}_L(t - \Delta t) &= \mathbf{i}_L(t - \Delta t) + \mathbf{g}_L \cdot \mathbf{v}_L(t - \Delta t) \\ \mathbf{I}_c(t - \Delta t) &= -\mathbf{i}_c(t - \Delta t) - \mathbf{g}_c \cdot \mathbf{v}_c(t - \Delta t) \end{aligned} \quad (2.20)$$

Consequently, nodal analysis is applied by substituting equation (2.19) and (2.20) into (2.4) and (2.5):

$$\begin{aligned} & [\mathbf{A}_c \cdot \mathbf{g}_c \cdot \mathbf{A}_c^T + \mathbf{A}_L \cdot \mathbf{g}_L \cdot \mathbf{A}_L^T + \mathbf{A}_R \cdot \mathbf{G} \cdot \mathbf{A}_R^T] \cdot \mathbf{e}(t) \\ &= -\mathbf{A}_I \cdot \mathbf{i}_I(t) - \mathbf{A}_L \cdot \mathbf{I}_L(t - \Delta t) - \mathbf{A}_C \cdot \mathbf{I}_C(t - \Delta t) \end{aligned} \quad (2.21)$$

Simple algebraic manipulation gives:

$$\begin{aligned} & \left[ \frac{2\mathbf{C}'}{\Delta t} + \mathbf{A}_L \cdot \frac{\Delta t}{2} \cdot \mathbf{L}^{-1} \cdot \mathbf{A}_L^T + \mathbf{G}' \right] \cdot \mathbf{e}(t) \\ &= -\mathbf{A}_I \cdot \mathbf{i}_I(t) - \mathbf{A}_L \cdot \mathbf{I}_L(t - \Delta t) - \mathbf{A}_C \cdot \mathbf{I}_C(t - \Delta t) \end{aligned} \quad (2.22)$$

Equation (2.22) will be used in next section to show the equivalency with the DSE approach.

In EMT type simulation field, Equation (2.22) is usually known as new node voltage update equations form as below in EMT type simulations:

$$\mathbf{Y}_{emt} \cdot \mathbf{e}(t) = \mathbf{I}_{his}(t - \Delta t) + \mathbf{I}_s(t) \quad (2.23)$$

Where:

$$\begin{aligned} \mathbf{I}_{his}(t - \Delta t) &= -\mathbf{A}_L \cdot \mathbf{I}_L(t - \Delta t) - \mathbf{A}_C \cdot \mathbf{I}_C(t - \Delta t) \\ \mathbf{I}_s(t) &= -\mathbf{A}_I \cdot \mathbf{i}_I(t) \end{aligned}$$

## 2.6 Comparison of Update Equations from Descriptor State Equations and Companion Circuit Based Method

As described above, the update equation for node voltages derived from Descriptor State Space Equations as shown in equation (2.17) is exactly identical to the equation used for EMT type simulation as shown in (2.23), which completes the proof of equivalency.

In this section, a simple example is provided that shows the resulting update equations for Dommel's method and DSE are the same. Also simulations for two different time steps using the two approaches are shown and are identical.

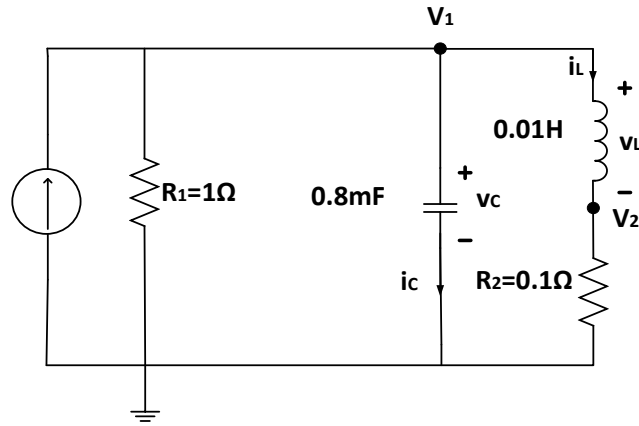


Figure 2-2 Example 1

The descriptor state space equations from MNA method can be formed as below:

From the circuit netlist, we have:

$$\begin{pmatrix} v_c \\ v_L \\ v_{R1} \\ v_{R2} \\ v_I \end{pmatrix} = \begin{pmatrix} A_c^T \\ A_L^T \\ A_{R1}^T \\ A_{R2}^T \\ A_I^T \end{pmatrix} \cdot e = \begin{pmatrix} 1 & 0 \\ 1 & -1 \\ 1 & 0 \\ 0 & 1 \\ -1 & 0 \end{pmatrix} \cdot \begin{pmatrix} V_1 \\ V_2 \end{pmatrix}, C = 0.0008, L = 0.01$$

Substituting equation (2.6) gives the descriptor state space equations:

$$\begin{aligned} & \begin{pmatrix} 0.0008 & 0 & 0 \\ 0 & 0 & 0 \\ 0 & 0 & 0.01 \end{pmatrix} \cdot \frac{d}{dt} \begin{pmatrix} V_1 \\ V_2 \\ i_L \end{pmatrix} \\ & = - \begin{pmatrix} 1 & 0 & 1 \\ 0 & 10 & -1 \\ -1 & 1 & 0 \end{pmatrix} \cdot \begin{pmatrix} V_1 \\ V_2 \\ i_L \end{pmatrix} - \begin{pmatrix} -1 \\ 0 \\ 0 \end{pmatrix} \cdot (i_s) \end{aligned} \quad (2.24)$$

Directly substituting the parameters to equation (2.17) gives the admittance matrix as below:

$$\begin{aligned} \mathbf{Y}_{emt} &= \frac{2\mathbf{C}'}{\Delta t} + \mathbf{G}' + \mathbf{A}_L \cdot \frac{\Delta t}{2} \cdot \mathbf{L}^{-1} \cdot \mathbf{A}_L^T \\ &= \begin{pmatrix} \frac{0.0016}{\Delta t} + 1 + 50 \cdot \Delta t & -50 \cdot \Delta t \\ -50 \cdot \Delta t & 10 + 50 \cdot \Delta t \end{pmatrix} \end{aligned} \quad (2.25)$$

With a history current source term:

$$\mathbf{I}_{his}(t - \Delta t) = \begin{pmatrix} -1 \\ 1 \end{pmatrix} \cdot I_L(t - \Delta t) + \begin{pmatrix} -1 \\ 0 \end{pmatrix} \cdot I_C(t - \Delta t) \quad (2.26)$$

The corresponding companion circuit formed from Dommel's method is shown below in Fig. 2-3:

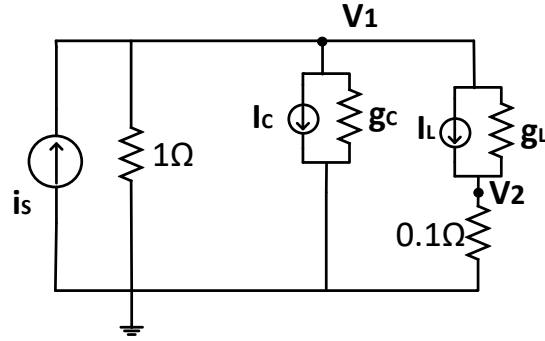


Figure 2-3 Companion Circuit for Example 1

In Fig. 2-3,  $g_C = \frac{0.0016}{\Delta t} s$  and  $g_L = 50 \cdot \Delta t s$  are the equivalent admittance term.

The history current source term  $I_C(t - \Delta t)$  and  $I_L(t - \Delta t)$  are:

$$I_C(t - \Delta t) = -\frac{0.0016}{\Delta t} \cdot v_C(t - \Delta t) - i_C(t - \Delta t)$$

$$I_L(t - \Delta t) = i_L(t - \Delta t) + 50 \cdot \Delta t \cdot v_L(t - \Delta t) \quad (2.27)$$

Assembling the nodal admittance matrix and history current vector from Fig.2-3 gives:

$$\mathbf{Y}_{emt} = \begin{pmatrix} \frac{0.0016}{\Delta t} + 1 + 50 \cdot \Delta t & -50 \cdot \Delta t \\ -50 \cdot \Delta t & 10 + 50 \cdot \Delta t \end{pmatrix} \quad (2.28)$$

And

$$\mathbf{I}_{his}(t - \Delta t) = \begin{pmatrix} -I_L(t - \Delta t) - I_C(t - \Delta t) \\ I_L(t - \Delta t) \end{pmatrix} \quad (2.29)$$

which is identical to equation (2.25) and (2.26), as it should be, because the DSE approach and Companion Circuit approach were proved to be identical in Section 2.4.

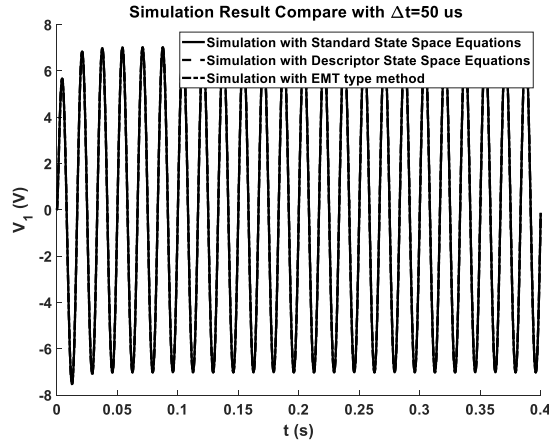


Figure 2-4 Node 1 voltage for  $\Delta t = 50 \mu s$

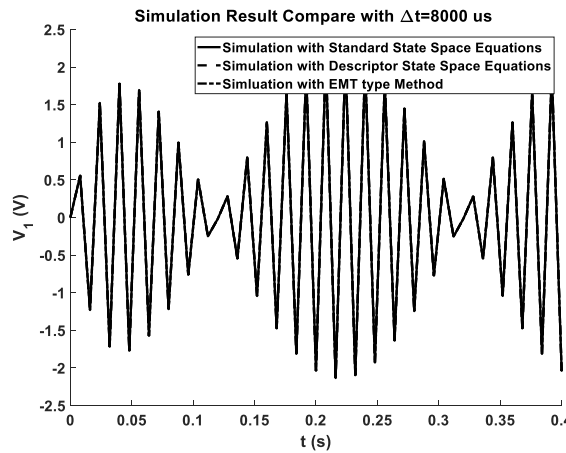


Figure 2-5 Node 1 voltage for  $\Delta t = 8000 \mu s$

Fig. 2-4. shows the voltage of node 1 for a time step of  $50 \mu s$ , using Dommel's method, as well as from integration of the DSEs and SVEs by Trapezoidal method. Similarly, Fig. 2-5. shows the same for a time step of  $8000 \mu s$ . In both cases the results are exactly overlapping, as they should be due to the exact equivalence. Note the  $8000 \mu s$  timestep is too large for accuracy and gives useless results, however, the point here was to show that regardless of the time step used, the two equivalent approaches yield the same results, accurate or otherwise!

## 2.6 Chapter Summary

In this chapter, transient simulation based on state variable approach is theoretically shown to be equivalent to Dommel's companion circuit/nodal analysis approach. Therefore, the stability conclusion drawn for the state space equations as shown in Chapters 3 and 4 could directly be applied for companion circuit method based simulations.

To show the equivalence, Dommel's method was first applied and the update equation consisting of the overall resultant admittance matrix and history terms was derived. Then Descriptor State Space Equations (DSEs) which can be directly obtained from the MNA method were introduced. By algebraic manipulation of the DSEs, the resulting update equations for node voltages were derived and have the form of an admittance matrix and history terms. The admittance matrix and history terms obtained from the DSEs are exactly the same, thereby proving the equivalence. Although DSEs rather than classical state variable equations (SVE), were used as the DSEs equations are easily obtainable for arbitrary circuits, the equivalence to SVEs immediately follows from earlier work [7-9] which has shown that DSEs can be transformed to SVEs.

A simple illustrative example was provided to demonstrate the equivalency. Simulations with different time steps were presented and show that the two methods yield identical simulation results.

### **3 Stability of Algorithms for Electro-Magnetic-Transient Simulation of Networks with Switches and Non-linear Inductors**

(This work was published in IEEE Transactions on Power Delivery [10])

This chapter extends the analysis of the stability of electromagnetic transient simulation algorithms to non-linear systems with switching elements and non-linear inductor branches. A theoretical analysis based on common quadratic Lyapunov function (CQLF) theory is used to investigate the stability of numerical algorithms for the simulation of lumped strictly passive *switched* circuits (LSPSC). It is proved that only when certain fundamental physical properties, i.e., passivity and invariance of Lyapunov energy function are satisfied, does the widely used Trapezoidal method result in stable simulations of such networks for any time step size. This research is the first time that the stability of the EMT simulation of circuits with switching elements has been proved [10].

It is valuable to point out that although the stability analysis in this section is based on state space equations, the conclusion is directly applied to the companion circuit based simulations, as those two models are theoretically proved to be equivalent in Chapter 2.

This chapter is organized as follows:

Lyapunov theory and the passivity property are briefly summarized in Section 3.1, after which Section 3.2 develops the theoretical approach to investigate the stability of numerical algorithms of switched circuits. Section 3.3 provides a counterexample to show that with the Trapezoidal rule the real-world stability of a switched system does not automatically guarantee the stability of the simulated system, which is contrary to the situation in a LTI system. Subsequently, a second example is used to show that the Backward Euler method can also result an unstable simulation of a real-world stable switched system. Section 3.4 shows that a non-linear inductor represented by a flux-current characteristic with an arbitrary number of piecewise linear segments can be considered as a special case of a circuit with switches. By applying the conclusions of Section 3.2, this proves that simulation of circuits with switches and such non-linear inductor models will be stable.

It should be noted that the focus of this paper is for BIBO stability of numerical algorithms in switched circuit simulation, and therefore excludes discussion of bounded numerical oscillation (sometimes referred to as chatter [22]). Also, although a simulation may be stable in the BIBO sense, it does not imply that the simulation is accurate.

### 3.1 Energy Function Based Stability Analysis

This section provides the background on Lyapunov function based stability analysis of actual switched circuits (not their simulations). These ideas are later expanded to simulated systems. First consider a switched network with lumped elements like capacitors, inductors, resistors etc.; where the switch is modeled as a bi-valued resistor (which can include ideal switches with zero/infinite resistor values). This approach is commonly used for the simulation of HVDC converters, FACTS controllers and so on. Each switch can be in the ON or OFF state, and is represented by a small resistance when ON and a large resistance when OFF. With  $s$  switches, there exist  $2^s$  different network configurations. Hence the system is described by  $2^s$  state space equations, each with state variable vector  $\mathbf{x}$ , input vector  $\mathbf{u}$  time-varying system matrix  $\mathbf{A}_i$  and input matrix  $\mathbf{B}_i$  as in (3.1):

$$\frac{d\mathbf{x}(t)}{dt} = \mathbf{A}_i \cdot \mathbf{x}(t) + \mathbf{B}_i \cdot \mathbf{u}(t); i \in \{1,2,3 \dots 2^s\} \quad (3.1)$$

The application of an integration method allows the conversion of the above continuous-time state space equation to a discrete state space equation:

$$\begin{aligned} \mathbf{x}((n+1) \cdot \Delta t) &= \mathbf{G}_i \cdot \mathbf{x}(n \cdot \Delta t) + \mathbf{H}_i \cdot \mathbf{u}(t); \\ i &\in \{1,2,3 \dots 2^s\} \end{aligned} \quad (3.2)$$

In (3.2),  $\mathbf{x}(n)$  represents value of the state variable in the  $n$ th simulation step. It should be noted that indices  $n$  and  $n+1$  identify the sample in the simulation, and these samples are not necessarily equally spaced in time. For example, the time distance between samples

may be the simulation time step  $\Delta t$  until a switching event. Following a switching interpolation as in Fig. 1-1, the next sample is at a time  $\delta t$  after the previous one.

### 3.1.1 Energy Function of Lumped Strictly Passive Switched Circuit (LSPSC) System

Note that as the switches are bi-valued resistors, capacitor voltages and inductor currents remain the state variables, regardless of the operation of the switches. Switching also does not alter the capacitance and inductance values. The energy stored in the LSPSC system at any time  $t$ , regardless of switching state is given as:

$$E(t) = \sum_{i=1}^{n_c} \frac{1}{2} \cdot C_i \cdot U_i(t)^2 + \sum_{j=1}^{n_L} \frac{1}{2} \cdot L_j \cdot I_j(t)^2 \quad (3.3)$$

The index  $i \in \{1, 2, \dots, n_c\}$  ranges over the set of inductances, and the index  $j \in \{1, 2, \dots, n_L\}$  ranges over the set of capacitors.  $U_i(t)$  and  $I_j(t)$  denote the voltage in capacitance  $C_i$  and current in inductance  $L_j$ . Note that the switching states do not figure in equation (3.3). As SVs  $U_i(t)$  and  $I_j(t)$  are state variables, i.e., continuous functions of time and hence  $E(t)$  is also continuous and does not change instantaneously when a switch operates.

Equation (3.3) is a quadratic energy function as in (3.4):

$$E = \mathbf{x}^T \cdot \mathbf{V} \cdot \mathbf{x} \quad (3.4)$$

Where  $\mathbf{x} = \begin{pmatrix} U_1 \\ \vdots \\ U_{n_c} \\ I_1 \\ \vdots \\ I_{n_L} \end{pmatrix}$  and  $\mathbf{V} = \begin{pmatrix} \frac{C_1}{2} & \dots & 0 & 0 & \dots & 0 \\ \vdots & \ddots & \vdots & \vdots & \ddots & \vdots \\ 0 & \dots & \frac{C_{n_c}}{2} & 0 & \dots & 0 \\ \vdots & \vdots & \vdots & \frac{L_1}{2} & \dots & \vdots \\ 0 & \dots & 0 & \vdots & \ddots & \vdots \\ 0 & \dots & 0 & 0 & \dots & \frac{L_{n_L}}{2} \end{pmatrix}$

Note that from (3.3),  $\forall \mathbf{x} \neq \mathbf{0}$ ,  $E > 0$ . From (3.4) and the definition of positive definiteness,  $\mathbf{V}$  is positive definite.

### 3.1.2 System Properties When Each State Is Strictly Passive

This section sets up the mathematical relationships that follow if every switching state is strictly passive. These are required in subsequent sections to investigate global stability for systems with operating switches. A network is passive, if over an arbitrary time period  $[t_0, t]$ , the energy injected into it is always greater than the energy stored in it [33, 34]. Mathematically,  $\forall t > t_0$ :

$$\int_{t_0}^t \mathbf{u}(s)^T \cdot \mathbf{y}(s) \cdot ds \geq E(t) - E(t_0) \quad (3.5)$$

Where  $\mathbf{u}(s)$  and  $\mathbf{y}(s)$  are input and output vectors.  $E(t)$  and  $E(t_0)$  denote the corresponding “energy” stored in the network at time  $t$  and time  $t_0$ , (with  $t > t_0$ ) in its energy storage components.

Setting  $t = t_0 + \Delta t$  in (3.5), dividing both sides by  $\Delta t$ , and taking the limit  $\Delta t \rightarrow 0$  gives the equivalent condition:

$$\mathbf{u}(t)^T \cdot \mathbf{y}(t) \geq \dot{E}(\mathbf{x}(t)) \quad (3.6)$$

Strict passivity requires a more stringent condition [16, 17]:

$$\mathbf{u}(t)^T \cdot \mathbf{y}(t) \geq \dot{E}(\mathbf{x}(t)) + \varphi(\mathbf{x}(t)) \quad (3.7)$$

Here  $\varphi(\mathbf{x}(t))$  is a positive definite function. Thus most RLC circuits are strictly passive, except for zero resistance circuits, e.g., an ideal voltage source directly connected across an inductor with zero resistance. The latter is passive, but not strictly passive as it satisfies (3.6) with an equality sign, but not (3.7).

If,  $\mathbf{u}(t) = 0$  (autonomous case), then  $\mathbf{u}(t)^T \cdot \mathbf{y}(t) = 0$ . Hence (3.7) implies (3.8):

$$\forall \mathbf{x}(t) \neq \mathbf{0}, \dot{E}(\mathbf{x}(t)) < 0 \quad (3.8)$$

Differentiating (3.4) and noting that for the autonomous system  $\dot{\mathbf{x}}(t) = \mathbf{A}_i \cdot \mathbf{x}(t)$ , yields (3.9):

$$\mathbf{x}^T(t) \cdot (\mathbf{A}_i^T \cdot \mathbf{V} + \mathbf{V} \cdot \mathbf{A}_i) \cdot \mathbf{x}(t) < 0; \quad i \in \{1, 2 \dots 2^s\} \quad (3.9)$$

As  $\mathbf{x}(t)$  is arbitrary, it is clear from equation (3.9) that  $\mathbf{A}_i^T \cdot \mathbf{V} + \mathbf{V} \cdot \mathbf{A}_i$  is a negative definite matrix. Hence the energy function  $E = \mathbf{x}^T \cdot \mathbf{V} \cdot \mathbf{x}$  satisfies both conditions for a

Lyapunov function, i.e., it is positive definite and its derivative is negative definite. This fact is used in the following section to prove asymptotic stability of the Autonomous Switched Network with strictly passive individual switching states.

### 3.1.3 Proof of Stability of the Real-World (physical) LSPSC

For a switched system as in equation (3.1), if there exists a positive definite matrix  $\mathbf{P}$  such that:

$$\forall i \in \{1,2,3 \dots 2^s\}, \mathbf{A}_i^T \cdot \mathbf{P} + \mathbf{P} \cdot \mathbf{A}_i < 0 \quad (3.10)$$

Then the scalar function  $\mathbf{x}^T \cdot \mathbf{P} \cdot \mathbf{x}$  is called a “common quadratic Lyapunov function” (CQLF). In (3.10) the symbol “<” indicates negative definiteness. In reference [12], the existence of common quadratic Lyapunov function (CQLF) is shown to be a sufficient condition for stability of a switched system.

Notice that (3.9) is of the form (3.10) with  $\mathbf{P} = \mathbf{V}$ ; thereby making (3.4) a CQLF. This proves that the autonomous real-world LSPSC system is asymptotically stable under arbitrary switching. The non-autonomous system is also stable, because from [13], the stability of the autonomous switched linear system also implies BIBO stability of the non-autonomous system. This conclusion can be applied to both continuous and discrete systems.

Now that it is established that the real-world LSPSC is stable, what can be said about the stability of its simulation with different integration methods? This is investigated in the next section.

## 3.2 Stability of Numerical Algorithms in LSPSC System Simulations

In this section, the stability of numerical simulation algorithms for LSPSC circuits are investigated using discrete-time Lyapunov energy function theory. Only the stability of the autonomous case is discussed, as Lyapunov stability of the autonomous system automatically implies BIBO stability of the non-autonomous system [13].

### 3.2.1 Global Stability of Numerical Algorithms in a Switched System (Discrete Time Lyapunov Theory)

Application of the numerical integration method converts the continuous time system in (3.1) into a discrete-time system as in (3.2). Reference [12] has shown that just like in continuous time systems, the existence of a CQLF is a *sufficient* condition for stability of a discrete-time switched system.

In the discrete-time form, the existence of a CQLF is equivalent to the existence of a positive definite matrix  $P$  [12], such that:

$$\forall i, \mathbf{G}_i^T \cdot \mathbf{P} \cdot \mathbf{G}_i - \mathbf{P} < \mathbf{0} \quad (3.11)$$

Here  $i \in I$ ; where  $I \in \{1,2,3 \dots 2^s\}$  is the index set which denotes the collection of all switching states.

In this paper, we show that  $v$  as in equation (3.4) can be selected as a candidate for  $P$ . We now check if  $v$  satisfies (3.11). If it does, the simulated system is stable under arbitrary switching.

Replacing  $P$  with  $v$  in equation (3.11) gives:

$$\mathbf{G}_i^T \cdot \mathbf{V} \cdot \mathbf{G}_i - \mathbf{V} < \mathbf{0} \quad (3.12)$$

which, by definition of negative definiteness implies that

$\forall \mathbf{x}(n \cdot \Delta t) \neq \mathbf{0}$ :

$$\mathbf{x}^T(n \cdot \Delta t) \cdot (\mathbf{G}_i^T \cdot \mathbf{V} \cdot \mathbf{G}_i - \mathbf{V}) \cdot \mathbf{x}(n \cdot \Delta t) < 0 \quad (3.13)$$

From equation (3.4) and the fact that  $\mathbf{x}((n+1) \cdot \Delta t) = \mathbf{G}_i \cdot \mathbf{x}(n \cdot \Delta t)$ , equation (3.13) can be shown to represent the “energy change” between time steps as proved in (3.14):

$$\begin{aligned} & \mathbf{x}^T(n \cdot \Delta t) \cdot (\mathbf{G}_i^T \cdot \mathbf{V} \cdot \mathbf{G}_i - \mathbf{V}) \cdot \mathbf{x}(n \cdot \Delta t) \\ &= \mathbf{x}^T((n+1) \cdot \Delta t) \cdot \mathbf{V} \cdot \mathbf{x}((n+1) \cdot \Delta t) - \mathbf{x}^T(n \cdot \Delta t) \cdot \mathbf{V} \cdot \mathbf{x}(n \cdot \Delta t) \\ &= E((n+1) \cdot \Delta t) - E(n \cdot \Delta t) \\ &\equiv \Delta E \end{aligned} \quad (3.14)$$

In equation (3.14)  $\Delta E$  is the energy variation during the time step. Hence (3.13) and (3.14) imply that if  $\Delta E$  is always negative, (3.12) is satisfied, and the system is asymptotically stable.

### 3.2.2 Energy Variation in Each Switching State with Different Numerical Integration Algorithms

The stability of different integration algorithms is now determined by substituting the corresponding matrix  $\mathbf{G}_i$  in (3.13) as shown next. The Trapezoidal integration algorithm is most commonly used in EMT simulations. It is A-stable for LTI systems. For comparison we include analysis of the Forward Euler (FE) and Backward Euler (BE) algorithms as well. The BE algorithm is L-stable for LTI systems, and is also sometimes used in EMT simulation [23].

#### 3.2.2.1 Stability of Algorithm for Forward Euler Integration

With the Forward Euler method,  $\mathbf{G}_i$  in (3.13) is given by:

$$\mathbf{G}_i = (\mathbf{I} + \mathbf{A}_i \cdot \Delta t) \equiv \mathbf{G}_{FEi} \quad (3.15)$$

Then (3.13) becomes:

$$\begin{aligned} \Delta E_F &= \mathbf{x}^T(n \cdot \Delta t) ((\mathbf{I} + \mathbf{A}_i^T \cdot \Delta t) \cdot \mathbf{V} \cdot (\mathbf{I} + \mathbf{A}_i \cdot \Delta t) - \mathbf{V}) \cdot \mathbf{x}(n \cdot \Delta t) \\ &= \mathbf{x}^T(n \cdot \Delta t) \cdot [(\mathbf{V} \cdot \mathbf{A}_i + \mathbf{A}_i^T \cdot \mathbf{V}) \cdot \Delta t + \mathbf{A}_i^T \cdot \mathbf{V} \cdot \mathbf{A}_i \cdot \Delta t^2] \cdot \mathbf{x}(n \cdot \Delta t) \end{aligned} \quad (3.16)$$

From (3.9), the matrix term  $(\mathbf{V} \cdot \mathbf{A}_i + \mathbf{A}_i^T \cdot \mathbf{V})$  is negative definite. Since the energy function matrix  $\mathbf{V}$  is positive definite and matrix  $\mathbf{A}_i$  is non-singular,  $\mathbf{A}_i^T \cdot \mathbf{V} \cdot \mathbf{A}_i$  is positive definite [35]. Thus (3.16) is the sum of a negative definite matrix  $(\mathbf{V} \cdot \mathbf{A}_i + \mathbf{A}_i^T \cdot \mathbf{V}) \cdot \Delta t$  and a positive definite matrix  $\mathbf{A}_i^T \cdot \mathbf{V} \cdot \mathbf{A}_i \cdot \Delta t^2$ . Hence,  $\Delta E_F$  can be positive or negative depending on which of these two terms dominates. Thus nothing can be determined about the stability from this particular energy function, i.e., the simulation may or may not be stable. However, this analysis still yields a lower bound on the critical time step. As  $\Delta t^2$  vanishes faster than  $\Delta t$ , it is always possible to find a sufficiently small  $\Delta t$ , say  $\Delta t_1$ , so

that the negative definite term is dominant. The simulation will be stable for any  $\Delta t$  smaller than  $\Delta t_1$ .

### 3.2.2.2 Stability of Algorithm for Backward Euler Integration

For the Backward Euler method (which is also A-stable in the LTI case),  $\mathbf{G}_i$  in (3.13) is given by:

$$\mathbf{G}_i = (\mathbf{I} - \mathbf{A}_i \cdot \Delta t)^{-1} \equiv \mathbf{G}_{BE_i} \quad (3.17)$$

And (3.13) becomes:

$$\begin{aligned} \Delta E_B &= \mathbf{x}^T(n \cdot \Delta t) \left( (\mathbf{I} - \mathbf{A}_i^T \cdot \Delta t)^{-1} \cdot \mathbf{V} \cdot (\mathbf{I} - \mathbf{A}_i \cdot \Delta t)^{-1} - \mathbf{V} \right) \cdot \mathbf{x}(n \cdot \Delta t) \\ &= \mathbf{x}^T(n \cdot \Delta t) \left( (\mathbf{I} - \mathbf{A}_i^T \cdot \Delta t)^{-1} \cdot [\mathbf{V} - (\mathbf{I} - \mathbf{A}_i^T \cdot \Delta t) \cdot \mathbf{V} \cdot (\mathbf{I} - \mathbf{A}_i \cdot \Delta t)] \cdot (\mathbf{I} - \mathbf{A}_i \cdot \Delta t)^{-1} \right) \cdot \mathbf{x}(n \cdot \Delta t) \\ &= \mathbf{x}^T(n \cdot \Delta t) \cdot (\mathbf{I} - \mathbf{A}_i^T)^{-1} \cdot [(\mathbf{V} \cdot \mathbf{A}_i + \mathbf{A}_i^T \cdot \mathbf{V}) \cdot \Delta t - \mathbf{A}_i^T \cdot \mathbf{V} \cdot \mathbf{A}_i \cdot \Delta t^2] \\ &\quad \cdot (\mathbf{I} - \mathbf{A}_i)^{-1} \cdot \mathbf{x}(n \cdot \Delta t) \end{aligned} \quad (3.18)$$

Since  $(\mathbf{V} \cdot \mathbf{A}_i + \mathbf{A}_i^T \cdot \mathbf{V}) \cdot \Delta t$  and  $-\mathbf{A}_i^T \cdot \mathbf{V} \cdot \mathbf{A}_i \cdot \Delta t^2$  are both negative definite, their sum is also negative definite. As a result, energy change  $\Delta E_B$  is always negative:

$$\forall \mathbf{x}(n \cdot \Delta t) \neq 0; \Delta E_B < 0 \quad (3.19)$$

Therefore, *the Backward Euler method always results in a stable simulation of a stable LSPSC system*, just like it does for the LTI circuit.

### 3.2.2.3 Stability of Algorithm for Trapezoidal Integration

For the Trapezoidal integration rule:

$$\mathbf{G}_i = \left( \mathbf{I} - \frac{\mathbf{A}_i \cdot \Delta t}{2} \right)^{-1} \cdot \left( \mathbf{I} + \frac{\mathbf{A}_i \cdot \Delta t}{2} \right) \cdot \mathbf{x}(n \cdot \Delta t) \equiv \mathbf{G}_{TR_i} \quad (3.20)$$

Thus (3.13) becomes:

$$\begin{aligned} \Delta E_{Tr} = \mathbf{x}^T(n \cdot \Delta t) & \left( \mathbf{I} + \frac{\mathbf{A}_i^T}{2} \cdot \Delta t \right) \cdot \left( \mathbf{I} - \frac{\mathbf{A}_i^T}{2} \cdot \Delta t \right)^{-1} \cdot \mathbf{V} \cdot \left( \mathbf{I} - \frac{\mathbf{A}_i}{2} \cdot \Delta t \right)^{-1} \\ & \cdot \left( \mathbf{I} + \frac{\mathbf{A}_i}{2} \cdot \Delta t \right) - \mathbf{V} \cdot \mathbf{x}(n \cdot \Delta t) \end{aligned} \quad (3.21)$$

As the commutation relation below (3.22) always holds (this is straightforward to show if the matrices are diagonalizable, but also holds if they are not (see Appendix A):

$$\left( \mathbf{I} + \frac{\mathbf{A}_i}{2} \right) \cdot \left( \mathbf{I} - \frac{\mathbf{A}_i}{2} \right)^{-1} = \left( \mathbf{I} - \frac{\mathbf{A}_i}{2} \right)^{-1} \cdot \left( \mathbf{I} + \frac{\mathbf{A}_i}{2} \right) \quad (3.22)$$

With some algebraic manipulation, equation (3.21) becomes:

$$\Delta E_{Tr} = \mathbf{x}^T(n \cdot \Delta t) \cdot \left( \mathbf{I} - \frac{\mathbf{A}_i}{2} \cdot \Delta t \right)^{-1} \cdot (\mathbf{A}_i^T \cdot \Delta t \cdot \mathbf{V} + \mathbf{V} \cdot \mathbf{A}_i \cdot \Delta t) \cdot \left( \mathbf{I} - \frac{\mathbf{A}_i}{2} \cdot \Delta t \right)^{-1} \cdot \mathbf{x}(n \cdot \Delta t) \quad (3.23)$$

Since  $(\mathbf{V} \cdot \mathbf{A}_i + \mathbf{A}_i^T \cdot \mathbf{V}) \cdot \Delta t$  is negative definite, post- multiplying it by *any arbitrary* nonsingular matrix  $\mathbf{W}$  and pre-multiplying it by  $\mathbf{W}^T$  still yields a negative definite matrix [35]. Thus,  $\left( \mathbf{I} - \frac{\mathbf{A}_i}{2} \cdot \Delta t \right)^{-1} \cdot (\mathbf{A}_i^T \cdot \Delta t \cdot \mathbf{V} + \mathbf{V} \cdot \mathbf{A}_i \cdot \Delta t) \cdot \left( \mathbf{I} - \frac{\mathbf{A}_i}{2} \cdot \Delta t \right)^{-1}$  is also negative definite, i.e.:

$$\forall \mathbf{x}(n \cdot \Delta t) \neq 0; \Delta E_{Tr} < 0 \quad (3.24)$$

Therefore, the *Trapezoidal method also always results in a stable simulation* for a stable LSPSC, just like it does for the LTI circuit. Note that this is true for *any arbitrary switching regime*, i.e., it **does not depend on the controller** that operates the switches, or on any measurement or interface delays.

The reader is cautioned that the above theorem only applies to lumped strictly passive switched networks and does not conclude anything about the stability of the simulation of non-passive switched networks. Non-passive switched network simulations with Trapezoidal or Backward Euler integration methods can be stable or unstable. This is easily shown by example, as in the following section.

### 3.2.3 The Stability of the Non-autonomous Case

Note that the proof was provided for systems without excitation, i.e., autonomous systems. However as proved in [13], Lyapunov stability for the autonomous system also implies

BIBO stability of the non-autonomous system. Hence, BE and Trapezoidal rule guarantee the stability of all LSPSC systems, autonomous as well as non-autonomous.

### 3.3 General Stability of Numerical Algorithms in Switched System Simulation

For linear time-invariant (LTI) systems, A-stable integration algorithms such as the Trapezoidal rule or BE *always* guarantee a stable *simulation* when the original system is stable [11, 22, 23]. There is no additional requirement, such as that the system be non-passive.

However, as proved in Section 3.2, the numerical stability of Trapezoidal and BE methods is only guaranteed if the following additional conditions are met:

1. Passivity of each switching state.
2. All switches are modelled as bi-valued resistors, which leads to a constant Lyapunov energy function when the switch operates.

Section 3.2 showed that Passivity and invariance of a Lyapunov energy function are *sufficient* conditions to prove the stability of LSPSC systems simulated using BE or Trapezoidal rule. However, consider the simulation of a *non-passive* switched networks. The proof of Section 3.2 *does not prove* that such systems will always be stable. Hence in this section, we show by counterexample that there is at least one non-passive system which is real world stable, but its simulation with Trapezoidal Rule or BE is *unstable*.

It is well known that Trapezoidal and Backward Euler integration methods result in stable simulations of stable LTI continuous-time systems, i.e., the left hand complex plane maps into the interior of the unit-circle. However, this is not true for switched circuits as can be proved with the following counterexample:

#### 3.3.1 Example 1 (simulation with Trapezoidal method)

Consider the second order circuit in Fig. 3-1. Switches  $S_1$  and  $S_2$  have resistance values of 1 M $\Omega$  for the off-state and 1 m $\Omega$  for the on state. The total arm resistance  $R_{e1}$  (inside

dotted box) will take on values of  $0.5 \Omega$  and  $-1.199 \Omega$  depending on switch  $S_1$  being off or on. Likewise arm resistance  $R_{e2}$  is  $0.5 \Omega$  or  $-0.499 \Omega$  depending on the state of  $S_2$ . As shown below, each switching state is by itself stable. However, the circuit is non-passive due to the negative resistances.

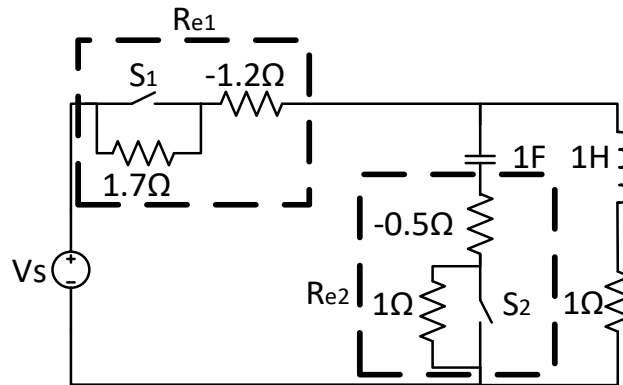


Figure 3-1 Second order circuit for Example 1

### 3.3.1.1 Numerical Stability of Permanent Switching States

If the circuit in Fig. 3-1 permanently resides in any one of the 4 switching states i.e.,  $(S_1, S_2) = (ON, ON)$ , etc.. It is straightforward to show that the circuit itself is stable. Let states 1, 2, 3 and 4 denote the four combinations for  $(ON, ON)$ ,  $(ON, OFF)$ ,  $(OFF, ON)$  and  $(OFF, OFF)$  as in Table 3-1. The corresponding eigenvalues for each state in Table 3-1 have negative real parts, indicating that if it remains permanently in any of the four switching states, it is stable.

Table 3-1 Eigenvalues for Each Switching State in Example 1

$S_2 \backslash S_1$	<i>ON</i>	<i>OFF</i>
<i>ON</i>	<p><i>State 1</i></p> $\lambda_1 = -0.0294 + 0.3411i$ $\lambda_2 = -0.0294 - 0.3411i$	<p><i>State 2</i></p> $\lambda_1 = -0.2135 + 0.4890i$ $\lambda_2 = -0.2135 - 0.4890i$
<i>OFF</i>	<p><i>State 3</i></p> $\lambda_1 = -750.4662$	<p><i>State 4</i></p> $\lambda_1 = -1.1250 + 0.4841i$

	$\lambda_2 = -2.0013$	$\lambda_2 = -1.1250 - 0.4841i$
--	-----------------------	---------------------------------

### 3.3.1.2 Stability with Periodic State Transitions

Reference [13], mathematically proves that the exponential stability of the *autonomous* switched linear system (i.e., that in equation (3.1) and (3.2) with  $\mathbf{u}(t) = 0$ ); is a necessary and sufficient condition for the BIBO stability of the *non-autonomous* system, i.e., with  $\mathbf{u}(t) \neq 0$ . Therefore, the stability of the simulated system can be determined by investigating the stability of the autonomous system. This is similar to the case in LTI systems, where the stability of  $\dot{\mathbf{x}}(t) = \mathbf{A} \cdot \mathbf{x}(t) + \mathbf{B} \cdot \mathbf{u}(t)$  can be analyzed only by considering eigenvalues of the system matrix  $\mathbf{A}$ , regardless of the feedforward term  $\mathbf{B}$ .

Now consider the case when the system is switched periodically with a 0.4 s period. For the first half period, i.e., [0.0 s, 0.2 s], switch  $S_1$  is ON and  $S_2$  is OFF. For the second half period,  $S_1$  is OFF and  $S_2$  is ON. Let  $\mathbf{x}(0) \neq 0$  be the initial condition for state variable vector  $\mathbf{x}$ . The corresponding theoretical solution for the state at the end of 0.4 is given by (3.25):

$$\mathbf{x}(0.4) = e^{A_3 \cdot 0.2} \cdot e^{A_2 \cdot 0.2} \cdot \mathbf{x}(0) \equiv \mathbf{G}_{TH} \cdot \mathbf{x}(0) \quad (3.25)$$

where the subscript *TH* denotes “theoretical”. Thus, the system matrix  $\mathbf{G}_{TH}$  for one period ([0 s, 0.4 s]) is:

$$\begin{aligned} \mathbf{G}_{TH} &= e^{A_3 \cdot 0.2} \cdot e^{A_2 \cdot 0.2} \\ &= \begin{pmatrix} -0.4319 & -0.2127 \\ 0.8621 & 0.4246 \end{pmatrix} \end{aligned}$$

Both eigenvalues of  $\mathbf{G}_{TH}$  are inside the unit circle:

$$\begin{aligned} \lambda_1 &= 7.1 \cdot 10^{-15} \\ \lambda_2 &= -0.0073 \end{aligned} \quad (3.26)$$

Now assume that this cycle is repeated with the 0.4 s period. The corresponding values for time  $0.4 \cdot k$  s is given by

$$\mathbf{x}(0.4 \cdot k) = \mathbf{G}_{TH} \cdot \mathbf{x}(0.4 \cdot (k - 1)) = \dots = \mathbf{G}_{TH}^k \cdot \mathbf{x}(0) \quad (3.27)$$

where  $k \in N^+$ .

As eigenvalues of  $\mathbf{G}_{TH}$  are in the unit circle,  $\lim_{k \rightarrow +\infty} \mathbf{G}_{TH}^k = \mathbf{0}$ , and hence the asymptotic trajectories of all state variables of the autonomous system converge to zero; indicating that the system is stable under the periodic 0.4 s switching regime.

The above analysis confirms that the real-world switched system is stable under the proposed switching regime. But is the *simulated* system stable? Consider the above system simulated with a Trapezoidal rule based integration method with time step  $\Delta t = 0.04$  s:

With a simulation time step  $\Delta t$ , and application of Trapezoidal integration, the corresponding system matrix  $\mathbf{G}_{tr_i}$  (where  $x((n+1) \cdot \Delta t) = \mathbf{G}_{tr_i} \cdot x(n \cdot \Delta t)$ ) is as in (3.28):

$$\mathbf{G}_{tr_i} = \left( I - \frac{\mathbf{A}_i \cdot \Delta t}{2} \right)^{-1} \cdot \left( I + \frac{\mathbf{A}_i \cdot \Delta t}{2} \right) \quad (3.28)$$

The numerical solution at time 0.4 s is the  $n^{\text{th}}$  step in the integration (where  $n = 0.4/\Delta t = 10$ ) is as shown below:

The corresponding state space equation is as below:

$$\begin{aligned} \mathbf{x}(0.4) &= \mathbf{x}(\Delta t \cdot 10) \\ &= \mathbf{G}_{tr_3} \cdot \mathbf{G}_{tr_3} \cdot \mathbf{G}_{tr_3} \cdot \mathbf{G}_{tr_3} \cdot \mathbf{G}_{tr_3} \cdot \mathbf{G}_{tr_2} \cdot \mathbf{G}_{tr_2} \cdot \mathbf{G}_{tr_2} \cdot \mathbf{G}_{tr_2} \cdot \mathbf{G}_{tr_2} \cdot \mathbf{x}(0) \\ &\equiv \mathbf{G}_{TR} \cdot \mathbf{x}(0) \end{aligned} \quad (3.29)$$

**TR** in the subscript indicates ‘‘Trapezoidal’’. Evaluation gives:

$$\mathbf{G}_{TR} = \begin{pmatrix} -1.4133 & -1.3536 \\ 0.2072 & 0.4218 \end{pmatrix} \quad (3.30)$$

However, one eigenvalues of  $\mathbf{G}_{TR}$  is larger than unity as shown below:

$$\begin{aligned} \lambda_1 &= -1.2450 \\ \lambda_2 &= 0.2535 \end{aligned} \quad (3.31)$$

Hence, as  $k \rightarrow +\infty$ , the system will not be bounded (as  $\mathbf{G}_{TR}^k$  is not be bounded). This counterexample confirms that in the case of a non-passive switched circuits, the simulation with Trapezoidal rule can be unstable even when the original switched system is stable.

It is valuable to note that if the circuit permanently stayed in any one switching state, the simulation result would be stable. This is to be expected as we are simulating a stable real world linear system without the non-linearity of switching. This is obvious from Table II

which shows the corresponding eigenvalues for each of the individual state matrices  $G_i$  in (3.2) for a time step of 0.04s. All eigenvalue magnitudes are less than unity.

Table 3-2 Eigenvalues for Each Switching State When Trapezoidal Method is Applied

$S2 \backslash S1$	<i>ON</i>	<i>OFF</i>
<i>ON</i>	<p><i>State 1</i></p> $\lambda_1 = 0.9558+0.0185i$ $\lambda_2 = 0.9558-0.0185i$	<p><i>State 2</i></p> $\lambda_1 = 0.9913+0.0194i$ $\lambda_2 = 0.9913 -0.0194i$
<i>OFF</i>	<p><i>State 3</i></p> $\lambda_1 = -0.8751$ $\lambda_2 = 0.9230$	<p><i>State 4</i></p> $\lambda_1 = 0.9987+0.0136i$ $\lambda_2 = 0.9987 -0.0136i$

This is confirmed by the simulation in Fig 3-2 carried out on the PSCAD/EMTDC program. The initial capacitor voltage is given as 1 kV while the inductance current is 0. For a  $\Delta t = 0.04$  s the simulation is unstable; whereas for  $\Delta t = 400 \mu s$ , it is stable.

This single counter-example proves that unlike for the LTI case, the Trapezoidal method (which is an A-stable method for LTI circuits) cannot always guarantee a stable simulation of a stable circuit with switches. Using the same procedure, it can be readily shown, that the Backward Euler method may also result in an unstable simulation result for a stable real-world switched circuit.

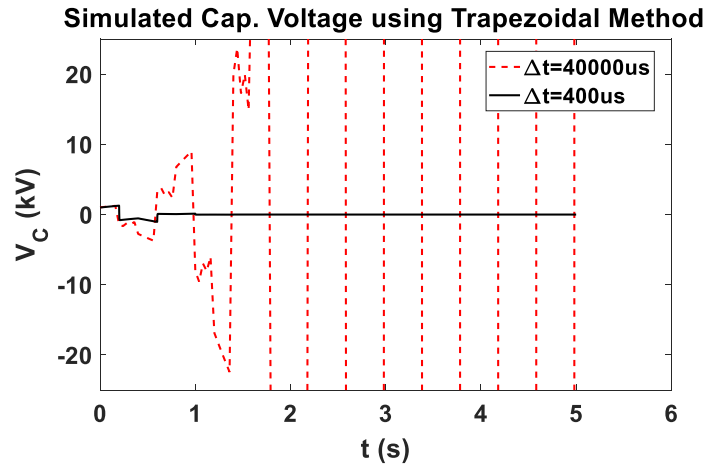


Figure 3-2 Validation using Simulation

### 3.3.2 Example 2 (Simulation with Backward Euler Method)

A slight modification to the parameters of the circuit of Example 1 gives the circuit of Fig. 3-3.

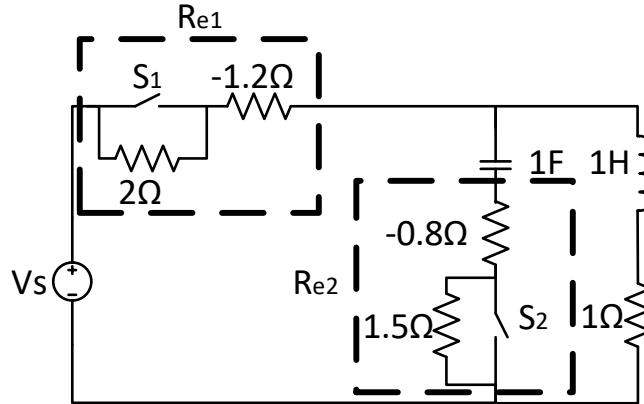


Figure 3-3 Second order circuit for Example 2

This circuit also has negative real part eigenvalues as shown in Table 3-3 below for every switching state and would thus be stable in every switching state. It should be noted that the real resistor of the switch should be used (i.e. 1 MΩ for the off-state and 1 mΩ for the on state) to form the matrix A to avoid the matrix to be singular or ill conditioning. The worst condition number of all switching state is  $1.49 \cdot 10^3$  (which is rounded to 3 digits) in switching state 3. Compared with the precision used in modern numerical solver (16 digits accuracy for MATLAB and 15 digits (double precision) for EMTDC/PSCAD), the accuracy lose is still negligible.

Table 3-3 Eigenvalues for Each Switching State in Example 2

$S2 \backslash S1$	<i>ON</i>	<i>OFF</i>
	<i>State 1</i>	<i>State 2</i>
<i>ON</i>	$\lambda_1 = -0.0101 + 0.3154i$ $\lambda_2 = -0.0101 - 0.3154i$	$\lambda_1 = -0.3390 + 0.5328i$ $\lambda_2 = -0.3390 - 0.5328i$
	<i>State 3</i>	<i>State 4</i>
<i>OFF</i>	$\lambda_1 = -357.1395$ $\lambda_2 = -5.0454$	$\lambda_1 = -1.0200 + 0.3995i$ $\lambda_2 = -1.0200 - 0.3995i$

Using the procedure discussed under Example 1, it can be shown that the real-world switched system is also stable when switched between the states  $(S1,S2) = (OFF,ON)$  and  $(ON, OFF)$  with a period of 1.6 s (i.e., it dwells in each state for 0.8 s). When simulated with a time step of 80  $\mu$ s using BE, the simulated system's discrete state matrix  $\mathbf{G}_{BE}$  become  $\lambda_1 = -0.2162$  and  $\lambda_2 = 0$ . As they are both less than 1 in magnitude, the system is stable. However, if the time step is increased to 0.4 s, then  $\lambda_1 = -1.1451$  and  $\lambda_2 = -2.5992 \cdot 10^{-6}$ . Now as  $|\lambda_1| > 1$ , the simulated system is unstable for this time step. Fig. 3-4. shows the theoretical solution for the real-world autonomous switched system and the Backward Euler method simulation for time steps of 80  $\mu$ s and 0.4 s respectively with an initial condition below:

$$\begin{pmatrix} v_C \\ i_L \end{pmatrix} = \begin{pmatrix} 2 \text{ V} \\ 2 \text{ A} \end{pmatrix}$$

As can be seen, the 80  $\mu$ s simulation is stable and essentially equals the analytical solution, but the 0.4 s is unstable as predicted.

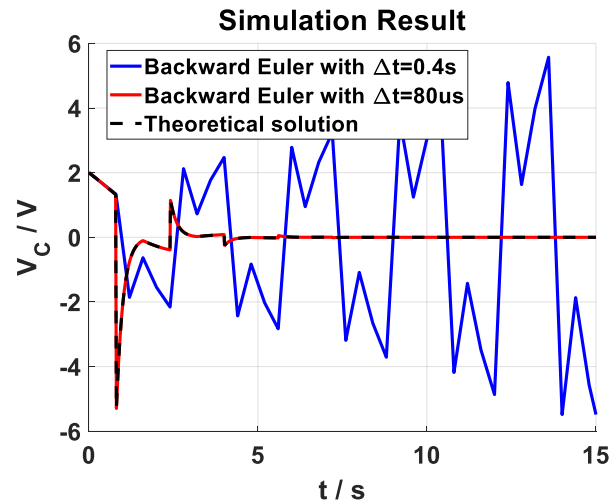


Figure 3-4. Simulation Validation

### 3.3.3 Discussion

Section 3.2 showed that a lumped strictly passive switched circuit will always have a stable simulation if the Trapezoidal or Backward Euler method is applied. However, it made no conclusion about the stability of a physical system which is stable, but where some individual states are not passive. The above counterexample 1 shows that for such

non-passive systems, it is possible for the simulation with the Trapezoidal method to be unstable, even when the original system is stable.

In power electronic circuit simulation, numerical oscillation is another important fact which mainly results from the stiffness property of certain switching state. Lots techniques are developed to suppress such phenomenon [11, 22, 23, 25, 36]. However, as shown in example 2, even with Backward Euler method is used (which is an L-stable algorithm), the instability still happen while the original system is stable.

### 3.4 Stability of Simulations of Non-linear Resistors and Inductors

#### 3.4.1 Stability of Simulation of Non-linear Resistors

Consider a resistor with non-linear voltage current characteristics such as in Fig. 3-5. The characteristic can be approximated by a number (arbitrarily large as needed for sufficient accuracy) of linear segments e.g.  $R, R_1, R_2 \dots$  etc.

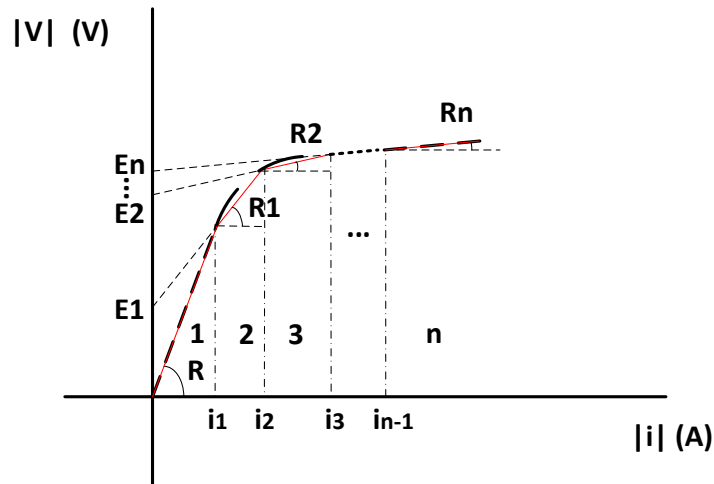


Figure 3-5 Non-linear resistor Voltage-Current curve

Each segment of the characteristic can be represented by a constant voltage source in series with a resistor, and can be switched when the current (or voltage) reaches threshold value, e.g. ,  $i_1, i_2, i_3$  etc.

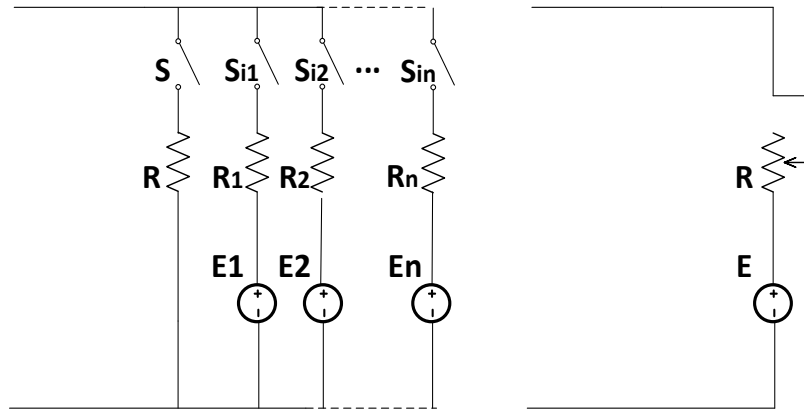


Figure 3-6 a) Piecewise linear model

b) Iterative method model

Alternatively, iterative method as shown in [37] can be used to calculate the corresponding values of voltage source  $E$  and resistor  $R$ .

For the Piecewise linear model, as we have already shown that such a system with passive elements, bi-valued switches and bounded voltage sources leads to a BIBO stable simulation, this means that non-linear resistors modelled in this way also results in stable simulations.

For the iterative method model, although the iteration procedure (as shown in [37]) might be complex, the resistor and voltage source are always finite, i.e.  $E \in [0, E_n]$  and  $R \in [R, R_n]$ . As a result, the stability of such can be analyzed as below:

- 1) In the autonomous condition, connecting any finite  $R$  to an LSPSC system retains the LSPSC property.
- 2) When Trapezoidal or Backward Euler method is applied, with bounded excitation (including the voltage source  $E$ ), the simulation of such a system will always BIBO stable as shown in section 3.2.

It is also valuable to notice that strictly speaking, the CQLF theory has not considered the condition where the number of switching state is infinite, which is the case for this iterative method. Further work might be needed to address this gap.

### 3.4.2 Stability of Simulation of Non-linear Inductors

In this section, the stability of a non-linear inductor is investigated. It will be shown that if such an element is modeled by a flux-current characteristic with an arbitrary number of piecewise linear segments, it can be considered as a special case of a circuit with

switches. By applying the conclusions of section 3.2, the simulation of circuits with switches and such inductors is stable.

### 3.4.2.1 Theoretical Analysis

In a power transmission circuit, inductors have iron cores and are therefore subject to saturation of the iron for high current values, which gives a non-linear flux-current characteristic as shown in Fig. 3-5. Hysteresis is not considered in this paper and it is assumed that the Flux-Current curve can be approximated to any level of accuracy using a finite number  $n$  of piecewise linear portions as shown by the dashed line [38]. The slope in any region  $k$  is the incremental inductance  $L_k$ .

In a switched inductance (SI) model, the piecewise linear flux-current characteristic of Fig. 3-7 is represented by a set of parallel inductances with switches as shown in Fig. 3-8. The switches operate when a slope change is encountered. Prof. Dommel introduced this model in the EMTP theory book [1]. Based on experience, he conjectured that the model was probably also absolutely stable. In this paper we provide a theoretical proof to confirm that Dommel's conjecture was indeed correct.

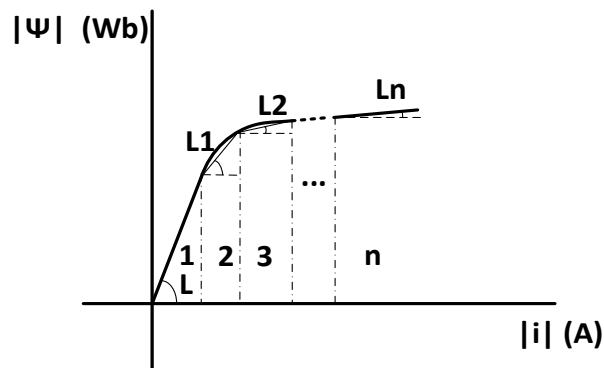


Figure 3-7 Non-linear Inductance Flux-Current Curve

Resistance  $R_L$  in Fig. 3-8 represents an internal resistance, which can be arbitrarily small but non-zero in order to maintain the required strict passivity property. The inductances  $L, L_{e1}, L_{e2}$  etc. in Fig. 3-8 can be determined recursively as below from the incremental inductances  $L, L_1, L_2$  etc. in Fig. 3-7. Note that as  $L_1 > L_2 \dots > L_n > 0$ , every  $L_{ek}$  is always positive.

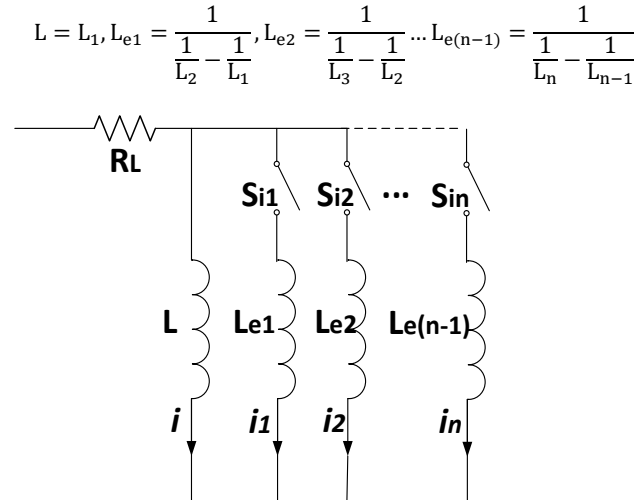


Figure 3-8 Piecewise linear model for non-linear inductance

The connection of the model in Fig. 3-8 to any other LSPSC circuit remains LSPSC, as the non-linear inductance is represented purely by switches and positive inductors and resistance [33]. Therefore, using the conclusion in section 3.2, the simulation by the Trapezoidal or Backward Euler method of a LSPSC system including non-linear inductances with the above representation, is always stable under arbitrary switching.

### 3.4.2.2 Case Study

In order to demonstrate the stability of the switched inductor model in Fig. 3-8, vis-à-vis a compensation based model [39]. Consider the simulation of an open circuited transformer rated at 230 kV: 230 kV line-line (i.e., 135 kV phase-neutral) energized via a 150 km transmission line as shown in Fig. 3-9, with data as in Table 3-4. The transformer core saturation is modeled by a magnetizing reactance which is represented by a non-linear inductor.

Coupling between transmission line phases is not modeled and only a single phase is simulated. The transformer is energized from the primary side and the transformer representation is referred to the primary

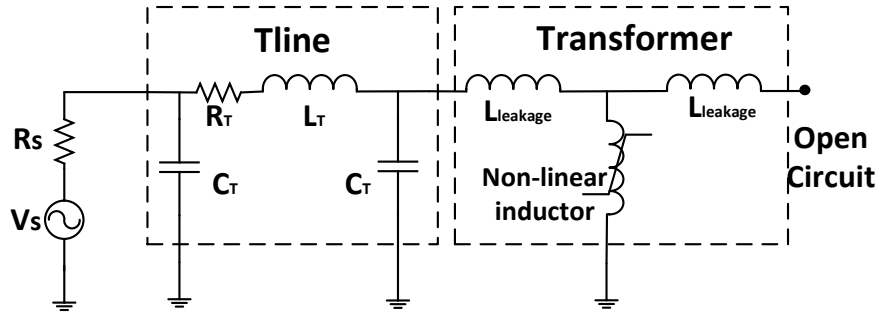


Figure 3-9 Transformer in open circuit

Table 3-4 Simulation System Parameters

<i>System Parameter</i>	<i>Value</i>
<i>Transformer Rated voltage</i>	<i>135kV/135 kV</i>
<i>Transformer Rated MVA</i>	<i>100 MVA</i>
<i>Transformer leakage inductor</i>	<i>0.2 P.U.</i>
<i>Transformer magnetizing inductor</i>	<i>66.3146 H</i>
<i>Transformer saturated inductor</i>	<i>0.2 P.U.</i>
<i>Rated frequency</i>	<i>60 Hz</i>
<i>T-line length</i>	<i>150 km</i>
<i>T-line resistance /m</i>	$3.5396 \cdot 10^{-5} \Omega/m$
<i>T-line inductive reactance/m</i>	$4.0166 \cdot 10^{-4} \Omega/m$
<i>T-line capacitive reactance /m</i>	$7.9315 \cdot 10^8 \Omega/m$
<i>Source voltage</i>	<i>1.17 P.U.</i>
<i>Source resistance Rs</i>	<i>1 <math>\Omega</math></i>

Core saturation is represented by a piecewise linear dual-slope flux-magnetizing current characteristic shown in Fig. 3-10 a. Two commonly used saturation approaches [39, 40] are examined:

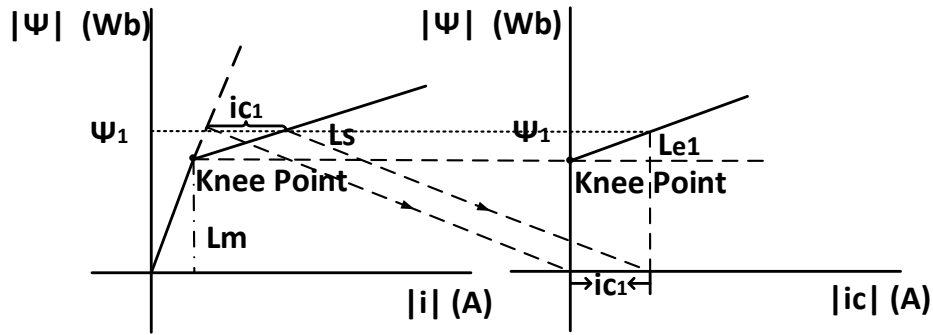


Figure 3-10 a) Flux-magnetizing current relationship b) Flux-compensation current relationship

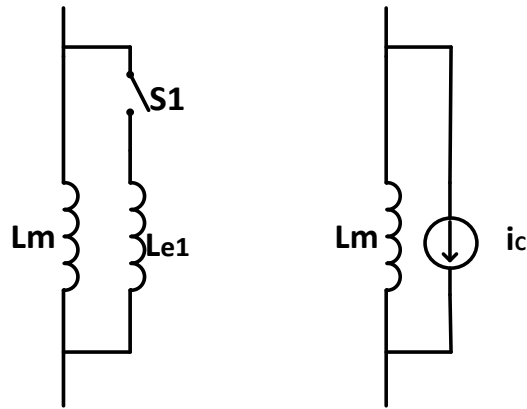


Figure 3-11a) Switched Inductor b) Compensation current source model

1) Switched inductor model as shown in Fig. 3-11 a.

In this model, inductor  $L_m$  is the unsaturated magnetizing inductor.  $L_{e1}$  is the inductor which is used to represent the core saturation inductance i.e. :

$$L_{e1} = \frac{1}{\frac{1}{L_s} - \frac{1}{L_m}}$$

Where  $L_s$  is the saturated inductor as shown in Table 3-4.

2) Current compensation model as shown in Fig. 3-11 b.

In the compensation source model, a compensation current source  $i_c$  is used to represent the core saturation, which injects a saturation current when the flux exceeds the knee (as in Fig. 3-10 b). The unsaturated inductance is also modelled by the inductance  $L_m$  as before.

The circuit is simulated in a Trapezoidal rule based EMT solver with a time step of  $10\ \mu\text{s}$ ,  $50\ \mu\text{s}$  and  $800\ \mu\text{s}$ . The transformer primary side voltage simulation results are shown in Fig. 3-12, Fig. 3-13 and Fig. 3-14.

With the  $10\ \mu\text{s}$  time step, both simulations are stable and essentially the same. However, with the larger simulation time step of  $50\ \mu\text{s}$ , it can be clearly seen the current compensation method is not stable, whereas with the SI model is stable, which is in agreement with the earlier proof that the SI model is always stable. Even with an unreasonable large time step of  $800\ \mu\text{s}$ , the simulation remains stable with the SI model, although the accuracy becomes very poor. Note the current compensation model result is not shown in Fig. 3-14, since it rapidly diverges to infinity.

Even with the SI method implemented here, there is a one time step delay, as the switching on and off of the inductors is determined by the flux in the previous time step. Although this may have accuracy implications, the simulation remains stable regardless of the time step. This is because, as shown in Section 3.2, the LSPSC system model is BIBO stable *regardless of the switching regime used*.

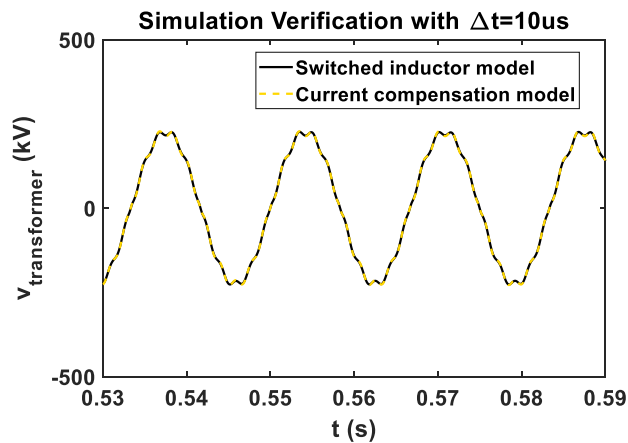


Figure 3-12 Transformer voltage simulation result with  $\Delta t = 10\ \mu\text{s}$

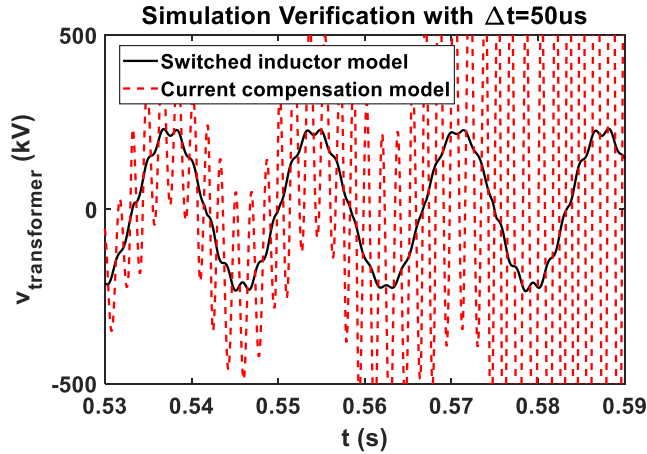


Figure 3-13 Transformer voltage simulation result with  $\Delta t = 50\mu s$

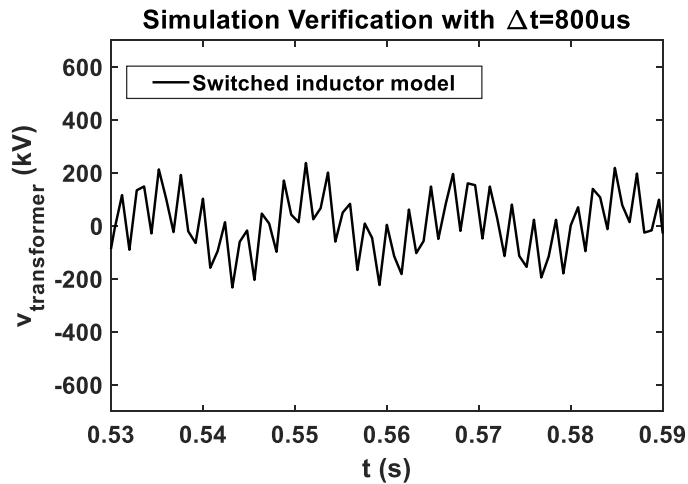


Figure 3-14 Transformer voltage simulation result with  $\Delta t = 800\mu s$

### 3.5 Chapter Conclusion

In this chapter, the stability of numerical algorithms in switched system simulations was theoretically analyzed. Using Common Quadratic Lyapunov function theory, we proved that the simulation of any strictly passive power electronic system with a bi-linear resistor switch representation and lumped elements (i.e., resistor, inductor and capacitor) is always stable regardless of the simulation time step, when the commonly used Trapezoidal or Backward Euler integration methods are employed. However, as shown by the counterexamples in Section 3.3, this is not always true when one or more individual

switching states are non-passive. In such a case, even if the real-world system is stable, its simulation can be unstable.

With the non-A stable Forward Euler method, we proved that the simulation of the LSPSC is stable for a sufficiently small time step, but may be unstable with larger time steps.

This chapter also proved that if a non-linear inductor is properly modelled as a set of parallel switched inductors (SI), it falls into the category of a passive circuits with bi-valued switches, and thus the conclusions derived for the stability of LSPSC simulation, becomes automatically applicable. Hence the SI modelling of circuits with non-linear inductors also results in a stable simulation with the Trapezoidal or Backward Euler methods.

## **4 Stability Evaluation of Interpolation, Extrapolation, and Numerical Oscillation Damping Methods Applied in EMT Simulation of Power Networks with Switching Transients**

(This work is going to be published in IEEE Transactions on Power Delivery)

It is known that A-stable or L-stable [11, 22, 23] methods result in stable simulations of stable Linear Time Invariant (LTI) systems. It was believed that these methods would also result in stable simulations of stable *switched* systems. Chapter 3 [10] showed that this was not generally true and Bounded Input Bounded Output (BIBO) stability of the simulation required the additional condition that every switching state be strictly passive. However, as shown in Section 1.4, the use of methods like interpolation or CDA steps essentially modifies the integration method at the instant of switching, and so the conclusions of Chapter 3 no longer directly apply. This chapter addresses this gap by extending the stability analysis to simulations that use CDA or interpolation which are widely used approaches in modern simulators. The stability analysis is based on state space equations. The equivalency of state space equations and Dommel's nodal analysis method was proved in Chapter 2, and is exploited in this Chapter.

Section 4.1 summarizes the background required for this paper, i.e., Common Quadratic Lyapunov Function (CQLF) theory, passivity and stability of numerical algorithms. Section 4.2 shows that the application of linear interpolation to locate the switching instant and get back to the original time step grid does not contribute to instability. Section 4.3 analyzes the stability of EMT type simulations of lumped strictly passive switched circuit (LSPSC) systems with CDA and also with interpolation. Section 4.4 analyzes the discontinuity problem and addresses the stability of the simulation with re-initialization methods. In Section 4.5, the proposed technique is applied to study the stability of other previously used interpolation methods [41, 42].

## 4.1 Energy Function Based Stability Analysis

This section summarizes Common Quadratic Lyapunov Function (CQLF) theory for stability analysis of the simulation algorithm, which is used in previous publications to investigate the stability of switched network simulations [10].

It should be noted that earlier Sections did not address the stability of simulation of switched systems that include interpolation or CDA steps. Later in this Section this CQLF theory is used to investigate the stability of such systems. It will be shown that if the energy variation for each switching state is always negative for the autonomous system (i.e., with zero excitation), then the non-autonomous system with bounded excitation is also always BIBO stable under arbitrary switching.

### 4.1.1 State-Space Model of Network with Switches

For most HVdc converters, FACTS controllers and so on, the system is typically modeled by a switched circuit with inductors, capacitors, resistors etc. For the power electronic switch, a bi-valued resistor is usually used to represent its dynamics. It is shown in [10] that a system with “ $s$ ” number of switches (and hence  $2^s$  switching states) can be described by the state space equations below:

$$\frac{d\mathbf{x}(t)}{dt} = \mathbf{A}_i \cdot \mathbf{x}(t) + \mathbf{B}_i \cdot \mathbf{u}(t); i \in \{1,2,3 \dots 2^s\} \quad (4.1)$$

Applying an integration method converts the continuous-time state space equation to a discrete state space equation:

$$\begin{aligned} \mathbf{x}(n+1) &= \mathbf{G}_i \cdot \mathbf{x}(n) + \mathbf{H}_i \cdot \mathbf{u}(n); \\ i &\in \{1,2,3 \dots 2^s\} \end{aligned} \quad (4.2)$$

It should be noted that indices  $n$  and  $n+1$  identify the sample in the simulation, and these samples are not necessarily equally spaced in time. For example, the time distance between samples may be the simulation time step  $\Delta t$  until a switching event. Following a switching interpolation as in Fig. 1-2, the next sample is at a time  $\delta t$  after the previous one.

The energy stored in such system at any time  $t$  could be defined as below:

$$E = \mathbf{x}^T \cdot \mathbf{V} \cdot \mathbf{x} \quad (4.3)$$

For a strictly passive network it can be shown that [10]:

$$\mathbf{x}^T(t) \cdot (\mathbf{A}_i^T \cdot \mathbf{V} + \mathbf{V} \cdot \mathbf{A}_i) \cdot \mathbf{x}(t) < 0; \quad i \in \{1, 2 \dots 2^s\} \quad (4.4)$$

#### 4.1.2 Common Quadratic Lyapunov Function Theory

For an *autonomous* switched system (i.e. equation (4.1) with zero input), if there exists a positive definite matrix  $\mathbf{P}$  such that:

$$\forall i \in \{1, 2, 3 \dots 2^s\}, \mathbf{A}_i^T \cdot \mathbf{P} + \mathbf{P} \cdot \mathbf{A}_i < \mathbf{0} \quad (4.5)$$

Then the scalar function  $\mathbf{x}^T \cdot \mathbf{P} \cdot \mathbf{x}$  is called a “common quadratic Lyapunov function” (CQLF). In reference [12], the existence of a Common Quadratic Lyapunov Function (CQLF) is shown to be a *sufficient* condition for stability of a switched system. In the discrete-time form, the existence of a CQLF is equivalent to the existence of a positive definite matrix  $\mathbf{P}$  [12], such that:

$$\forall i, \mathbf{G}_i^T \cdot \mathbf{P} \cdot \mathbf{G}_i - \mathbf{P} < \mathbf{0} \quad (4.6)$$

Here  $i \in \{1, 2, 3 \dots 2^s\}$  i.e., it belongs to the index set of all possible switching states. In reference [13], it is also theoretically proved that if an autonomous switched system is stable, the non-autonomous system will be BIBO stable.

#### 4.1.3 Stability of Numerical Simulation Algorithms

In [10], for the autonomous switched system, the definition of energy variation during each time step is introduced. It was shown, that if this variation is negative, then the system is BIBO stable. This approach was used to theoretically prove that the simulation of a LSPSC system using the Trapezoidal or Backward Euler methods is guaranteed stable. The procedure can be summarized as below:

If Lyapunov function  $V$  as in equation (3.4) is a candidate for  $P$ , then the condition for stability is that  $\mathbf{G}_i^T \cdot \mathbf{V} \cdot \mathbf{G}_i - V$  be negative definite. By definition of negative definiteness, this gives the condition in equation (4.7):

$$\forall \mathbf{x}(n \cdot \Delta t) \neq \mathbf{0}; \mathbf{x}^T(n) \cdot (\mathbf{G}_i^T \cdot \mathbf{V} \cdot \mathbf{G}_i - V) \cdot \mathbf{x}(n) < 0 \quad (4.7)$$

Denoting the energy in the  $n^{\text{th}}$  time step as  $E(n) = \mathbf{x}(n)^T \cdot \mathbf{V} \cdot \mathbf{x}(n)$ , equation (4.7) becomes (4.8):

$$\begin{aligned} & \mathbf{x}^T(n) \cdot (\mathbf{G}_i^T \cdot \mathbf{V} \cdot \mathbf{G}_i - V) \cdot \mathbf{x}(n) \\ &= E(n+1) - E(n) \\ &\equiv \Delta E \end{aligned} \quad (4.8)$$

In equation (4.8),  $\Delta E$  is the energy variation from  $n\Delta t$ , to  $(n+1)\Delta t$ . Hence (4.7) and (4.8) imply that if  $\Delta E$  is always negative, (4.6) is satisfied, and the system is asymptotically stable.

Based on this technique, the stability of the Trapezoidal and Backward Euler method in LSPSC system simulation was theoretically proven to be stable in earlier work [10]. A similar procedure will be adopted to investigate the stability of systems with CDA or interpolation.

## **4.2 Stability of simulation when interpolation is used to locate the switching instant**

The interpolation technique is often used for locating the switching instant and suppressing numerical oscillation. In this section, the stability of the simulation with the use of this technique is analyzed. Use of interpolation for suppressing numerical oscillation is investigated later in Section 4.3.

### **4.2.1 Impact on Simulation Stability with Interpolation Technique Used for Locating the Switching Event**

In general, the switching instant does not coincide with the simulation grid, and may occur between time steps. In order to overcome this challenge, the interpolation technique has been used in many EMT programs such as NETOMAC and PSCAD/EMTDC.

In this section, the stability of this procedure is analyzed. It is shown that such processes add additional switching states to the switched system in equation (4.2). Applying CQLF theory to the new resulting range of switching states shows that using interpolation does not influence stability of the LSPSC system. These additional states occur at times not on the original time step grid. The reader is referred to the discussion at the end of Section 4.1.1, i.e., the actual time difference between the  $n$ th and  $n+1$  th samples may be different for each  $n$ .

#### 4.2.2 Locating the Switching Instant

Consider an EMT simulation using Trapezoidal simulation with a nominal time step of  $\Delta t_{TR}$ . The predicted time evolution of the state vector with Trapezoidal rule is as follows:

$$\begin{aligned} \mathbf{x}_p(t + \Delta t_{TR}) &= \left(I - \frac{A_i}{2} \cdot \Delta t_{TR}\right)^{-1} \cdot \left(I + \frac{A_i}{2} \cdot \Delta t_{TR}\right) \cdot \mathbf{x}(t) + \left(I - \frac{A_i}{2} \cdot \Delta t_{TR}\right)^{-1} \cdot \mathbf{B}_i \cdot \\ &\quad \Delta t_{TR} \cdot \frac{\mathbf{u}(t) + \mathbf{u}(t + \Delta t_{TR})}{2} \\ &\equiv \mathbf{G}_{TR_i} \cdot \mathbf{x}(t) + \mathbf{H}_{TR_i} \cdot \mathbf{u}'(t) \end{aligned} \quad (4.9)$$

The subscript  $p$  indicates that this is a prediction of the state at  $t + \Delta t_{TR}$ , by assuming that the state did not change in between. Assume that a switching from state  $i$  to  $j$  occurs between time step, say in the interval  $(t, t + \Delta t_{TR})$ . Linear interpolation fixes the time of switch operation to  $t + k \cdot \Delta t_{TR}$  where  $0 < k < 1$  and the activated switching state changed from  $i$  to  $j$ . Using (4.9) We interpolate to this point as below:

$$\begin{aligned} \mathbf{x}(t + k \cdot \Delta t_{TR}) &= \mathbf{x}(t) + (\mathbf{x}_p(t + \Delta t_{TR}) - \mathbf{x}(t)) \cdot k \\ &= [\mathbf{I} + k \cdot (\mathbf{G}_{TR_i} - \mathbf{I})] \cdot \mathbf{x}(t) + k \cdot \mathbf{H}_{TR_i} \cdot \mathbf{u}'(t) \\ &\equiv \mathbf{G}_{Int_{ij}} \cdot \mathbf{x}(t) + \mathbf{H}_{Int_{ij}} \cdot \mathbf{u}'(t) \end{aligned} \quad (4.10)$$

The equation above also shows that the interpolation procedure can be treated as a new switching state with system matrix  $\mathbf{G}_{Int_{ij}}$  and input matrix  $\mathbf{H}_{Int_{ij}}$ . It is also valuable to

note that although the time step for this switching state is  $k \cdot \Delta t_{TR}$  (instead of  $\Delta t_{TR}$ ), it is nevertheless the  $n+1$ <sup>th</sup> point in the discrete sequence as indicated in equation (4.2):

$$\mathbf{x}(n+1) = \mathbf{G}_{Int_{iji}} \cdot \mathbf{x}(n) + \mathbf{H}_{Int_{iji}} \cdot \mathbf{u}'(n) \quad (4.11)$$

From [10], the global stability of the switched system simulation with this new switching state can be analyzed by checking if the energy variation of this switching state with zero input is always negative as below:

$$\begin{aligned} \Delta E_{Int_{iji}} &= \mathbf{x}^T(n \cdot \Delta t) \cdot \left( \mathbf{G}_{Int_{iji}}^T \cdot \mathbf{V} \cdot \mathbf{G}_{Int_{iji}} - \mathbf{V} \right) \cdot \mathbf{x}(n \cdot \Delta t) \\ &= \mathbf{x}^T(n \cdot \Delta t) \cdot k\mathbf{V} \cdot \mathbf{G}_{TR_i} - \mathbf{V} + \mathbf{G}_{TR_i}^T \cdot \mathbf{V} - \mathbf{V} + k \cdot \mathbf{G}_{TR_i}^T \cdot \mathbf{V} \cdot \mathbf{G}_{TR_i} - \\ &\quad k \cdot \mathbf{V} \cdot \mathbf{G}_{TR_i} - k \cdot \mathbf{G}_{TR_i}^T \cdot \mathbf{V} + k \cdot \mathbf{V} \cdot \mathbf{x}(n \cdot \Delta t) \end{aligned} \quad (4.12)$$

Note from [10] we have:

$$\mathbf{G}_{TR_i}^T \cdot \mathbf{V} \cdot \mathbf{G}_{TR_i} - \mathbf{V} < 0 \quad (4.13)$$

Substituting into equation (4.12) gives:

$$\begin{aligned} \Delta E_{Int_{iji}} &< \mathbf{x}^T(n \cdot \Delta t) \cdot k\mathbf{V} \cdot \mathbf{G}_{TR_i} - \mathbf{V} + \mathbf{G}_{TR_i}^T \cdot \mathbf{V} - \mathbf{V} - k \cdot \mathbf{V} \cdot \mathbf{G}_{TR_i} - k \cdot \mathbf{G}_{TR_i}^T \cdot \mathbf{V} \\ &\quad + 2k \cdot \mathbf{V} \cdot \mathbf{x}(n \cdot \Delta t) \\ &= \mathbf{x}^T(n \cdot \Delta t) \cdot k(1-k) \left( (\mathbf{V} \cdot (\mathbf{G}_{TR_i} - \mathbf{I}) + (\mathbf{G}_{TR_i}^T - \mathbf{I}) \cdot \mathbf{V}) \right) \cdot \mathbf{x}(n \cdot \Delta t) \end{aligned} \quad (4.14)$$

Letting  $K1 = k \cdot (1-k)$ , for  $k \in (0,1)$ . Note that  $0 < K1 < 1$ . Equation (4.14) above can be rewritten as (4.15):

$$\Delta E_{Int_{iji}} < K1 \cdot \mathbf{x}^T(n \cdot \Delta t) \cdot \left( (\mathbf{V} \cdot (\mathbf{G}_{TR_i} - \mathbf{I}) + (\mathbf{G}_{TR_i}^T - \mathbf{I}) \cdot \mathbf{V}) \right) \cdot \mathbf{x}(n \cdot \Delta t) \quad (4.15)$$

Since  $K1$  is always positive, the equation above is always true if the middle matrix term  $(\mathbf{V} \cdot (\mathbf{G}_{TR_i} - \mathbf{I}) + (\mathbf{G}_{TR_i}^T - \mathbf{I}) \cdot \mathbf{V})$ , is negative definite. This is proven by utilizing the fact for LSPSC system,  $\mathbf{G}_{TR_i}^T \cdot \mathbf{V} \cdot \mathbf{G}_{TR_i} - \mathbf{V} < 0$  thus:

$$\begin{aligned}
& \mathbf{x}^T(n \cdot \Delta t) \cdot \left( (\mathbf{V} \cdot (\mathbf{G}_{TR_i} - \mathbf{I}) + (\mathbf{G}_{TR_i}^T - \mathbf{I}) \cdot \mathbf{V}) \right) \cdot \mathbf{x}(n \cdot \Delta t) \\
& < \mathbf{x}^T(n \cdot \Delta t) \cdot (\mathbf{V} \cdot (\mathbf{G}_{TR_i} - \mathbf{I}) + (\mathbf{G}_{TR_i}^T - \mathbf{I}) \cdot \mathbf{V}) \cdot \mathbf{x}(n \cdot \Delta t) + \\
& \quad \mathbf{x}^T(n \cdot \Delta t) \cdot [\mathbf{V} - \mathbf{G}_{TR_i}^T \cdot \mathbf{V} \cdot \mathbf{G}_{TR_i}] \cdot \mathbf{x}(n \cdot \Delta t) \\
& = -\mathbf{x}^T(n \cdot \Delta t) \cdot [(\mathbf{G}_{TR_i} - \mathbf{I})^T \cdot \mathbf{V} \cdot (\mathbf{G}_{TR_i} - \mathbf{I})] \cdot \mathbf{x}(n \cdot \Delta t) \tag{4.16}
\end{aligned}$$

Matrix  $\mathbf{V}$  is positive definite and  $(\mathbf{G}_{TR_i} - \mathbf{I})$  is always non-singular for LSPSC systems (follows from the fact that eigenvalues of  $\mathbf{G}_{TR_i}$  are within the unit circle as each simulation state is strictly passive). Hence the matrix term  $-(\mathbf{G}_{TR_i} - \mathbf{I})^T \cdot \mathbf{V} \cdot (\mathbf{G}_{TR_i} - \mathbf{I})$  is negative definite. Therefore, from (4.16):

$$\begin{aligned}
& \mathbf{x}^T(n \cdot \Delta t) \cdot (\mathbf{V} \cdot (\mathbf{G}_{TR_i} - \mathbf{I}) + (\mathbf{G}_{TR_i}^T - \mathbf{I}) \cdot \mathbf{V}) \cdot \mathbf{x}(n \cdot \Delta t) \\
& < -\mathbf{x}^T(n \cdot \Delta t) \cdot [(\mathbf{G}_{TR_i} - \mathbf{I})^T \cdot \mathbf{V} \cdot (\mathbf{G}_{TR_i} - \mathbf{I})] \cdot \mathbf{x}(n \cdot \Delta t) \\
& < 0 \tag{4.17}
\end{aligned}$$

Substituting (4.17) back into (4.15) gives:

$$\begin{aligned}
\Delta E_{Int_{ij}} & < K1 \cdot \mathbf{x}^T(n \cdot \Delta t) \cdot \left( (\mathbf{V} \cdot (\mathbf{G}_{TR_i} - \mathbf{I}) + (\mathbf{G}_{TR_i}^T - \mathbf{I}) \cdot \mathbf{V}) \right) \cdot \mathbf{x}(n \cdot \Delta t) \\
& < 0 \tag{4.18}
\end{aligned}$$

Equation (4.18) shows that locating the switching instant using linear interpolation contributes to a negative change in energy. If all other steps in the numerical simulation also result in negative energy changes, then the entire simulation will be stable.

It should be noted that this proof actually only relies on the fact that the real energy function is a CQLF for all discrete switching states, i.e.  $\mathbf{G}_{TR_i}^T \cdot \mathbf{V} \cdot \mathbf{G}_{TR_i} - \mathbf{V} < \mathbf{0}$ . Although in the above analysis,  $\mathbf{G}_{TR_i}$  represented a Trapezoidal integration rule, it can be seen that the stability proof (i.e., equations (4.13) – (4.18)) is general and applies to any integration method for which  $\mathbf{G}_i^T \cdot \mathbf{V} \cdot \mathbf{G}_i - \mathbf{V} < \mathbf{0}$ ,  $\mathbf{G}_i$  being the corresponding system matrix for state  $i$ , using that integration method. The Backward Euler algorithm also has the same property as shown in [12], and would result in stable simulation if such interpolation were applied.

### 4.2.3 Additional Interpolation for Synchronizing to Original Time Grid

In order to get back into synchronism with the original time grid (i.e., integer multiples of  $\Delta t_{TR}$ ) the solution at time  $t + \Delta t_{TR}$  is obtained by linearly interpolating between  $\mathbf{x}(t + k \cdot \Delta t_{TR})$  and  $\mathbf{x}(t + k \cdot \Delta t_{TR} + \Delta t_{TR})$ . Noting that  $t$  was assumed to be an integer multiple of  $\Delta t_{TR}$ , and so time  $t + \Delta t_{TR}$  lies on the original time grid.

Once this is done,  $\mathbf{x}(t + k \cdot \Delta t_{TR} + \Delta t_{TR})$  is discarded, and the next points in the solution continue on the original time grid, i.e., at instances time  $t + \Delta t_{TR}$ ,  $t + 2\Delta t_{TR}$ ,  $t + 3\Delta t_{TR}$  ... etc. until the next switching event.

$$\begin{aligned}
 \mathbf{x}(t + \Delta t_{TR}) &= \mathbf{x}(t + k \cdot \Delta t_{TR}) + (\mathbf{x}(t + k \cdot \Delta t_{TR} + \Delta t_{TR}) - \mathbf{x}(t + k \cdot \Delta t_{TR})) \\
 &\quad \cdot (1 - k) \\
 &= \left[ \mathbf{I} + (\mathbf{G}_{TRj} - \mathbf{I}) \cdot (1 - k) \right] \cdot \mathbf{x}(t + k \cdot \Delta t_{TR}) + (1 - k) \cdot \mathbf{H}_{TRj} \cdot \\
 &\quad \mathbf{u}(t + k \cdot \Delta t_{TR}) \\
 &\equiv \mathbf{G}_{Intijj} \cdot \mathbf{x}(t) + \mathbf{H}_{Intijj} \cdot \mathbf{u}'(t)
 \end{aligned} \tag{4.19}$$

Because  $0 < k < 1$  we also have  $0 < (1 - k) < 1$ . Hence, the same steps used in (4.10)-(4.18) can be repeated by substituting  $\bar{k} = (1 - k)$  for  $k$  in equation (4.10):

$$\mathbf{x}(t + \Delta t_{TR}) = \left[ \mathbf{I} + \bar{k} \cdot (\mathbf{G}_{TRi} - \mathbf{I}) \right] \cdot \mathbf{x}(t) + \bar{k} \cdot \mathbf{H}_{TRi} \cdot \mathbf{u}'(t) \tag{4.20}$$

Noting that (4.20) is identical with (4.10), from the treatment in Section 4.1.2, the corresponding energy variation  $\Delta E_{Intijj}$  is also always negative:

$$\Delta E_{Intijj} < 0 \tag{4.21}$$

Therefore, the application of linear interpolation for re-synchronizing with the original time-grid also results in the reduction of stored energy and by the argument in Section 4.1.3, does not contribute to instability.

### 4.3 Stability of Numerical Oscillation Suppression Strategy

The operation of the switch can lead to the phenomenon of ‘‘chatter’’ when the system is switched into a stiff switching state as explained in [11, 22]. It is valuable to note that this

means that even when chatter is not suppressed, the simulation is stable in the BIBO sense, as it does not become infinite. This is consistent with earlier research conclusions that the Trapezoidal rule results in the stable simulation of a lumped strictly passive switched circuit [10].

However, the question of whether the simulation is stable when a chatter suppression strategy such as Critical Damping Adjustment (CDA) or interpolation is applied will be answered for the first time in this section.

### 4.3.1 Stability of Critical Damping Adjustment (CDA)

In some EMT simulators (e.g., EMTP) [24], two steps of backward Euler (BE) with a half time step are taken to suppress the numerical oscillation after the switching operation. This method is referred to as “Critical Damping Adjustment” (CDA). CDA has the advantage that the admittance matrix with a half time step BE, is identical with the admittance matrix from a full time step Trapezoidal rule and so no matrix re-factorization is required in this step.

As proved in [10], for an *autonomous* LSPSC system, the energy variation in each BE step is always negative (regardless of time step) when the backward Euler method is applied, i.e., :

$$\Delta E_{BE} = \mathbf{x}^T(n) \left( (\mathbf{I} - \mathbf{A}_i^T \cdot \Delta t_{BE})^{-1} \cdot \mathbf{V} \cdot (\mathbf{I} - \mathbf{A}_i \cdot \Delta t_{BE})^{-1} - \mathbf{V} \right) \cdot \mathbf{x}(n) < 0 \quad (4.22)$$

As a result, as discussed in part 4.1.3, the new switching states introduced by CDA method do not contribute to instability.

### 4.3.2 Stability of Interpolation

Instead of using CDA, programs such as PSCAD use a linear interpolation technique to suppress the numerical oscillation [19]. This procedure is a special case of the interpolation introduced in Section 4.2 where  $k=0.5$ . The proof in Section 4.2.2 states that any  $k \in$

(0,1), does not contribute to instability of LSPSC system simulation. Hence this interpolation based chatter removal does not destabilize the simulation.

#### 4.4 Stability of Re-Initialization procedure

As discussed in Section 1.4.2, and referring to Fig. 1-3, a straightforward application of the companion circuit leads to an erroneous history current for calculating the network solution at  $t = 2\Delta t$  (the switch opens at time  $\Delta t$ ). This is because the last solution of inductor voltage was at  $t = \Delta t_-$ , which is different from the solution at  $t = \Delta t_+$  (although the inductor current is continuous, the voltage is not). Correctly calculating the history term to be used in the solution at  $2\Delta t$  requires the voltage at  $\Delta t_+$ . Two techniques for re-initializing the simulation [7] in companion circuit simulation were presented in the introduction: i) half time step BE and ii) instantaneous solution. By examining the change in energy of the corresponding autonomous circuit, it will be shown that with the half time step BE method, the re-initialization does not contribute to instability.

##### 4.4.1 The Discontinuity of Derivative Problem

Assume the switching state changes from state  $i$  to  $j$  at  $t = n \cdot \Delta t$ , the corresponding time instants before and after the switching operations are written as  $n \cdot \Delta t_-$  and  $n \cdot \Delta t_+$ . All state variables remain continuous (i.e.  $\mathbf{x}(n \cdot \Delta t_-) = \mathbf{x}(n \cdot \Delta t_+) \equiv \mathbf{x}(n \cdot \Delta t)$ ). However, due to the variation of system matrix (the matrix  $A_i$  changes to  $A_j$  in equation (4.1)), the derivative can change instantaneously, i.e.:

$$\begin{aligned}\dot{\mathbf{x}}(n \cdot \Delta t_-) &= \mathbf{A}_i \cdot \mathbf{x}(n \cdot \Delta t) + \mathbf{B}_i \cdot \mathbf{u}(n \cdot \Delta t) \\ \dot{\mathbf{x}}(n \cdot \Delta t_+) &= \mathbf{A}_j \cdot \mathbf{x}(n \cdot \Delta t) + \mathbf{B}_i \cdot \mathbf{u}(n \cdot \Delta t) \\ \text{i.e., } \dot{\mathbf{x}}(n \cdot \Delta t_+) &\neq \dot{\mathbf{x}}(n \cdot \Delta t_-)\end{aligned}\tag{4.23}$$

The traditional application of the companion circuit based simulation produces a different answer. This is because the history current sources are calculated based on the pre-switching network admittance values.

The correct use of the Trapezoidal rule should be as follows:

$$\begin{aligned}
& \mathbf{x}((n+1) \cdot \Delta t) \\
&= \left( \mathbf{I} - \frac{\mathbf{A}_j \cdot \Delta t}{2} \right)^{-1} \cdot \left( \mathbf{I} + \frac{\mathbf{A}_j \cdot \Delta t}{2} \right) \cdot \mathbf{x}(n \cdot \Delta t) + \mathbf{H}_j \cdot \mathbf{u}(t) \\
&\equiv \mathbf{x}(n \cdot \Delta t) + \frac{\dot{\mathbf{x}}(n \cdot \Delta t_+) + \dot{\mathbf{x}}((n+1) \cdot \Delta t)}{2} \cdot \Delta t
\end{aligned} \tag{4.24}$$

where

$$\begin{aligned}
\dot{\mathbf{x}}(n \cdot \Delta t_+) &= \mathbf{A}_j \cdot \mathbf{x}(t_0) + \mathbf{B}_j \cdot \mathbf{u}(t_0) \\
\dot{\mathbf{x}}((n+1) \cdot \Delta t) &= \mathbf{A}_j \cdot \mathbf{x}((n+1) \cdot \Delta t) + \mathbf{B}_j \cdot \mathbf{u}((n+1) \cdot \Delta t)
\end{aligned}$$

However, in the direct use of the companion circuit approach, the inductor voltages and capacitor currents *before* switching are used in the history current sources (only the conductance matrix is changed). Actually, this is tantamount to using the matrix  $\left( \mathbf{I} - \frac{\mathbf{A}_j \cdot \Delta t}{2} \right)^{-1} \cdot \left( \mathbf{I} + \frac{\mathbf{A}_i \cdot \Delta t}{2} \right)$  instead of  $\left( \mathbf{I} - \frac{\mathbf{A}_j \cdot \Delta t}{2} \right)^{-1} \cdot \left( \mathbf{I} + \frac{\mathbf{A}_j \cdot \Delta t}{2} \right)$  in the state variable solution (where state  $i$  is the switching state before switching while  $j$  is the one after).

Actually, calculating the new history term is impractical (especially when the circuit is index-2) [6, 11]. Several techniques are developed to approximate the post-switching derivative term or even totally avoid using the discontinuous term, which will be discussed next. The stability of simulation with these techniques will also be discussed.

#### 4.4.2 Techniques for Re-initialization

In order to overcome the above discontinuity problem, a suitable initial condition should be calculated from which the correct post-switching derivative can be determined. They are referred as re-initialization. There are mainly two methods for achieving this.

The first one uses a half-time step Backward Euler integration after the instant of switching. NETOMAC uses this for calculating the new initial condition. Other programs such as EMTP [24] and MicroTran [7] use the Backward Euler method for two half time

steps to move forward. Note that the history term with BE is the state variable (i.e., inductor current in the previous time step) which is continuous. Hence, this method also gives the benefit of using the correct post-switching derivative term. As discussed in Section 4.3.2, the BE steps always reduce the energy of the LSPSC system simulation, and so does not contribute to instability.

Another way to do the re-initialization is the “Instantaneous Solution Interpolation” method [21], which is used in PSCAD/ EMTDC. In this approach, the post-switching terms are approximated by updating the new admittance matrix and re-solving the nodal equations. This strategy can also be proved to be stability preserving using a similar analysis as in the previous sections. A proof is included in the Appendix.

## **4.5 Application to Other Methods for Re-synchronizing to Original Time Grid**

In this section, the technique is used to examine the stability of two other interpolation techniques mentioned in literature. These are used for re-synchronizing to the original time grid. They include a) Flexible Integration for Readjustment in Simulation of Transients (FIRST) [41] and Extrapolation[42]. If each application of the interpolation procedure yields a reduction in stored energy for the autonomous case, then the procedure is guaranteed not to contribute to instability. However, if this step results in  $\Delta E > 0$ , then no conclusion can be made as to the stability.

As in the above sections, the stability of autonomous system is first examined, from which the BIBO stability of the non-autonomous system immediately follows as proved in [13].

### **4.5.1 Flexible Integration for Readjustment in Simulation of Transients (FIRST)**

Assuming the switching instant occurs in the time interval  $[(k - 1)\Delta t, k\Delta t]$ , and is flagged by the switch current computed at  $k\Delta t$  becoming negative. As shown in Fig. 4-1, linear interpolation, is used to locate the switching instant at  $(k - 1 + \delta)\Delta t$ , where  $\delta \in [0,1]$ . Next, the solution is interpolated to this instant and reported at  $k\Delta t$ . Then, as

indicated by the red arrow in Fig. 4-1, the solution at  $(k + 1)\Delta t$  is calculated from the interpolated solution at time instant  $(k - 1 + \delta)\Delta t$  using the *FIRST* method as shown in Fig. 4-1.

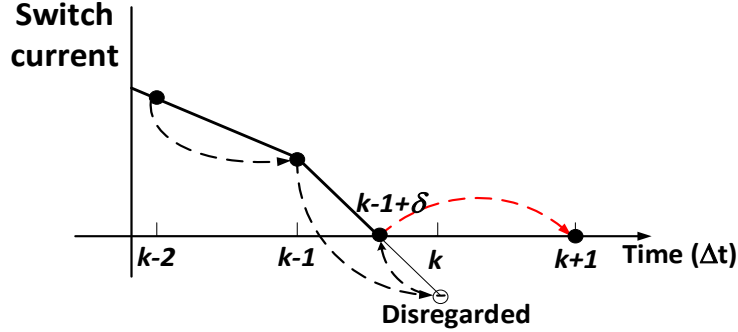


Figure 4-1 Interpolations methods for re-synchronizing to original time grid

*FIRST* proposes a generalized numerical integration method [41] to calculate the solution at  $(k + 1)\Delta t$  from the solution at  $(k - 1 + \delta)\Delta t$  :

$$x((k + 1)\Delta t) = \mathbf{G}_{FIRST_i} \cdot x(k - 1 + \delta)\Delta t, \quad (4.25)$$

where

$$\mathbf{G}_{FIRST_i} = \left( I - \frac{A_i}{2} \cdot (2 - \delta)\Delta t \cdot (2 - \epsilon) \right)^{-1} \cdot \left( I + \frac{A_i}{2} \cdot (2 - \delta)\Delta t \cdot \epsilon \right)$$

With  $\epsilon = 2 - 2/(2 - \delta)$ .

Note that  $\delta \in [0,1]$  implies  $\epsilon \in [0,1]$ . Note that (4.25) is the equation for the autonomous system without any excitation term. We need only investigate the autonomous system as its stability immediately implies the BIBO stability of the non-autonomous case[13].

Reference [41] uses the BE integration method and shows that with this method, the companion circuit implementation of this results in an invariant admittance matrix for all  $\delta \in [0,1]$ , thus avoiding additional admittance matrix inversions.

$\mathbf{G}_{FIRST_i}$  corresponds to a new switching state for which using (4.25), the corresponding energy change  $\Delta E_{FIRST}$  is:

$$\begin{aligned}
\Delta E_{FIRST} &= \mathbf{G}_{FIRST_i}^T \cdot \mathbf{V} \cdot \mathbf{G}_{FIRST_i} - V \\
&= \mathbf{x}(k' \cdot \Delta t) \cdot \left( \left( \mathbf{I} - \frac{\mathbf{A}_i}{2} \cdot \Delta t' \cdot (2 - \epsilon) \right)^{-1} \right)^T \cdot (\mathbf{A}_i^T \cdot \Delta t' \cdot \mathbf{V} + \mathbf{V} \cdot \mathbf{A}_i \cdot \Delta t' - \\
&\quad (2 - 2 \cdot \epsilon) \cdot \mathbf{A}_i^T \cdot \mathbf{V} \cdot \mathbf{A}_i \cdot \Delta t'^2) \cdot \left( \mathbf{I} - \frac{\mathbf{A}_i}{2} \cdot \Delta t' \cdot (2 - \epsilon) \right)^{-1} \cdot \mathbf{x}(k' \cdot \Delta t) \quad (4.26)
\end{aligned}$$

Where we have used  $k' = (k - 1 + \delta)$  and  $\Delta t' = (2 - \delta)\Delta t$  to reduce the size of the expression.

Since both  $(\mathbf{V} \cdot \mathbf{A}_i + \mathbf{A}_i^T \cdot \mathbf{V}) \cdot \Delta t'$  and  $-\mathbf{A}_i^T \cdot \mathbf{V} \cdot \mathbf{A}_i \cdot \Delta t'^2$  are negative definite and  $(2 - 2 \cdot \epsilon) \geq 0$ , the summation of  $\mathbf{A}_i^T \cdot \Delta t' \cdot \mathbf{V} + \mathbf{V} \cdot \mathbf{A}_i \cdot \Delta t' - (2 - 2 \cdot \epsilon) \cdot \mathbf{A}_i^T \cdot \mathbf{V} \cdot \mathbf{A}_i \cdot \Delta t'^2$  is negative definite. Hence, the corresponding energy change  $\Delta E_{FIRST}$  is always negative, and therefore does not contribute to instability.

### 4.5.2 Extrapolation

In this method [42], extrapolation is used to approximate the value at time instant  $(k + 1)\Delta t$  in Fig. 4. The procedure is summarized as below:

$$\mathbf{x}((k + 1)\Delta t) = [\mathbf{I} + k_{ex} \cdot (\mathbf{G}_{TR_i} - \mathbf{I})] \cdot \mathbf{x}((k - 1 + \delta)\Delta t) \quad (4.27)$$

Where  $k_{ex} = 2 - \delta$  stays in the interval  $[1, 2]$ , which implies that  $k_{ex} \geq 1$ .

Noting equation (4.27) is in the same form of equation (4.10) with  $k$  replaced by  $k_{ex}$ . However, the stability proof used in equations (4.10) through (4.18) requires  $k < 1$ . However, as  $k_{ex} \geq 1$ , the corresponding newly introduced switching may result in  $\Delta E > 0$ . As energy is not reduced in this step, we cannot conclusively say that the system will be stable under an arbitrary switching regime if this interpolation/extrapolation method is used.

### 4.5.3 Verification by Simulation

In this section, a simple example as shown in Fig. 4-2 is used to verify the proposed conclusion. In order to avoid the ambiguity that the instability is a result of improper re-initialization, the capacitor current is re-calculated after each switching to ensure a correct initial condition.

In the example of Fig. 4-2, switch  $S_1$  is modeled as a bi-valued resistor which has resistance values of  $1\text{ M}\Omega$  for the off-state and  $10\text{ m}\Omega$  for the on state. The circuit is excited by a  $100\text{ V}$  dc source  $V_s$ . The system is simulated with a time step of  $0.1\ \mu\text{s}$ ,  $86\ \mu\text{s}$  and  $87\ \mu\text{s}$  respectively.

In the simulation, the switch is periodically turned off for  $8.3\ \Delta t$  and turned on for  $1.7\ \Delta t$ . Note this control signal is related to the simulation time step. With this regime, every switching instant falls between integer time step multiples. For the turn-on event at  $8.3\ \Delta t$ , we have  $\delta = 0.3$  and consequently,  $\epsilon = 2 - 2/(2 - \delta) = 0.8235$ .

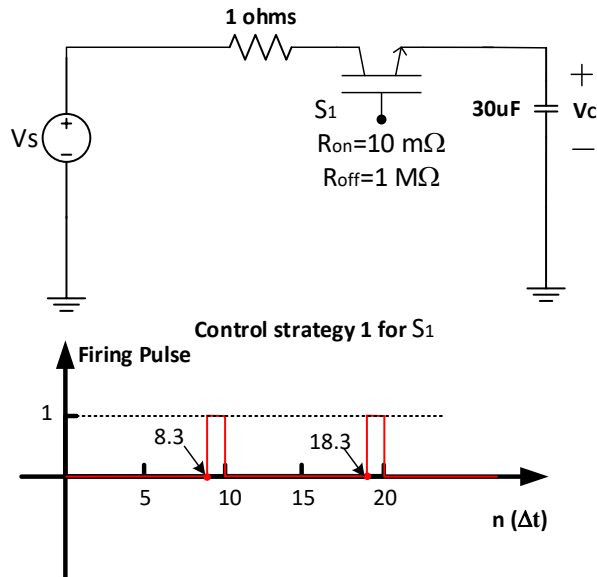


Figure 4-2 Example for unstable simulation resulted from interpolation

When the switch is on, the corresponding state space equation is:

$$\frac{dv_C(t)}{dt} = -\frac{v_C(t)}{(R+R_{on})\cdot C} + \frac{v_s(t)}{(R+R_{on})\cdot C}; \quad (4.28)$$

The corresponding system matrix is  $A_{on} = -(R + R_{on})C = -33003.33$ .

1) *FIRST* method

We already know that  $\Delta E < 0$  for *FIRST* as shown in Section 4.5.1, so the simulation must always be stable.

2) Extrapolation method

This method uses the standard Trapezoidal integration. So, substituting the circuit parameters into equation (4.27) gives, with  $\delta = 0.3$ ,  $k_{ex} = 2 - 0.3 = 1.7$  gives:

For  $\Delta t = 0.1\mu s$ , we get a negative change in energy:

$$\mathbf{G}_{ext_{on}}^T \cdot \mathbf{V} \cdot \mathbf{G}_{ext_{on}} - \mathbf{V} = -1.6757 \cdot 10^{-7} < 0$$

For  $\Delta t = 86\mu s$ , the energy change is still negative

$$\mathbf{G}_{ext_{on}}^T \cdot \mathbf{V} \cdot \mathbf{G}_{ext_{on}} - \mathbf{V} = -1.6326 \cdot 10^{-7} < 0 \quad (4.29)$$

However, for  $\Delta t = 87\mu s$ , we get a positive change in energy:

$$\mathbf{G}_{ext_{on}}^T \cdot \mathbf{V} \cdot \mathbf{G}_{ext_{on}} - \mathbf{V} = 1.2220 \cdot 10^{-7} > 0$$

Therefore, the simulation will be stable with  $\Delta t = 0.1\mu s$  and  $\Delta t = 86\mu s$ .

However, for  $\Delta t = 87\mu s$  there is a possibility that the simulation is unstable.

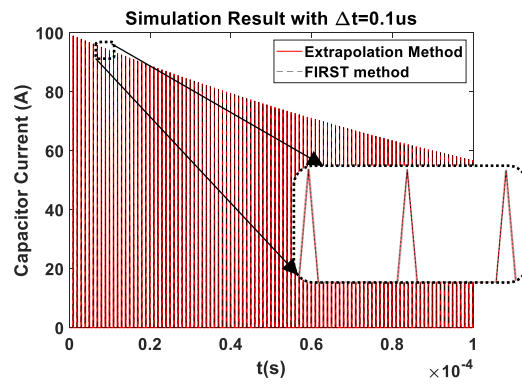


Figure 4-3 Capacitor current with  $\Delta t=0.1\mu s$

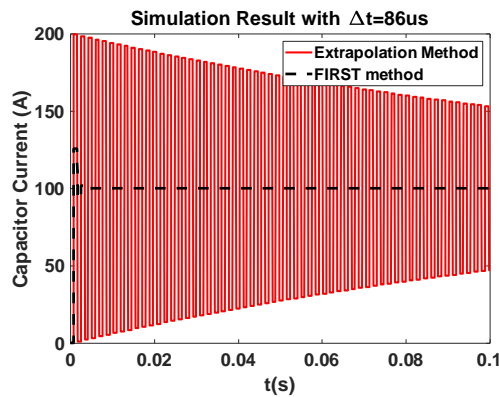


Figure 4-4 Capacitor current with  $\Delta t=86\mu s$

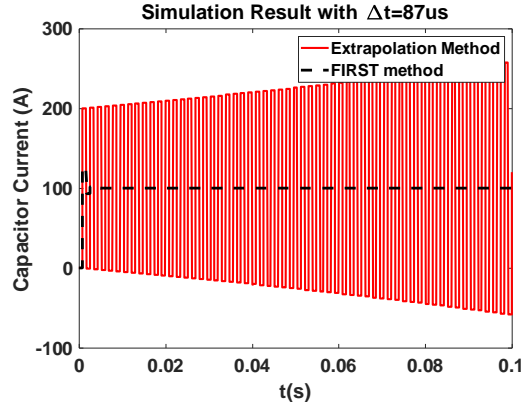


Figure 4-5 Capacitor current with  $\Delta t=87\mu s$

Fig. 4-3 shows the capacitor current waveform for the FIRST and Extrapolation methods for a time step  $\Delta t = 0.1 \mu s$ . As our energy analysis for this smaller time step has shown, both methods result in a stable simulation and indeed have essentially overlapping results due to the small time step. When the time step is increased to  $86 \mu s$ , as proved by the energy analysis in (4.29), the simulations are stable, although the accuracy is poor as seen in Fig. 4-4. As indicated by the energy analysis, slightly increasing the time step to  $87 \mu s$  as in Fig. 4-5, *FIRST* gives a stable simulation, as proved by the energy analysis in Section 4.5.1. However, Extrapolation has no theoretical guarantee of stability and in this case does result in an unstable simulation.

## 4.6 Chapter Conclusions

This chapter extended the state of the art of the stability analysis of simulations for networks with binary resistor switch models. In such simulations, special numerical strategies are used to accurately reproduce the dynamics of switching. For instance, linear interpolation is used to accurately locate the switching instant when the switch operates at a non-integral multiple of a time step. Interpolation and Critical Damping Adjustment (CDA) are used to eliminate numerical oscillations.

A theoretical framework was developed to analyze the stability of these strategies. Application of Interpolation or Critical Damping Adjustment (CDA) was shown to be tantamount to introduction of additional switching states. By using Common Quadratic

Lyapunov function theory, it was theoretically proved that transitions into or out of these states always results in a reduction of stored energy for an autonomous system, which earlier researchers have shown is a sufficient condition for BIBO stability. Hence the use of commercial packages based on these approaches can rest easy that these features will not result in an unstable simulation of a real-world stable system, if each switching state is strictly passive.

The chapter also showed that the approach can be used to analyze any interpolation or extrapolation strategy. Two methods reported in literature for getting back on the time grid, (*FIRST* and Extrapolation) were investigated. *FIRST* was found to be always stable regardless of time step, whereas Extrapolation could potentially result in an unstable simulation due to the energy reduction criterion is not met.

## 5. Accuracy Evaluation of Electromagnetic Transients Simulation

In this Chapter, firstly, the limitation of the component level accuracy evaluation is illustrated by a simple example in Section 5.1, which is straightforward enough for other researchers to replicate for comparative studies. In order to overcome this limitation, Section 5.2 proposes a state space equations based theoretical method to globally evaluate the simulation accuracy. After that, for the purpose of implementing the proposed method to a larger “practical sized” power networks, the “simulation accuracy spectrum” technique is introduced in Section 5.3. The accuracy spectrum can be computed without forming the state space equations, thus can easily be applied to a large network. As shown in Section 5.4, it can be extended to networks with frequency dependent transmission line elements in addition to the RLCM elements (resistor, inductor, capacitor and mutual inductor). Finally Section 5.5 shows application examples to verify the proposed method.

### 5.1 Previous Approaches for Accuracy Evaluation and their Limitations

#### 5.1.1 Component Level Accuracy Evaluation

In [22, 23], the authors compare the frequency response of individual dynamic elements (e.g., inductor, capacitor, etc.) to the frequency response of its corresponding discrete time domain model. The discretized model is obtained by applying a selected integration method (such as Trapezoidal rule) with a time step  $\Delta t$  and then converting the resulting difference equation to the frequency domain using the mapping:

$$z^{-1} = e^{-j\omega\Delta t} \quad (5.1)$$

Pioneering work by the authors of [22] showed the errors in magnitude and phase as a function of frequency and time step for individual inductor or capacitor elements for different integration methods. Trapezoidal integration was shown to have a magnitude error but not a phase angle error for the admittance of any individual element, whereas the Backward Euler method was shown to exhibit spurious damping due to both magnitude and phase errors. One conclusion of this approach was that the accuracy degraded with

frequency for each element. This chapter will show that when multiple elements are present, additional consideration has to be taken when analyzing accuracy and it may happen that in certain cases the accuracy may be better at higher frequency than at certain lower frequencies.

### 5.1.2 Limitation of Component Level Accuracy Evaluation

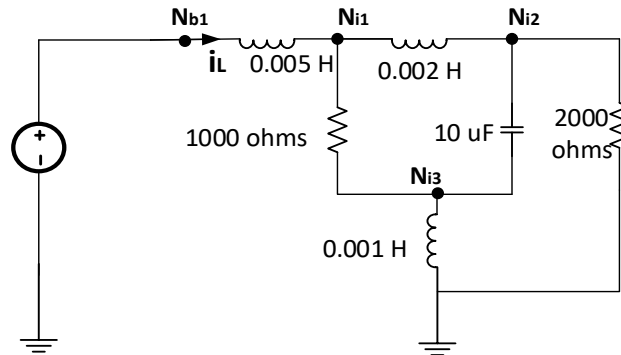


Figure 5-1 Simple RLC circuit

Considering the RLC circuit in Fig. 5-1. Following the steps in [22], Fig. 5-2 shows the simulation accuracy for just the 0.005 H inductor connecting to node  $N_{b1}$  as obtained using the approach in [2,3]. The y axis shows the ratio of the simulated inductor admittance and original inductor admittance for any inductor in the circuit (they are all the same). The graph for the capacitor is the inverse. Reference [22] also shows that the phase of any inductor or capacitor simulated by Trapezoidal method has no numerical error. Therefore, an obvious conclusion could directly be drawn that the simulation accuracy becomes worse in the frequency excitation becomes higher.

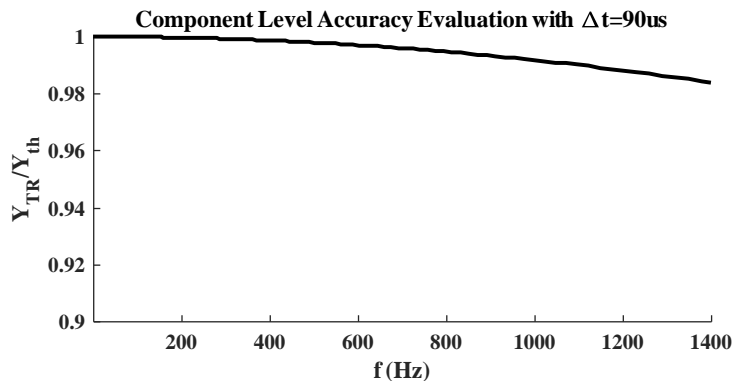


Figure 5-2 Numerical accuracy of Inductor

In order to verify the conclusion, the lumped network as shown in Fig. 5-1 is implemented in an Electrotactic transient simulator. A 132.79 V (RMS value) voltage source is used as an input with two frequencies: 560Hz and 800 Hz. The corresponding current response  $i_{out}$  is as shown in Fig. 5-3 (which is  $i_L$  in Fig. 5-1).

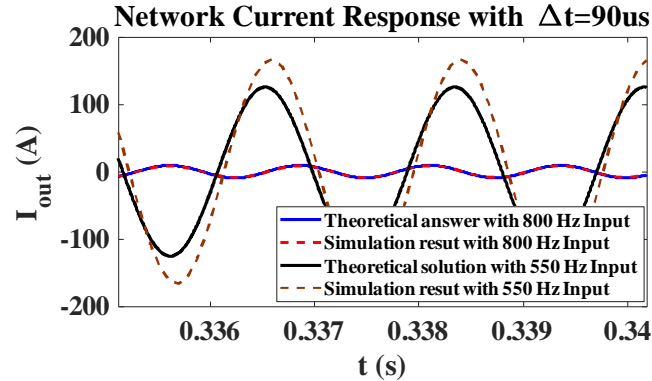


Figure 5-3 Simulation result

It is clearly shown that when the input frequency is 800 Hz, the current response matches well with the theoretical one. However, if the input voltage frequency reduced to 550 Hz, the current 1.33 times larger, and displaced by 15.84 degrees from the theoretical. This is contrary to the conclusion of earlier papers which state that accuracy should always degrade as frequency increases for a given time step.

Therefore, in order to fairly reflect the simulation accuracy, it is important to consider the circuit as a whole, which is done in this paper. In next section, the theoretical background will be built to see the accuracy of whole simulation.

## 5.2 Proposed Methods for Accuracy Evaluation of EMT Simulation

### 5.2.1 Theoretical Foundation of Simulation Accuracy Evaluation [43]

Let the network equations be represented in state variable form:

$$\dot{\mathbf{x}}(t) = \mathbf{A} \cdot \mathbf{x}(t) + \mathbf{B} \cdot \mathbf{u}(t) \quad (5.2)$$

The corresponding discrete-time state equations become:

$$\mathbf{x}(n \cdot \Delta t) = \mathbf{G} \cdot \mathbf{x}((n-1) \cdot \Delta t) + \mathbf{H} \cdot \mathbf{u}(n \cdot \Delta t) \quad (5.3)$$

Matrices  $\mathbf{G}$  and  $\mathbf{H}$  depend on time step and the selected integration method. For example, for Trapezoidal method they are as in equation (5.6) in the next section.

Since all the states in the circuit can be represented as a linear combination of state variables, the simulation accuracy of those state variables gives a complete description of the entire system's simulation accuracy.

In the frequency domain, the transfer function relating state variables  $\mathbf{X}(j\omega)$  to the input  $\mathbf{U}(j\omega)$  in the actual (continuous time) system is given by equation (5.4). In the discrete time domain (where  $\mathbf{x}$  and  $\mathbf{u}$  only assume values at integer multiples of the timestep, i.e.,  $\mathbf{x}(n) \equiv \mathbf{x}(n \cdot \Delta t)$ ). The frequency response of state variables  $\mathbf{X}(z)$  resulting from the excitation  $\mathbf{U}(z)$  is given by equation (5.5):

For the original continuous system:

$$\begin{aligned} \mathbf{X}(j\omega) &= \mathbf{F}_o(j\omega) \cdot \mathbf{U}(j\omega) \\ \text{where } \mathbf{F}_o(j\omega) &= (j\omega \mathbf{I} - \mathbf{A})^{-1} \cdot \mathbf{B} \end{aligned} \quad (5.4)$$

For the discrete system:

$$\begin{aligned} \mathbf{X}(z) &= \mathbf{F}_d(z) \cdot \mathbf{U}(z) \\ \text{where } \mathbf{F}_d(z) &= (\mathbf{I} - \mathbf{G}z^{-1})^{-1} \cdot \mathbf{H} \end{aligned} \quad (5.5)$$

By the mapping function  $z^{-1} = e^{-j\omega\Delta t}$ , the frequency response of the discrete system ( $\mathbf{F}_d(j\omega)$ ) can be calculated.

### 5.2.2 Method I: Global Evaluation of Simulation Accuracy

When Trapezoidal method is applied, the corresponding  $\mathbf{G}$  and  $\mathbf{H}$  matrices will be:

$$\begin{aligned} \mathbf{G} &= \left(\mathbf{I} - \frac{\mathbf{A} \cdot \Delta t}{2}\right)^{-1} \left(\mathbf{I} + \frac{\mathbf{A} \cdot \Delta t}{2}\right) \\ \mathbf{H} &= \left(\mathbf{I} - \frac{\mathbf{A} \cdot \Delta t}{2}\right)^{-1} \cdot \mathbf{B} \cdot \Delta t \cdot \frac{1+z^{-1}}{2} \end{aligned} \quad (5.6)$$

Subsequently, substituting equation (5.6) to (5.5) gives the transfer function with the excitation to all state variables.

Implementing the method above to the circuit shown in Fig. 5-1 gives Fig. 5-4, where the transfer function used in Y axis is corresponding to the inductor current connecting to  $N_{b1}$ .

The figure above clearly predicts the accuracy loss at 550 Hz, with the current being 1.33 times the theoretical value. This matches the simulation result as shown in Fig. 5-4.

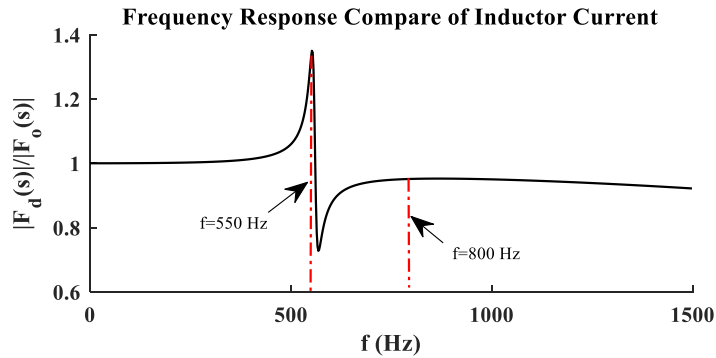


Figure 5-4 Simulation accuracy of inductor current

### 5.2.3 Challenge for Practical Application

The above analysis method is general and applies to the accuracy analysis of any linear network. However, in most simulations, the state space equations as in (5.2) are typically never calculated due to the significant effort, particularly for very large networks.

Additionally, when distributed parameter elements such as transmission lines [2, 44, 45] are included in the simulation, formulation of equation (5.2) will become very complicated. The definition of time constant is also not valid (with distributed component), which is used in [1] to determine the simulation time step.

In Section 5.3, the proposed method above is modified for convenient application to large systems. In Section 5.4, a methodology is proposed to include the consideration of distributed parameter components.

## 5.3 Method 2: Simulation Accuracy Considering Driving Port Admittances

The above procedure (Method I) requires the network equations in state variable (SV) form, which are not easily available in an EMT formulation based on Dommel's approach. Also, the presence of distributed elements does not allow for an SV formulation, without using approximations. However, as seen from Eqn. (5.4) and Eqn. (5.5), the above accuracy analysis method actually only needs the transfer functions such as  $F_o$  and  $F_d$ , which relate each state variable to the excitation and have a large dimension. In this section, instead of using  $F_o$  and  $F_d$ , it will show that if we use the driving point admittance, the accuracy can be quantified directly from the network's netlist data, which makes it applicable to large systems.

### 5.3.1 The Equivalent Admittance Matrix from Boundary Ports

The linear ac system admittance seen from those boundary ports can be used to define an accuracy index. Unlike the transfer functions  $F_o$  and  $F_d$  in Section III.B, which relate all SVs to the applied excitation, this transfer function only relates the port current to the applied port excitation voltage.

A major advantage of this approach is that the transfer function can be easily formed by the well-known network reduction techniques, i.e. without the requirement of state space equations. However, there is a tradeoff. Any mode internal to the network which is not observable from the driving port are not included in the accuracy estimation. In practice, due to the nature of power system structure, the high frequency harmonics from the external excitation usually only transfer locally (near the driving ports), thus those modes are usually not be excited so much from the driving port and hence this is generally not a serious limitation. In the Appendix C, an alternative approach based on modified nodal analysis (MNA) is proposed, where admittance is modified to reflect all the internal modes.

Consider the network  $\mathcal{N}$  shown in Fig. 5-5 in which  $N_b$  represents a multi-phase port with boundary nodes  $N_{b1}, N_{b2} \dots N_{bn}$  connecting to external sources. All non-boundary nodes, e.g.,  $N_{i1}, N_{i2}, N_{i3}$  of the network are referred to as internal nodes.

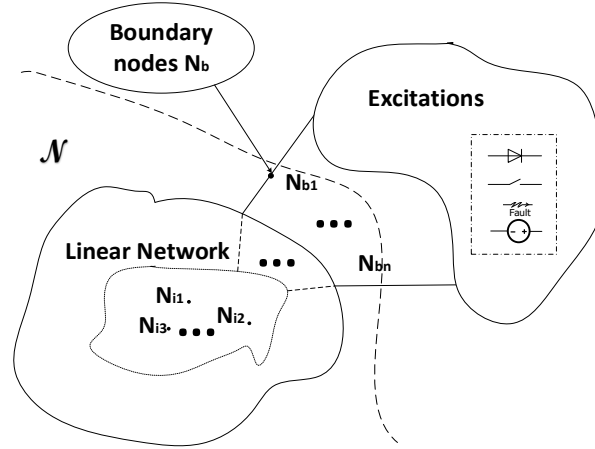


Figure 5-5 Network showing boundary and internal buses

The voltage current relationship for  $\mathcal{N}$  can be described as:

$$\begin{pmatrix} \mathbf{I}_b(s) \\ \mathbf{I}_i(s) \end{pmatrix} = \mathbf{Y}_{\mathcal{N}}(s) \cdot \mathbf{V} = \begin{pmatrix} \mathbf{Y}_{bb}(s) & \mathbf{Y}_{bi}(s) \\ \mathbf{Y}_{bi}^T(s) & \mathbf{Y}_{ii}(s) \end{pmatrix} \cdot \begin{pmatrix} \mathbf{V}_b(s) \\ \mathbf{V}_i(s) \end{pmatrix} \quad (5.7)$$

Where  $\mathbf{V}_b$  and  $\mathbf{V}_i$  are boundary and internal nodes voltages respectively.  $\mathbf{I}_b$  denotes the current vector entering the boundary nodes.  $\mathbf{I}_i$  represents internal currents injections. As all excitation is at external nodes,  $\mathbf{I}_i=0$ .

Applying Gaussian elimination gives the corresponding Norton admittance  $\mathbf{Y}_b$  as seen from the boundary.

$$\mathbf{Y}_b(s) = \mathbf{Y}_{bb}(s) - \mathbf{Y}_{bi}(s) \cdot \mathbf{Y}_{ii}(s)^{-1} \cdot \mathbf{Y}_{bi}^T(s) \quad (5.8)$$

### 5.3.2 Bi-linear Transformation

In equation (5.8), the matrices are functions of frequency. If  $\mathbf{Y}_b(s)$  is a rational function of  $s$ , it can be converted to state equations. However, when distributed parameters, e.g., cable or transmission lines, although  $\mathbf{Y}_b(s)$  can be realized as a function of  $s$ , the

realization is not a rational function, due mainly to the presence of transportation lag. Hence conversion to SVs form is not possible for the real-world system.

EMT type simulations typically use the Trapezoidal method to discretize the system equations. The corresponding  $z$  domain transfer function for the network admittance  $Y_{\mathcal{N}}(s)$  is obtained with a bilinear transformation by replacing  $s$  with  $s \approx \frac{2 \cdot (z-1)}{\Delta t \cdot (z+1)} \equiv s_{TR}(z)$ . Noting  $z = e^{j\omega\Delta t}$ , the final form for the simulated transfer function

can be obtained by replacing the original  $s$  in (5.8) by:

$$s_{TR}(j\omega, \Delta t) \approx \frac{2 \cdot (z-1)}{\Delta t \cdot (z+1)} = \frac{2 \cdot (e^{j\omega\Delta t} - 1)}{\Delta t \cdot (e^{j\omega\Delta t} + 1)} \quad (5.9)$$

With  $s = s_{TR}(j\omega, \Delta t)$  equation (5.8) gives the simulated transfer function  $Y_{bTR}(j\omega, \Delta t)$  as a functions of  $\omega$ .

$$Y_{bTR}(j\omega, \Delta t) = Y_b(s) \Big|_{s=s_{TR}(j\omega, \Delta t)} \quad (5.10)$$

Thus no explicit symbolic algebra is necessary and  $Y_{bTR}(j\omega, \Delta t)$  can be determined at each frequency point. Also, the method is directly modifiable for other integration methods by selecting the applicable transformation instead of the bilinear transformation. The proposed procedure does not require the generation of state space equations and hence is easier to apply to analyze accuracy of large networks.

Unlike previous methods, distributed parameter transmission lines or cables can be included in the accuracy investigation as will be shown later in section 5.4.

### 5.3.3 Simulation Accuracy Spectrum

Using the proposed Method 2, an index for accuracy can be developed. With the  $s$ -domain and discretized admittance matrices  $Y_b(j\omega)$  and  $Y_{bTR}(j\omega, \Delta t)$  as described in Eqn. (5.10), the relative error matrix  $\Delta Y_{eb}(j\omega, \Delta t)$  is formed as in equation (5.11):

$$\Delta \mathbf{Y}_b^{ij}(j\omega, \Delta t) = \frac{|\mathbf{Y}_b^{ij}(j\omega) - \mathbf{Y}_{bTR}^{ij}(j\omega, \Delta t)|}{|\mathbf{Y}_b^{ij}(j\omega)|} \quad (5.11)$$

The closer the simulated system is to the real system, the closer are the value of the elements of  $\Delta \mathbf{Y}_b(j\omega, \Delta t)$  to zero.

In a practical large power system case, the electrical connection among far away nodes might be very small, which makes the denominator of equation (5.11) approach zero, and so the ratio (5.11) becomes numerically non-robust. In order to overcome this limitation, the relative error matrix  $\Delta \mathbf{Y}_{eb}(j\omega, \Delta t)$  is slightly modified as in shown in (5.12), by making the denominator the largest magnitude of the equivalent admittance,  $\max_j(|\mathbf{Y}_b^{ij}(j\omega)|)$ , connected to the  $i^{\text{th}}$  port, instead of just  $|\mathbf{Y}_b^{ij}(j\omega)|$ .

$$\Delta \mathbf{Y}_{bm}^{ij}(j\omega, \Delta t) = \frac{|\mathbf{Y}_b^{ij}(j\omega) - \mathbf{Y}_{bTR}^{ij}(j\omega, \Delta t)|}{\max_j(|\mathbf{Y}_b^{ij}(j\omega)|)} \quad (5.12)$$

Finally, an “*accuracy spectrum*” index is proposed as in equation (5.13) which tracks the largest element in matrix  $\Delta \mathbf{Y}_{bm}(j\omega, \Delta t)$  at each frequency.

$$\mathcal{A}(j\omega, \Delta t) = \max_{i,j} \Delta \mathbf{Y}_{bm}(j\omega, \Delta t)_{ij} \quad (5.13)$$

### 5.3.4 Advantage of the Proposed Index

Compared with previous methods [22, 23], the proposed index considers the complete network (from its driving point) rather than individual components. It is also more easily applicable to large networks compared to Method I described in Section 5.2, as the formation of SV equations is not required.

It is also valuable to notice that the accuracy is measured with respect to a driving point port. Generally speaking, all modes of the circuit are included in the response, except in the case where such modes are not observable. To consider all the modes, the method should be modified as shown in Appendix C.

## 5.4 Consideration of Distributed Parameter Elements

This section discusses the required representation for a discretized distributed transmission line or underground/underwater cable required for accuracy analysis. This has not been considered in earlier accuracy analysis approaches [1, 11].

### 5.4.1 Transmission Line Formulation

Although not directly representable by a rational transfer function (without approximation), a frequency dependent transmission line is nevertheless a linear system and can be represented in frequency domain as indicated in [46] as shown below. Starting from the well known Telegrapher's Equation (5.14):

$$\begin{aligned} -\frac{dV(\omega, x)}{dx} &= Z(\omega) \cdot I(\omega, x) \\ -\frac{dI(\omega, x)}{dx} &= Y(\omega) \cdot V(\omega, x) \end{aligned} \quad (5.14)$$

In (5.14),  $V(\omega, x)$  and  $I(\omega, x)$  are voltage and current in the transmission line at a distance  $x$  along the line.  $Y(\omega)$  and  $Z(\omega)$  are per unit length admittance and impedance. Eqn. (5.14) is *exactly* representable by a frequency dependent model as in Fig 5-6, referred to as an Equivalent PI model [47]:

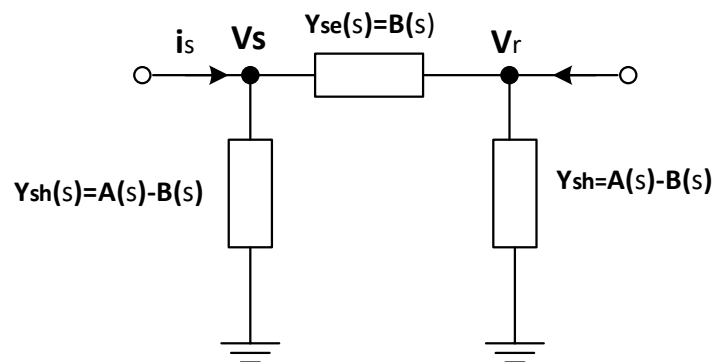


Figure 5-6 Exact PI model of Transmission line

Where:

$$\begin{aligned}
\mathbf{Y}_{SH}(s) &= \mathbf{A}(s) - \mathbf{B}(s), \quad \mathbf{Y}_{SE}(s) = \mathbf{B}(s) \\
\mathbf{A}(s) &= \mathbf{Y}_C(s) \cdot (\mathbf{I} + \mathbf{H}(s)^2) \cdot (\mathbf{I} - \mathbf{H}(s)^2)^{-1} \\
\mathbf{B}(s) &= 2 \cdot \mathbf{Y}_C(s) \cdot \mathbf{H}(s) \cdot (\mathbf{I} - \mathbf{H}(s)^2)^{-1}
\end{aligned}$$

And

(5.15)

$$\begin{aligned}
\mathbf{H}(s) &= e^{-\sqrt{\mathbf{Z}(s) \cdot \mathbf{Y}(s)} \cdot l} \\
\mathbf{Y}_C(s) &= \mathbf{Z}(s)^{-1} \sqrt{\mathbf{Z}(s) \cdot \mathbf{Y}(s)}
\end{aligned}$$

Note that the above representation holds true for multiphase and multi-circuit lines. For example, for a 3-phase line,  $\mathbf{Z}(j\omega)$  and  $\mathbf{Y}(j\omega)$  are  $3 \times 3$  matrices. Equation (5.15) is used to get the theoretical admittance  $\mathbf{Y}_{sh}(s) = \mathbf{A}(s) - \mathbf{B}(s)$  and  $\mathbf{Y}_{se}(j\omega) = \mathbf{B}(j\omega)$ . Similarly, for a double circuit 3-phase line, the matrices would be of dimension  $6 \times 6$ .

#### 5.4.2 Discretized Model in EMT Type Simulation

To implement the frequency dependent model into EMT type simulations of multi-phase and multi-circuit lines, several techniques have been reported in literature. The discussion below considers the Universal Line Model [45] from Morched, Gustavsen, and Tartibi, although, the proposed method is general and can be used to analyze accuracy of other EMT implementations of transmission lines or cables.

In the Universal Line Model (ULM) [45],  $\mathbf{Y}_C(s)$  and  $\mathbf{H}(s)$  in Eqn. (5.15) are approximated respectively by  $\mathbf{Y}_C'(s)$ , which is a rational function of frequency and  $\mathbf{H}'(s)$ , which is a product of a rational function and a fixed travel time delay [45, 48]. For a line with  $N_c$  conductors (or conducting elements):

$$\begin{aligned}
\mathbf{Y}'_c(s)_{mn} &= \sum_{i=1}^{N_{Y_c}} \frac{(c_{Y_{c_i}})_{mn}}{s - (p_{Y_{c_i}})} \\
\mathbf{H}'(s)_{mn} &= \sum_{k=1}^n \left[ \sum_{i=1}^{(N_H)_k} \frac{(c_{H_{ik}})_{mn}}{s - p_{H_{ik}}} \right] \cdot e^{-s\tau_k} \\
m \in \{1, \dots, N_c\}, \quad n \in \{1, \dots, N_c\},
\end{aligned} \tag{5.16}$$

Where  $N_{Y_c}$  and  $(N_H)_k$  are the number of poles for  $\mathbf{Y}'_c(s)$  and the  $k^{\text{th}}$  mode of  $\mathbf{H}'(s)$ , and  $(c_{Y_{c_i}})_{mn}$  and  $(c_{H_{ik}})_{mn}$  are residues.

Subsequently, the rational function parts are included in the EMT simulation environment using the Trapezoidal rule (or other integration method of choice), with the delay part as an actual transportation lag, i.e., all the delay terms are included in the form of history current sources. Applying the bi-linear transformation to the rational function terms only (not to the delay terms  $e^{-s\tau_k}$ , as these are implemented as physical delays and not by modelled by the Trapezoidal rule), the simulated model in the frequency domain can be calculated with the help of equation (5.9) as below :

$$\begin{aligned}
\mathbf{Y}'_c(j\omega, \Delta t)_{mn} &= \sum_{i=1}^{N_{Y_c}} \frac{(c_{Y_{c_i}})_{mn}}{s_{TR}(j\omega, \Delta t) - (p_{Y_{c_i}})} \\
\mathbf{H}'(j\omega, \Delta t)_{mn} &= \sum_{k=1}^n \left[ \sum_{i=1}^{(N_H)_k} \frac{(c_{H_{ik}})_{mn}}{s_{TR}(j\omega, \Delta t) - p_{H_{ik}}} \right] \cdot e^{-j\omega\tau_k}
\end{aligned} \tag{5.17}$$

Substituting the results to (5.15) gives the shunt and series admittances  $\mathbf{Y}_{SH}(j\omega, \Delta t)$  and  $\mathbf{Y}_{SE}(j\omega, \Delta t)$ , which could then be used to find  $\mathbf{Y}_{\mathcal{N}}(s_{TR})$  and subsequently  $\mathbf{Y}_b(s_{TR})$  in equation (5.7) and (5.8). Thus the accuracy of networks with transmission lines or cables can also be determined by the procedure as shown in Section 5.3.

## 5.5 Application of Proposed Method

In this sections, two examples are used to demonstrate the proposed accuracy evaluation method. The first considers a system with a frequency dependent transmission line. Due to its distributed parameter property, state-space equations (and eigenvalues) do not exist for such networks, and hence, previously proposed time constant based approaches [1] are not applicable. The second examples considers the IEEE 39 bus system connecting to a LCC-HVdc network.

### 5.5.1 System with a Distributed Parameter Transmission Line

In EMT type simulations, the frequency dependent transmission line is often modeled by the universal line model (ULM), which uses Vector Fitting [49] with passivity enforcement [50] to approximate the admittance matrix  $\mathbf{Y}_C$  and propagation matrix  $\mathbf{H}$  by rational functions. As passivity enforcement often comes at the expense of some accuracy loss, an important question is how these approximations influence the simulation accuracy. Note the error introduced by approximation and passivity enforcement is usually not predictable as it is the result of a least-squared fitting, it is not possible to quantify the numerical error by traditional truncation error based analysis (in the form of  $O(\Delta t^k)$ ).

Alternatively, the accuracy can be evaluated by the method in this paper. In this section, the EMT model's accuracy is investigated by comparison with an accurate frequency domain formulation as described in Section 5.3 and 5.4. It will be shown that by the proposed method, it is easy to include the effect of a frequency dependent line model in the accuracy evaluation of the network.

A simple example as shown in Fig. 5-7 is presented, in which a 1453.51 km long single-phase frequency dependent transmission line (modeled using ULM [8]) is connected to an RLC circuit.

Parameters for vector fitting  $\mathbf{Y}_C(s)$  and  $\mathbf{H}(s)$  are as in Table 5-1. as below. Three different fitting errors [49] in the vector fitting procedure, 5% and 2% and 0.05% are considered.

Table 5-1 Frequency Dependent Model Parameters

Curve fitting starting frequency	0.05
Curve fitting end frequency	10000
Maximum fitting error for $Y_C(s)$	a) 0.05%, b) 2%, c) 5 %
Maximum fitting error for $H(s)$	a) 0.05%, b) 2%, c) 5%

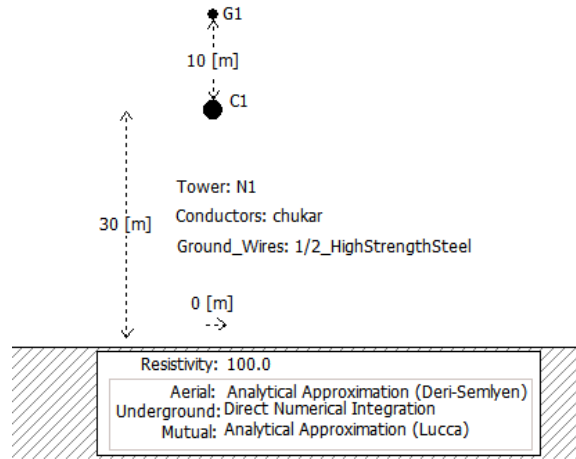
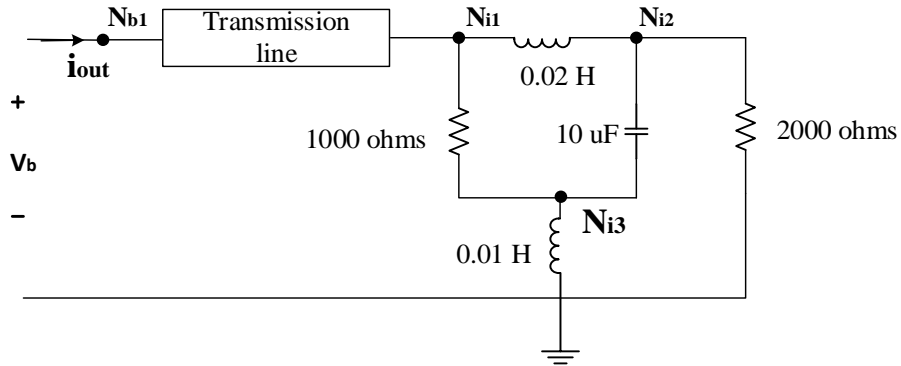


Figure 5-7 Network and transmission line configuration

The corresponding theoretically calculated simulation accuracy spectrum for a time step of  $\Delta t = 10 \mu s$  is shown in Fig. 5-8 for different fitting accuracies as listed in Table 5-1.

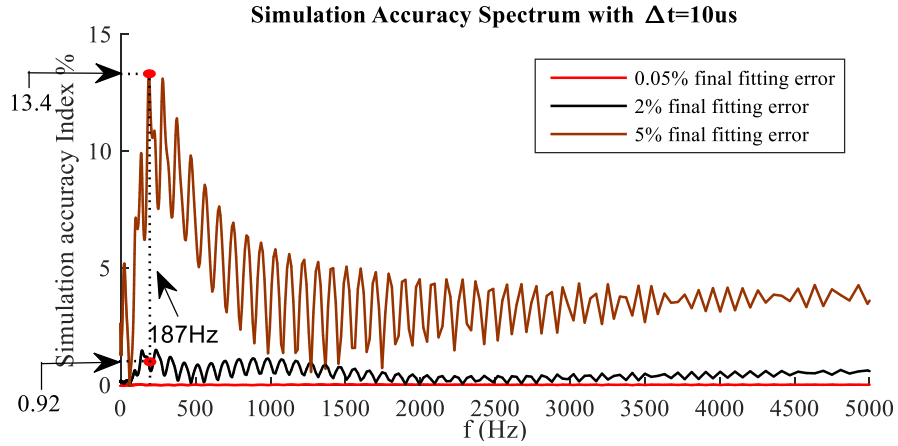


Figure 5-8 Simulation accuracy spectrum with  $\Delta t = 10 \mu s$

From Fig. 5-8, it can be seen that with a 5% fitting error, the maximum inaccuracy in the accuracy spectrum is 13.4% and occurs at 187 Hz. For smaller fitting errors, the accuracy improves, as expected, falling to below 1% for a fitting error of 2 %.

The above theoretically calculated inaccuracy values can be verified using EMT simulation. The ULM transmission line model in the EMT program is as described earlier in Section 5.4 [45]. Fig 5-9 shows the relative difference current  $i_{difference}$  for the 187 Hz excitation between theoretical and simulated values of  $i_{out}$  (as shown in in Fig 5-7).

$$i_{difference} = \frac{i_{out,theory} - i_{out,simulated}}{\max(|i_{out,theory}|)} \quad (5.18)$$

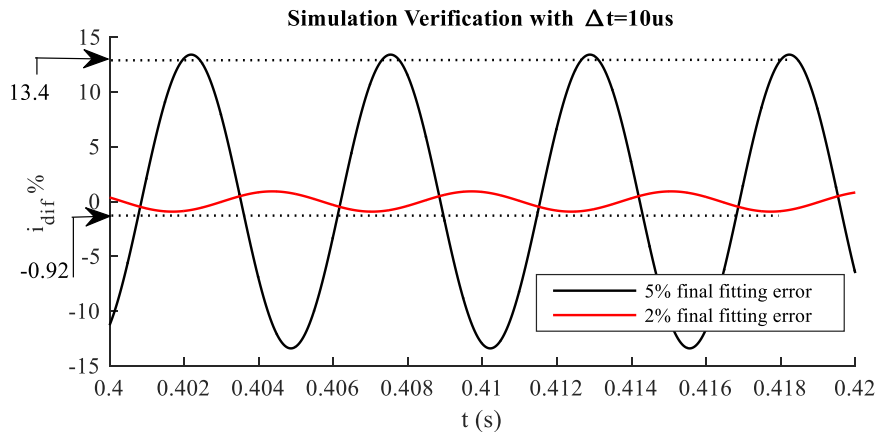


Figure 5-9 Impact of fitting error on simulation (  $\Delta t = 10 \mu s$ )

The plots in Fig. 5-9 are for two different fitting errors, 5% and 2%. For the 5% fitting error, the maximum error is 13.4%, which precisely agrees with the prediction by the theoretically calculated simulation accuracy spectrum in Fig. 5-8. Similarly, for the, 2% fitting error the peak value of  $i_{difference}$  is 0.92%, which also precisely matches with the theoretical simulation accuracy spectrum.

This is as expected, because  $i_{out}$  is the current response at the driving point  $N_{b1}$ , thus  $i_{out}(\omega) = Y_b(\omega) \cdot V_b(\omega)$ . Hence by comparison of (5.18) with (5.12) and (5.13)), the peak value of  $i_{difference}$  is the same as the simulation accuracy index in the corresponding frequency.

In Fig 5-10, the theoretically calculated simulation accuracy spectrum error of two frequency points are shown with time steps of  $10\mu s$ . The fitting accuracy is 2%. Simulation accuracy is measured as with the application of two different excitation signals, one at 194 Hz and the other at 4927 Hz.

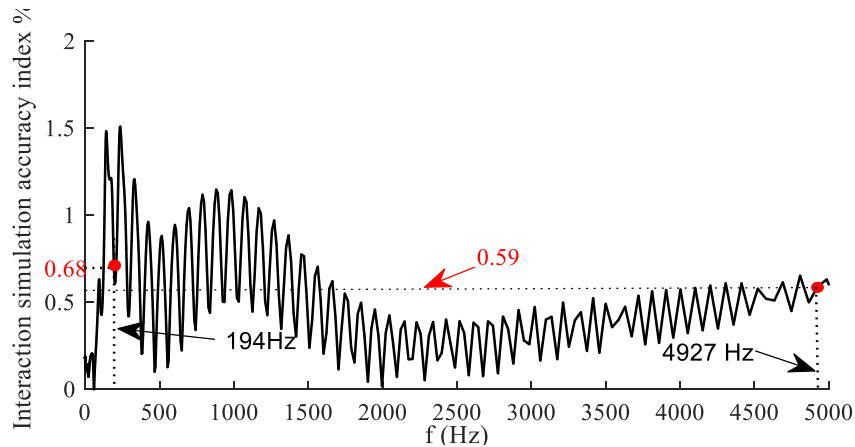


Figure 5-10 Simulation accuracy spectrum with 2% fitting error and  $\Delta t = 10\mu s$

The above conclusion is also observed in the actual EMT simulation. As before, the relative difference current  $i_{difference}$  is shown in Fig. 5-11. With the 194 Hz excitation, the peak of  $i_{difference}$  is 0.68, while at 4927 Hz it is 0.59, again in excellent agreement with the theoretically calculated values in Fig. 5-10.

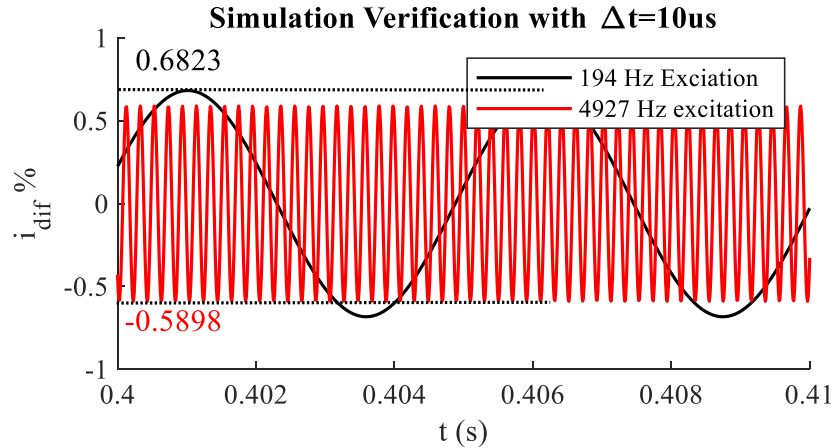


Figure 5-11 EMT simulation verification with different  $\Delta t$

### 5.5.2 Accuracy of EMT Simulation of IEEE 39 BUS System

In this section, the proposed technique is applied to the simulation of a larger system -the IEEE-39 bus system [51]. In this example, the transmission lines are modelled by nominal PI models. This allows the determination of explicit eigenvalues which are not available if the lines are modeled as distributed elements. The purpose of this case was to examine whether the 39-bus network would be modelled accurately enough over the frequency range required when an 12 Pulse LCC-HVdc Converter, which generates low and high frequency harmonics and other transients is connected at the BUS 26 as shown in Fig. 5-12.

The eigenvalues of the network are shown in Fig. 5-13. According to the some earlier research [7], the rule of thumb is to set the simulation time step based on the smallest time constant, which corresponding to largest eigenvalue, i.e.  $-2.3546 \cdot 10^5$ . Following this treatment, one tenth of the smallest time constant would give the simulation time step of  $0.42 \mu s$ . However, as shown below, accuracy spectrum analysis shows that if performance from the driving point is of interest, a much larger time step is sufficient.

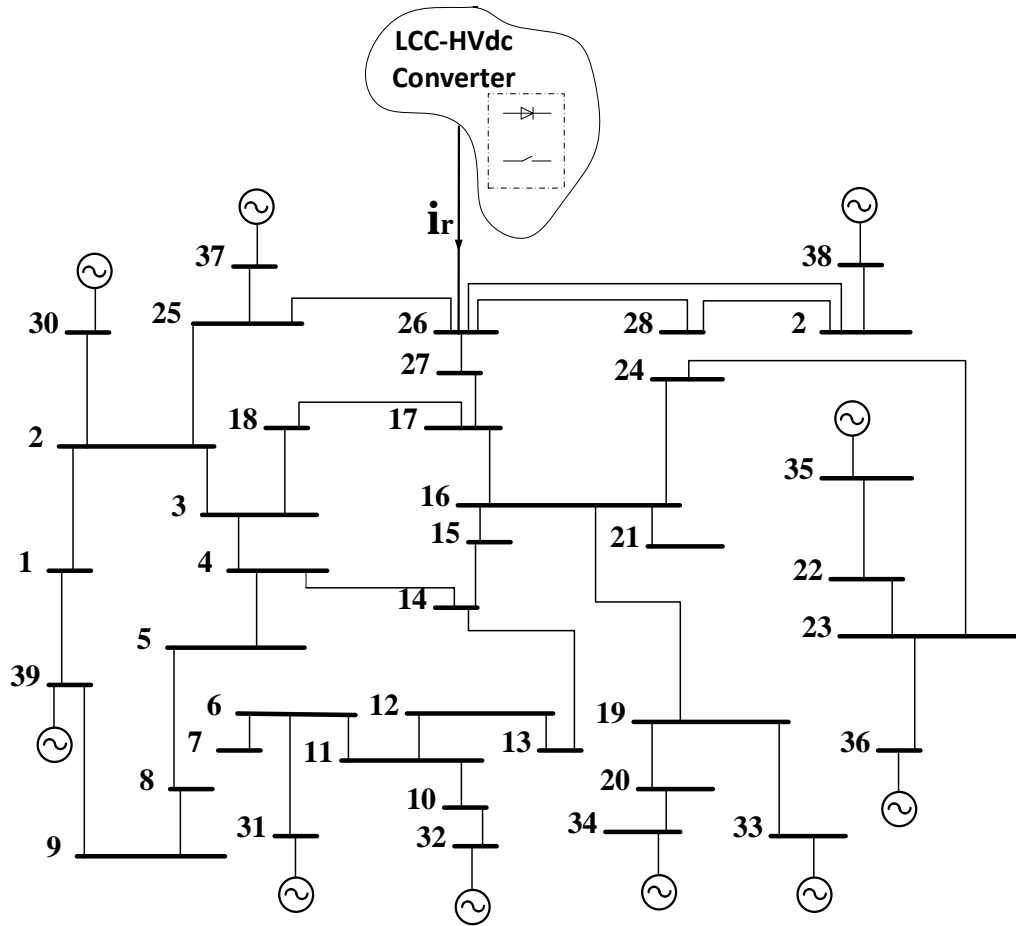


Figure 5-12 Topology of studied system

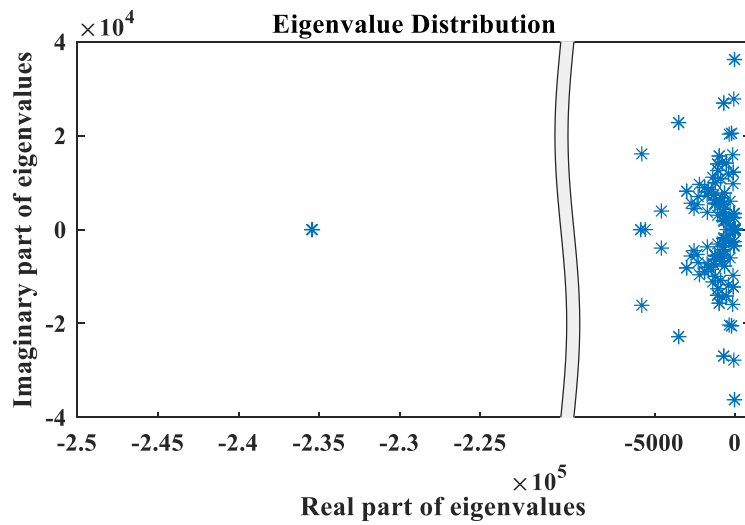


Figure 5-13 Eigenvalue distribution

In practice, the frequency range of interest in such 12 Pulse LCC-HVdc system simulations (particularly on real-time simulators) is in the 0 kHz - 1500 kHz. Fig. 5-14 shows the accuracy spectrum determined by the proposed approach for different time steps. The maximum error is observed in the neighborhood of 1500 Hz. If a maximum error of 2% or less is required, a time step of 8  $\mu$ s would suffice. This is much larger than the 0.42  $\mu$ s time step suggested by using the rule of thumb based on system time constants [7].

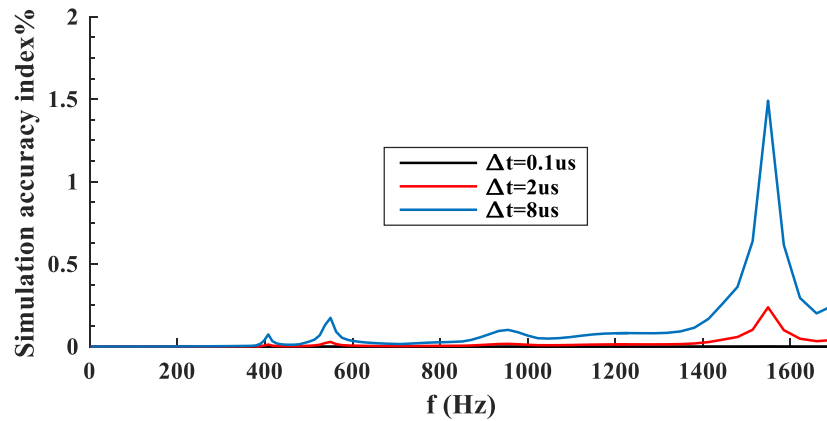


Figure 5-14 Simulation accuracy spectrum

In order to verify whether the frequency spectrum is a good measure of accuracy, a comparison was made with EMT simulation which used timesteps of  $\Delta t = 0.1\mu$ s and  $\Delta t = 8\mu$ s. At  $t = 1.3$  s, a dc fault is applied, and cleared by force retarding the HVdc converter. Normal operation is resumed 75 ms later. The corresponding simulation result of BUS 26 Phase A voltage and current response  $i_r$ . Phase A current are shown in Fig. 5-15, with a simulation time step of  $0.1\mu$ s and  $8\mu$ s. It can be clearly observed that there is no visible difference between the simulation time step of  $0.1\mu$ s and  $8\mu$ s even in the transient period, which confirms that the simulation time step is small enough.

Note the simulation time step predicted by the proposed method is significantly larger than the one from the time constant based method. This is because although the very fast modes do exist in the internal system (as evinced from the eigenvalue plot), such modes

are at least not observable from the driving ports, and hence are not reflected in the accuracy spectrum.

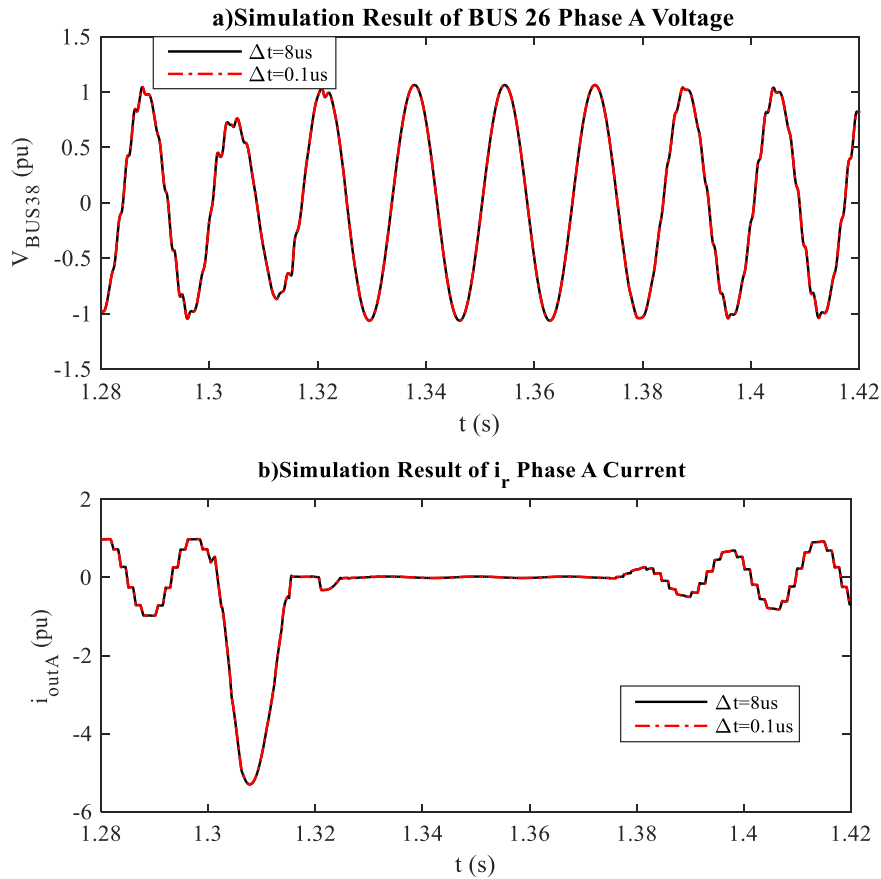


Figure 5-15 Simulation validation

## 5.6 Chapter Summary

In this chapter, a novel technique is proposed to assess the accuracy of electro-magnetic transient simulations for practical power systems.

Firstly, a simple lumped circuit example is used to show the limitation of individual element based numerical accuracy evaluation. In order to fill this gap, section 5.2 proposed a state space equations based method to globally evaluate the accuracy of electro-magnetic transient simulations. Analysis shows that the accuracy may vary with frequency and time

step, and it is not always the case that for a given timestep, the accuracy at low frequencies is better than at high frequencies. For application in larger systems, a simulation accuracy spectrum is introduced which examines the accuracy from the network's driving point. The approach is also shown to be viable to analyze the accuracy of distributed element systems such as frequency-dependent transmission lines, which cannot be handled by state-variable based approaches. The proposed approaches are validated by two EMT simulation examples.

## 6 Concluding Remarks and Future Work

### 6.1 Summary of Results

In this thesis, a set of novel methods were developed to evaluate the numerical stability and accuracy of electromagnetic transient simulations. The main contribution can be summarized as below:

1. In order to adapt the existing stability analysis techniques for analyzing the stability of companion circuit based electromagnetic transient simulation, firstly, the equivalency of state space equations models and electromagnetic companion circuit methods was mathematically proved. Using this powerful theorem, for any linear RLCM circuit, the stability conclusions obtained by state space formulation can be directly applied to a companion circuit model based simulation.
2. Next, Common Quadratic Lyapunov Function (CQLF) theory was adopted to analyse the numerical stability of lumped switched network simulations, with bi-valued resistive switches. Using rigorous analysis, it was shown by counterexamples that Trapezoidal and Backward Euler method do not always result in stable simulations of such systems, even when the original real-world system is stable. This conclusion is different from that for the simulation of lumped linear (non-switched) systems, which always have a stable simulation under Trapezoidal and BE.
3. The additional requirement that every switching state be strictly passive was shown to be a sufficient condition for Bounded Input Bounded Output (BIBO) stability of the simulation of lumped switched networks by Trapezoidal and Backward Euler methods. It was also shown that if non-linear inductor or resistors are represented by a set of parallel switched inductors or resistors, the simulation falls into the category of a passive circuits with bi-valued switches, and thus the conclusions derived for the stability of LSPSC simulation, become automatically applicable.

4. Interpolation and Critical Damping Adjustment (CDA) are methods used in literature to prevent numerical oscillation. Interpolation is also used to more accurately reflect the switching instant if it falls between time steps. Using CQLF theory, the thesis showed that the widely used strategies such as linear interpolation and CDA always result a stable simulation if the original switched system is strictly passive in all switching states. It is also shown that the developed approach can be used to determine the stability of other practical interpolation and extrapolation methods in simulation.
  
5. Methods for accuracy analysis of electromagnetic simulations were developed, which, unlike previous approaches, consider the entire circuit as opposed to individual elements. The results show that simulation accuracy at low frequencies is sometimes poorer than at high frequency thus the proposed method is necessary for proper evaluating the accuracy of power network simulations. Furthermore, if only the accuracy at a given set of driving points was of interest, a more convenient approach was developed which did not require formation of state space equations and consequently could be used for large networks. The method was also adopted to include networks containing distributed parameter transmission lines or cables.

## 6.2 Publications Resulting from the Thesis

The following journal and conference papers resulted from the research in this thesis:

1. H. Zhao, S. Fan, and A. M. Gole, "Stability of Algorithms for Electro-Magnetic-Transient Simulation of Networks with Switches and Non-linear Inductors," in **IEEE Transactions on Power Delivery**, vol. 35, no. 1, pp.377-385, Feb. 2020.
2. H. Zhao, S. Fan, and A. M. Gole, " Stability Evaluation of Interpolation, Extrapolation, and Numerical Oscillation Damping Methods Applied in EMT Simulation of Power Networks with Switching Transients," to be published in **IEEE Transactions on Power Delivery (accepted July 2020)**

3. H. Zhao, S. Fan, and A. M. Gole, "Equivalency of State Space Models and EMT Companion Circuit Models," *International Conference on Power Systems Transients (IPST)*, Perpignan, France, June 16-20, 2019.
4. H. Zhao, Yi Zhang, and A. M. Gole, "Accuracy Evaluation of Electromagnetic Transients Simulation," under preparation for *IEEE Transactions on Power Delivery*

### 6.3 Future Work

There still exist several valuable topics for further research, which are shortly summarized as below:

**Extension to Analysis of Stability of Other Numerical Algorithms:** In this thesis, the numerical stability analysis is demonstrated with the Trapezoidal rule (the most widely used algorithm in commercial EMT packages) and BE as typical examples. However, the methodology proposed in this thesis is general and could be extendable to analyze other numerical algorithms, e.g. 2S-Dirk.

**Analyzing the Stability and Accuracy of Multi-rate Simulation:** In order to accurately represent the non-linear characteristic of the power electronics, a very small simulation time step in the order of 1-10  $\mu\text{s}$  is usually required. However, if the entire system is modeled with this small time step without recourse to system reduction, the computation burden become excessive when the external ac network is very large. In order to reduce the computation, the system is split into slow and fast subsystems and uses large and small time steps for slow-varying and fast-varying subsystems respectively [52-54]. Further extending the technique proposed in this thesis to study the stability and accuracy of such system is a valuable research topic.

**Developing Better Interface for Multi-rate Simulation:** Furthermore, a special interface [52] is required to decouple the slow and fast subsystems in Multi-rate simulations. Based on the stability and accuracy analysis, it might be possible to design a more robust and accurate interface for such simulations.

**Efficient and Robust Simulation of Very Large Power System:** In general, the simulation of very large ac networks is computational expensive. However, as shown in the accuracy analysis, the interested phenomenon only required a limited frequency range. It will be valuable to develop new technique by considering this fact to reduce the computation burden.

## References

- [1] H. W. Dommel, *Electromagnetic transients program (EMTP) theory book*: Bonneville Power Administration, 1986.
- [2] H. W. Dommel, "Digital Computer Solution of Electromagnetic Transients in Single- and Multiphase Networks," *IEEE Transactions on Power Apparatus and Systems*, vol. PAS-88, pp. 388-399, 1969.
- [3] N. Balabanian, S. Seshu, and T. A. Bickart, "Electrical network theory," 1969.
- [4] A.-R. Sana, J. Mahseredjian, X. Dai-Do, and H. Dommel, "Treatment of discontinuities in time-domain simulation of switched networks," *Mathematics and computers in simulation*, vol. 38, pp. 377-387, 1995.
- [5] J. Mahseredjian, V. Dinavahi, and J. A. Martinez, "Simulation Tools for Electromagnetic Transients in Power Systems: Overview and Challenges," *IEEE Transactions on Power Delivery*, vol. 24, pp. 1657-1669, 2009.
- [6] L. O. Chua, *Computer-aided analysis of electronic circuits : algorithms and computational techniques / Leon O. Chua, Pen-Min Lin*. Englewood Cliffs, N.J.: Englewood Cliffs, N.J. : Prentice-Hall, 1975.
- [7] N. Watson, J. Arrillaga, and J. Arrillaga, *Power systems electromagnetic transients simulation* vol. 39: 1st, 2003.
- [8] B. Brogliato, *Dissipative Systems Analysis and Control Theory and Applications*, 2nd Edition.. ed.: London : Springer London : Imprint: Springer, 2006.
- [9] J. A. Hollman and J. R. Marti, "Step-by-step eigenvalue analysis with EMTP discrete-time solutions," *IEEE Transactions on Power Systems*, vol. 25, pp. 1220-1231, 2010.
- [10] H. Zhao, S. Fan, and A. M. Gole, "Stability of Algorithms for Electro-Magnetic-Transient Simulation of Networks with Switches and Non-linear Inductors," *IEEE Transactions on Power Delivery*, 2019.
- [11] J. Tant and J. Driesen, "On the Numerical Accuracy of Electromagnetic Transient Simulation with Power Electronics," *IEEE Transactions on Power Delivery*, vol. PP, pp. 1-1, 2018.
- [12] L. Hai and P. J. Antsaklis, "Stability and Stabilizability of Switched Linear Systems: A Survey of Recent Results," *Automatic Control, IEEE Transactions on*, vol. 54, pp. 308-322, 2009.
- [13] G. Michaletzky and L. Gerencser, "BIBO stability of linear switching systems," *Automatic Control, IEEE Transactions on*, vol. 47, pp. 1895-1898, 2002.
- [14] R. N. Shorten and K. S. Narendra, "On the stability and existence of common Lyapunov functions for stable linear switching systems," in *Proceedings of the 37th IEEE Conference on Decision and Control (Cat. No.98CH36171)*, 1998, pp. 3723-3724 vol.4.

- [15] J. Zhao and D. J. Hill, "A notion of passivity for switched systems with state-dependent switching," *Journal of control theory and applications*, vol. 4, pp. 70-75, 2006.
- [16] M. Zefran, F. Bullo, and M. Stein, "A notion of passivity for hybrid systems," vol. 1, ed. USA, 2001, pp. 768-773.
- [17] D. Liberzon and A. S. Morse, "Basic problems in stability and design of switched systems," *IEEE Control Systems*, vol. 19, pp. 59-70, 1999.
- [18] K. Krueger and R. Lasseter, "HVDC simulation using NETOMAC," *IEEE Montech'86*, 1986.
- [19] A. Gole, "Modeling of power electronic apparatus: Additional interpolation issues," *IPST'97*, pp. 23-28, 1997.
- [20] T. Noda and A. Ametani, "XTAP," in *Numerical analysis of power system transients and dynamics*, ed: IET, 2014, pp. 169-208.
- [21] G. Irwin, D. Woodford, and A. Gole, "Precision simulation of PWM controllers," in *Proc. of IPST (International Power Systems Transients) conference*, 2001.
- [22] J. R. Marti and J. Lin, "Suppression of numerical oscillations in the EMT power systems," *IEEE Transactions on Power Systems*, vol. 4, pp. 739-747, 1989.
- [23] K. Strunz, "Position-dependent control of numerical integration in circuit simulation," *IEEE Transactions on Circuits and Systems II: Express Briefs*, vol. 51, pp. 561-565, 2004.
- [24] J. Mahseredjian, S. Denetière, L. Dubé, B. Khodabakhchian, and L. Gérin-Lajoie, "On a new approach for the simulation of transients in power systems," *Electric power systems research*, vol. 77, pp. 1514-1520, 2007.
- [25] T. Noda, K. Takenaka, and T. Inoue, "Numerical Integration by the 2-Stage Diagonally Implicit Runge-Kutta Method for Electromagnetic Transient Simulations," *IEEE Transactions on Power Delivery*, vol. 24, pp. 390-399, 2009.
- [26] C. WG33, "Guide lines for Representation of Network Elements when Calculating Transients," *CIGRE Technical Brochure*, 1990.
- [27] H. Zhao, S. Fan, and A. M. Gole, "Equivalency of State Space Models and EMT Companion Circuit Models," presented at the Proc. of IPST (International Power Systems Transients) conference, Perpignan, France 2019.
- [28] Q. Chen, S. Weng, and C. Cheng, "A Practical Regularization Technique for Modified Nodal Analysis in Large-Scale Time-Domain Circuit Simulation," *IEEE Transactions on Computer-Aided Design of Integrated Circuits and Systems*, vol. 31, pp. 1031-1040, 2012.
- [29] R. K. H. Galvão, K. H. Kienitz, and S. Hadjiloucas, "Conversion of descriptor representations to state-space form: an extension of the shuffle algorithm," *International Journal of Control*, vol. 91, pp. 2199-2213, 2018.
- [30] H. Chung-Wen, A. Ruehli, and P. Brennan, "The modified nodal approach to network analysis," *IEEE Transactions on Circuits and Systems*, vol. 22, pp. 504-509, 1975.

- [31] P. Misra, P. Van Dooren, and V. Syrmos, "Pole-zero representation of descriptor systems," *Automatica*, vol. 31, pp. 907-912, 1995.
- [32] G. H. Golub and C. F. Van Loan, *Matrix computations* vol. 3: JHU Press, 2012.
- [33] H. K. Khalil, "Nonlinear systems. 2002," *ISBN*, vol. 130673897, p. 9780130673893, 2002.
- [34] J. C. Geromel, P. Colaneri, and P. Bolzern, "Passivity of switched linear systems: Analysis and control design," *Systems & Control Letters*, vol. 61, pp. 549-554, 2012.
- [35] D. S. Bernstein, *Matrix mathematics : theory, facts, and formulas*, 2nd ed.. ed. Princeton, N.J.: Princeton, N.J. : Princeton University Press, 2009.
- [36] D. Shu, X. Xie, S. Zhang, and Q. Jiang, "Hybrid method for numerical oscillation suppression based on rational-fraction approximations to exponential functions," *IET Generation, Transmission & Distribution*, vol. 10, pp. 2825-2832, 2016.
- [37] T. L. Maguire and A. M. Gole, "Digital simulation of flexible topology power electronic apparatus in power systems," *IEEE Transactions on Power Delivery*, vol. 6, pp. 1831-1840, 1991.
- [38] M. Vakilian and R. C. Degeneff, "A method for modeling nonlinear core characteristics of transformers during transients," *Power Delivery, IEEE Transactions on*, vol. 9, pp. 1916-1925, 1994.
- [39] H. W. Dommel, "Transformer models in the simulation of electromagnetic transients," in *Proc. 5th power systems computation conference*, 1975, pp. 1-5.
- [40] C. Muller, "User's Guide on the Use of PSCAD," *Manitoba, Canada: Manitoba HVDC Research Centre*, 2010.
- [41] K. Strunz, "Flexible numerical integration for efficient representation of switching in real time electromagnetic transients Simulation," *IEEE Transactions on Power Delivery*, vol. 19, pp. 1276-1283, 2004.
- [42] M. O. Faruque, V. Dinavahi, and X. Wilsun, "Algorithms for the accounting of multiple switching events in digital simulation of power-electronic systems," *IEEE Transactions on Power Delivery*, vol. 20, pp. 1157-1167, 2005.
- [43] A. M. Gole, "Power Systems Transient Simulation," 1998.
- [44] J. R. Marti, "Accurate Modelling of Frequency-Dependent Transmission Lines in Electromagnetic Transient Simulations," *IEEE Transactions on Power Apparatus and Systems*, vol. PAS-101, pp. 147-157, 1982.
- [45] A. Morched, B. Gustavsen, and M. Tartibi, "A universal model for accurate calculation of electromagnetic transients on overhead lines and underground cables," *IEEE Transactions on Power Delivery*, vol. 14, pp. 1032-1038, 1999.
- [46] B. Gustavsen, "Passivity Enforcement for Transmission Line Models Based on the Method of Characteristics," *IEEE Transactions on Power Delivery*, vol. 23, pp. 2286-2293, 2008.
- [47] A. Tavighi, J. R. Martí, V. A. Galván, and J. A. Gutierrez-Robles, "Time-Window-Based Discrete-Time Fourier Series for Electromagnetic Transients in Power Systems," *IEEE Transactions on Power Delivery*, vol. 33, pp. 2551-2561, 2018.

- [48] B. Gustavsen and A. Semlyen, "Simulation of transmission line transients using vector fitting and modal decomposition," *IEEE Transactions on Power Delivery*, vol. 13, pp. 605-614, 1998.
- [49] B. Gustavsen and A. Semlyen, "Rational approximation of frequency domain responses by vector fitting," *IEEE Transactions on power delivery*, vol. 14, pp. 1052-1061, 1999.
- [50] B. Gustavsen and A. Semlyen, "Enforcing passivity for admittance matrices approximated by rational functions," *IEEE Transactions on Power Systems*, vol. 16, pp. 97-104, 2001.
- [51] I. Hiskens, "IEEE PES task force on benchmark systems for stability controls," *IEEE PES, New Jersey, USA*, pp. 1-23, 2013.
- [52] T. Maguire, I. Park, and P. Forsyth, "An Interface Technique for Multi-rate EMT Simulations."
- [53] A. Semlyen and F. De Leon, "Computation of electromagnetic transients using dual or multiple time steps," *IEEE Transactions on Power Systems*, vol. 8, pp. 1274-1281, 1993.
- [54] F. A. Moreira and J. R. Martí, "Latency techniques for time-domain power system transients simulation," *IEEE transactions on Power Systems*, vol. 20, pp. 246-253, 2005.

## Appendix A – Matrix commutation relation proof

Assuming matrix  $\mathbf{A}$  can be represented as below:

$$\mathbf{A} = \mathbf{T} \cdot \mathbf{J} \cdot \mathbf{T}^{-1} \quad (\text{A.1})$$

where:

$$\mathbf{J} = \begin{bmatrix} \mathbf{J}_1 & \cdots & \mathbf{0} \\ \vdots & \ddots & \vdots \\ \mathbf{0} & \cdots & \mathbf{J}_n \end{bmatrix}$$

And  $\mathbf{J}_i$  is Jordan Block.

As a result, we could have:

$$\mathbf{I} + \frac{\mathbf{A}}{2} = \mathbf{T} \cdot \left( \frac{1}{2} \cdot \mathbf{J} + \mathbf{I} \right) \cdot \mathbf{T}^{-1} \quad (\text{A.2})$$

and

$$\begin{aligned} \left( \mathbf{I} - \frac{\mathbf{A}}{2} \right)^{-1} &= \left( \mathbf{T} \cdot \left( \mathbf{I} - \frac{1}{2} \cdot \mathbf{J} \right) \cdot \mathbf{T}^{-1} \right)^{-1} \\ &= \mathbf{T} \cdot \left( \mathbf{I} - \frac{1}{2} \cdot \mathbf{J} \right)^{-1} \cdot \mathbf{T}^{-1} \end{aligned} \quad (\text{A.3})$$

where  $\mathbf{I}$  is a Identity matrix.

Their product gives:

$$\begin{aligned} &\left( \mathbf{I} + \frac{\mathbf{A}}{2} \right) \cdot \left( \mathbf{I} - \frac{\mathbf{A}}{2} \right)^{-1} \\ &= \mathbf{T} \cdot \left( \frac{1}{2} \cdot \mathbf{J} + \mathbf{I} \right) \cdot \mathbf{T}^{-1} \cdot \mathbf{T} \cdot \left( \mathbf{I} - \frac{1}{2} \cdot \mathbf{J} \right)^{-1} \cdot \mathbf{T}^{-1} \\ &= \mathbf{T} \cdot \left( \frac{1}{2} \cdot \mathbf{J} + \mathbf{I} \right) \cdot \left( \mathbf{I} - \frac{1}{2} \cdot \mathbf{J} \right)^{-1} \cdot \mathbf{T}^{-1} \end{aligned} \quad (\text{A.4})$$

Since for each Jordan Block  $\mathbf{J}_i$ :

$$\frac{1}{2} \cdot J_i + I = \begin{bmatrix} \frac{\lambda_i}{2} + 1 & 1 & \dots & 0 \\ 0 & \frac{\lambda_i}{2} + 1 & \dots & \vdots \\ \vdots & \vdots & \ddots & \vdots \\ 0 & \dots & \frac{\lambda_i}{2} + 1 & 1 \\ & & 0 & \frac{\lambda_i}{2} + 1 \end{bmatrix} \equiv M \quad (\text{A.5})$$

and

$$(I - \frac{1}{2} \cdot J_i)^{-1} = \begin{bmatrix} \frac{1}{1 - \frac{\lambda_i}{2}} & \frac{-1}{(1 - \frac{\lambda_i}{2})^2} & \dots & \frac{(-1)^{n-2}}{(1 - \frac{\lambda_i}{2})^{n-1}} & \frac{(-1)^{n-1}}{(1 - \frac{\lambda_i}{2})^n} \\ 0 & \frac{1}{1 - \frac{\lambda_i}{2}} & \dots & \frac{(-1)^{n-3}}{(1 - \frac{\lambda_i}{2})^{n-2}} & \frac{(-1)^{n-2}}{(1 - \frac{\lambda_i}{2})^{n-1}} \\ \vdots & \vdots & \ddots & \vdots & \vdots \\ 0 & \dots & \dots & \frac{1}{1 - \frac{\lambda_i}{2}} & \frac{-1}{(1 - \frac{\lambda_i}{2})^2} \\ & & & 0 & \frac{1}{1 - \frac{\lambda_i}{2}} \end{bmatrix} \equiv M' \quad (\text{A.6})$$

Thus:

$$\begin{aligned} & \left( \frac{1}{2} \cdot J_i + I \right) \cdot (I - \frac{1}{2} \cdot J_i)^{-1} \\ = & \begin{bmatrix} \frac{\lambda_i}{2} + 1 & 1 & \dots & 0 \\ 0 & \frac{\lambda_i}{2} + 1 & \dots & \vdots \\ \vdots & \vdots & \ddots & \vdots \\ 0 & \dots & \frac{\lambda_i}{2} + 1 & 1 \\ & & 0 & \frac{\lambda_i}{2} + 1 \end{bmatrix} \cdot \begin{bmatrix} \frac{1}{1 - \frac{\lambda_i}{2}} & \frac{-1}{(1 - \frac{\lambda_i}{2})^2} & \dots & \frac{(-1)^{n-2}}{(1 - \frac{\lambda_i}{2})^{n-1}} & \frac{(-1)^{n-1}}{(1 - \frac{\lambda_i}{2})^n} \\ 0 & \frac{1}{1 - \frac{\lambda_i}{2}} & \dots & \frac{(-1)^{n-3}}{(1 - \frac{\lambda_i}{2})^{n-2}} & \frac{(-1)^{n-2}}{(1 - \frac{\lambda_i}{2})^{n-1}} \\ \vdots & \vdots & \ddots & \vdots & \vdots \\ 0 & \dots & \dots & \frac{1}{1 - \frac{\lambda_i}{2}} & \frac{-1}{(1 - \frac{\lambda_i}{2})^2} \\ & & & 0 & \frac{1}{1 - \frac{\lambda_i}{2}} \end{bmatrix} \quad (\text{A.7}) \end{aligned}$$

$$\equiv \mathbf{K}$$

where:

$$K_{xy} = \sum_{k=1}^n \mathbf{M}_{xk} \cdot \mathbf{M}'_{ky}$$

Since only  $\mathbf{M}_{xx}$  and  $\mathbf{M}_{x(x+1)}$  are not 0 in  $x^{\text{th}}$  row:

$$K_{xy} = \left(\frac{\lambda_i}{2} + 1\right) \cdot \mathbf{M}'_{xy} + \mathbf{M}'_{(x+1)y} \quad (\text{A.8})$$

Similarly:

$$\begin{aligned} & \left(\mathbf{I} - \frac{1}{2} \cdot \mathbf{J}_i\right)^{-1} \cdot \left(\frac{1}{2} \cdot \mathbf{J}_i + \mathbf{I}\right) \\ = & \begin{bmatrix} \frac{1}{1-\frac{\lambda_i}{2}} & \frac{-1}{(1-\frac{\lambda_i}{2})^2} & \dots & \frac{(-1)^{n-2}}{(1-\frac{\lambda_i}{2})^{n-1}} & \frac{(-1)^{n-1}}{(1-\frac{\lambda_i}{2})^n} \\ \mathbf{0} & \frac{1}{1-\frac{\lambda_i}{2}} & \dots & \frac{(-1)^{n-3}}{(1-\frac{\lambda_i}{2})^{n-2}} & \frac{(-1)^{n-2}}{(1-\frac{\lambda_i}{2})^{n-1}} \\ \vdots & \vdots & \ddots & \vdots & \vdots \\ \mathbf{0} & \dots & \frac{1}{1-\frac{\lambda_i}{2}} & \frac{-1}{(1-\frac{\lambda_i}{2})^2} & \frac{1}{1-\frac{\lambda_i}{2}} \\ \mathbf{0} & \dots & \mathbf{0} & \frac{1}{1-\frac{\lambda_i}{2}} & \mathbf{0} \end{bmatrix} \cdot \begin{bmatrix} \frac{\lambda_i}{2} + 1 & \mathbf{1} & \dots & \mathbf{0} \\ \mathbf{0} & \frac{\lambda_i}{2} + 1 & \dots & \mathbf{0} \\ \vdots & \vdots & \ddots & \vdots \\ \mathbf{0} & \dots & \frac{\lambda_i}{2} + 1 & \mathbf{1} \\ \mathbf{0} & \dots & \mathbf{0} & \frac{\lambda_i}{2} + 1 \end{bmatrix} \quad (\text{A.9}) \\ & \equiv \mathbf{K}' \end{aligned}$$

where

$$K'_{xy} = \sum_{k=1}^n \mathbf{M}'_{xk} \cdot \mathbf{M}_{ky}$$

Due to the fact that only  $\mathbf{M}_{yy}$  and  $\mathbf{M}_{(y-1)y}$  are not 0 in  $y^{\text{th}}$  column

$$= \mathbf{M}'_{x(y-1)} + \mathbf{M}'_{xy} \cdot \left(\frac{\lambda_i}{2} + 1\right)$$

Due to the fact of  $(y-1) - x = y - (x+1)$ ,  $\mathbf{M}'_{x(y-1)} = \mathbf{M}'_{(x+1)y}$ . Therefore:

$$\mathbf{K}' = \mathbf{K} \quad (\text{A.10})$$

Since all Jordan blocks follows this rule, the whole equation can be rewritten as:

$$\begin{aligned}
& \left(I + \frac{A}{2}\right) \cdot \left(I - \frac{A}{2}\right)^{-1} \\
&= T \cdot \left(\frac{1}{2} \cdot J + I\right) \cdot \left(I - \frac{1}{2} \cdot J\right)^{-1} \cdot T^{-1} \\
&= T \cdot \left(I - \frac{1}{2} \cdot J\right)^{-1} \cdot \left(\frac{1}{2} \cdot J + I\right) \cdot T^{-1} \\
&= \left(I - \frac{A}{2}\right)^{-1} \cdot \left(I + \frac{A}{2}\right) \tag{A.11}
\end{aligned}$$

Q.E.D.

## Appendix B – Stability of Instantaneous Solution Interpolation

The stability of instantaneous solution interpolation is analyzed below. The strategy used in the paper is followed, i.e., the stability of the autonomous system is investigated from which the BIBO stability of the non-autonomous system automatically follows as proved in [13].

Assume the activated switching state is changed from  $m_0$  to  $m_1$  at  $t = t_0$  where  $m_0$  and  $m_1 \in \{1, 2 \dots 2^s\}c$ . In the instantaneous interpolation method, the system matrices before and after the switching are different. The solution at  $t_{0+}$  is modified from that at  $t_{0-}$  using equation (A1), which uses two different state matrices  $A_{m_0}$  and  $A_{m_1}$ . The reference shows that using this procedure reduces spurious power loss.

$$\mathbf{x}(t_{0+}) = \mathbf{x}(t_{0-}) + \frac{A_{m_1} \cdot \mathbf{x}(t_{0+}) + A_{m_0} \cdot \mathbf{x}(t_{0-})}{2} \cdot \Delta t \quad (\text{B.1})$$

Collecting the terms with  $\mathbf{x}(t_{0+})$  on the left-hand side and inverting the resulting left-hand side matrix gives:

$$\mathbf{x}(t_{0+}) = \left( \mathbf{I} - \frac{A_{m_1}}{2} \cdot \Delta t_{TR} \right)^{-1} \cdot \left( \mathbf{I} + \frac{A_{m_0}}{2} \cdot \Delta t_{TR} \right) \cdot \mathbf{x}(t_{0-}) \quad (\text{B.2})$$

If the circuit only has this single switching event and subsequently stays in state  $m_1$ , this is equivalent to a (Trapezoidal rule based) simulation of an LTI system with state matrix  $A_{m_1}$ . As state  $m_1$  is strictly passive, the simulation will be stable.

Now consider switching to another state  $m_2$  at time  $t_1$  after  $n_1$  time steps, i.e.,  $t_1 = t_0 + n_1 \cdot \Delta t$ . We are assuming a precise switching on the time step so that interpolation is not required in order to simplify the proof, but it can be shown to be true even if interpolation were used.

$$\mathbf{x}(t_{1+}) = \left( \mathbf{I} - \frac{A_{m_2}}{2} \cdot \Delta t_{TR} \right)^{-1} \cdot \left( \mathbf{I} + \frac{A_{m_1}}{2} \cdot \Delta t_{TR} \right) \cdot \mathbf{x}(t_{1-}) \quad (\text{B.3})$$

Hence the relationship between  $\mathbf{x}(t_{1+})$  and  $\mathbf{x}(t_{0-})$  can be described below:

$$\mathbf{x}(t_{1+}) = \left( \mathbf{I} - \frac{A_{m_2}}{2} \cdot \Delta t_{TR} \right)^{-1} \cdot \left( \mathbf{I} + \frac{A_{m_1}}{2} \cdot \Delta t_{TR} \right) \cdot \mathbf{G}_{TR_{m_1}}^{n_1} \cdot \left( \mathbf{I} - \frac{A_{m_1}}{2} \cdot \Delta t_{TR} \right)^{-1} \cdot \left( \mathbf{I} + \frac{A_{m_0}}{2} \cdot \Delta t_{TR} \right) \cdot \mathbf{x}(t_{0-}) \quad (\text{B.4})$$

Note that in [21], the Trapezoidal method is used so  $\mathbf{G}_{TR_{m_1}} = \left( \mathbf{I} - \frac{A_{m_1}}{2} \cdot \Delta t_{TR} \right)^{-1} \cdot \left( \mathbf{I} + \frac{A_{m_1}}{2} \cdot \Delta t_{TR} \right)$ .

Also, it can be shown that the following commutation relation applies:

$$\begin{aligned} & \left( \mathbf{I} - \frac{A_{m_1}}{2} \cdot \Delta t_{TR} \right)^{-1} \cdot \left( \mathbf{I} + \frac{A_{m_1}}{2} \cdot \Delta t_{TR} \right) \\ &= \left( \mathbf{I} + \frac{A_{m_1}}{2} \cdot \Delta t_{TR} \right) \cdot \left( \mathbf{I} - \frac{A_{m_1}}{2} \cdot \Delta t_{TR} \right)^{-1} \end{aligned} \quad (\text{B.5})$$

Due to the commutation relation above, equation (A6) can be derived by moving the term  $\left( \mathbf{I} - \frac{A_{m_1}}{2} \cdot \Delta t_{TR} \right)^{-1}$  to the left as marked by the arrow below:

$$\begin{aligned} \mathbf{x}(t_{1+}) &= \left( \mathbf{I} - \frac{A_{m_2}}{2} \cdot \Delta t_{TR} \right)^{-1} \cdot \left( \mathbf{I} + \frac{A_{m_1}}{2} \cdot \Delta t_{TR} \right) \cdot \mathbf{G}_{TRm_1}^{n_1} \cdot \left( \mathbf{I} - \frac{A_{m_1}}{2} \cdot \Delta t_{TR} \right)^{-1} \cdot \left( \mathbf{I} + \frac{A_{m_0}}{2} \cdot \Delta t_{TR} \right) \cdot \mathbf{x}(t_{0-}) \\ &= \left( \mathbf{I} - \frac{A_{m_2}}{2} \cdot \Delta t_{TR} \right)^{-1} \cdot \left( \mathbf{I} - \frac{A_{m_1}}{2} \cdot \Delta t_{TR} \right)^{-1} \cdot \left( \mathbf{I} + \frac{A_{m_1}}{2} \cdot \Delta t_{TR} \right) \cdot \mathbf{G}_{TRm_1}^{n_1} \cdot \left( \mathbf{I} + \frac{A_{m_0}}{2} \cdot \Delta t_{TR} \right) \cdot \mathbf{x}(t_{0-}) \\ &= \left( \mathbf{I} - \frac{A_{m_2}}{2} \cdot \Delta t_{TR} \right)^{-1} \cdot \mathbf{G}_{TRm_1}^{n_1+1} \cdot \left( \mathbf{I} + \frac{A_{m_0}}{2} \cdot \Delta t_{TR} \right) \cdot \mathbf{x}(t_{0-}) \end{aligned} \quad (\text{B.6})$$

As a result, although a new switching state  $\left( \mathbf{I} - \frac{A_{m_1}}{2} \cdot \Delta t_{TR} \right)^{-1} \cdot \left( \mathbf{I} + \frac{A_{m_0}}{2} \cdot \Delta t_{TR} \right)$  as shown in equation (A2) is introduced when the circuit is switching to state  $m_1$ , the  $m_1$  related term  $\left( \mathbf{I} - \frac{A_{m_1}}{2} \cdot \Delta t_{TR} \right)^{-1}$  will become  $\mathbf{G}_{TRm_1}$  when switched out by combining with term  $\left( \mathbf{I} + \frac{A_{m_1}}{2} \cdot \Delta t_{TR} \right)$ . In other words, in the global view, by switching in and out of state  $m_1$  with instantaneous solution interpolation method, will not introduce new  $m_1$  related switching state.

Similarly, without losing generality, assuming the system is in switching state  $m_0$  with initial value of  $\mathbf{x}(t_0)$  at time  $t_0$ , after  $k^{\text{th}}$  switching, the corresponding solution can be written as:

$$\mathbf{x}(t) = \mathbf{G}_{TRm_k}^{n_k} \cdot \left( \mathbf{I} - \frac{A_{m_k}}{2} \cdot \Delta t_{TR} \right)^{-1} \cdot \mathbf{G}_{TRm_{k-1}}^{n_{k-1}+1} \dots \mathbf{G}_{TRm_1}^{n_1+1} \cdot \left( \mathbf{I} + \frac{A_{m_0}}{2} \cdot \Delta t_{TR} \right) \cdot \mathbf{G}_{TRm_0}^{n_0} \cdot \mathbf{x}(t_0) \quad (\text{B.7})$$

where  $m_i$  is the corresponding switching state after  $i^{\text{th}}$  switching and  $n_i \cdot \Delta t_{TR}$  is the duration the system stays in switching state  $m_i$ .

Noting that regardless of the number of switching  $k$ , there are only two new switching matrices  $\left( \mathbf{I} - \frac{A_{m_k}}{2} \cdot \Delta t_{TR} \right)^{-1}$  and  $\left( \mathbf{I} + \frac{A_{m_0}}{2} \cdot \Delta t_{TR} \right)$  added only once respectively.

Simulation of LSPSC system with Trapezoidal method is shown to be exponentially stable under arbitrary switching in [10]. According to [33], this is equivalent to say that for a  $\mathbf{x}(t) = \mathbf{G}_{TRm_k}^{n_k} \cdot \mathbf{G}_{TRm_{k-1}}^{n_{k-1}+1} \dots \mathbf{G}_{TRm_1}^{n_1+1} \cdot \mathbf{G}_{TRm_0}^{n_0} \cdot \mathbf{x}(t_0)$ . With a bounded initial condition,  $\|\mathbf{x}(t_0)\| < c_1$  where  $c_1 > 0$ , there exist positive constants  $c_2$  and  $\lambda$  that:

$$\|\mathbf{x}(t)\| \leq c_2 \cdot \|\mathbf{x}(t_0)\| \cdot e^{-\lambda \cdot (t-t_0)} \quad (\text{B.8})$$

Since  $(\mathbf{I} - \frac{A_{m_{k+1}}}{2} \cdot \Delta t_{TR})^{-1}$  and  $(\mathbf{I} + \frac{A_{m_0}}{2} \cdot \Delta t_{TR})$  are finite, a positive constant  $c_3$  can always be found such that:

$$\|(\mathbf{I} - \frac{A_{m_{k+1}}}{2} \cdot \Delta t_{TR})^{-1}\| \cdot \|(\mathbf{I} + \frac{A_{m_0}}{2} \cdot \Delta t_{TR})\| \leq c_3 \quad (\text{B.9})$$

Hence the norm  $\|\mathbf{x}(t)\|$  of the simulation solution with instantaneous solution interpolation will be:

For a bounded input  $\|\mathbf{x}(t_0)\| < c_1$  :

$$\begin{aligned} \|\mathbf{x}(t)\| &= \|\mathbf{G}_{TRm_{k+1}}^{n_{k+1}} \cdot (\mathbf{I} - \frac{A_{m_{k+1}}}{2} \cdot \Delta t_{TR})^{-1} \cdot \mathbf{G}_{TRm_k}^{n_{k+1}} \dots \mathbf{G}_{TRm_1}^{n_1+1} (\mathbf{I} + \frac{A_{m_0}}{2} \cdot \Delta t_{TR})\| \cdot \|\mathbf{x}(t_0)\| \\ &\leq \|(\mathbf{I} - \frac{A_{m_{k+1}}}{2} \cdot \Delta t_{TR})^{-1}\| \cdot \|(\mathbf{I} + \frac{A_{m_0}}{2} \cdot \Delta t_{TR})\| \cdot \|\mathbf{G}_{TRm_{k+1}}^{n_{k+1}} \cdot \mathbf{G}_{TRm_k}^{n_{k+1}} \dots \mathbf{G}_{TRm_1}^{n_1+1}\| \cdot \|\mathbf{x}(t_0)\| \\ &\leq c_3 \cdot c_2 \cdot \|\mathbf{x}(t_0)\| \cdot e^{-\lambda \cdot (t-t_0)} \end{aligned} \quad (\text{B.10})$$

Since  $c_3 \cdot c_1$  is still a positive number, the system is still exponentially stable. When the excitation is included, the system will still be BIBO stable.

Q.E.D.

## Appendix C – Modified admittance approach for simulation accuracy evaluation

In this section, the modified admittance will be introduced as a new transfer function to define an accuracy index. Compared with the equivalent admittance used in section 5, this transfer function reflects all the internal modes.

Similar to Section 5, consider the network  $\mathcal{N}$  shown in Fig. C-1 with.  $N_b$  represents a multi-phase port with boundary nodes  $N_{b1}, N_{b2} \dots N_{bn}$  connecting to external sources. All non-boundary nodes, e.g.,  $N_{i1}, N_{i2}, N_{i3}$  of the network are referred to as internal nodes.

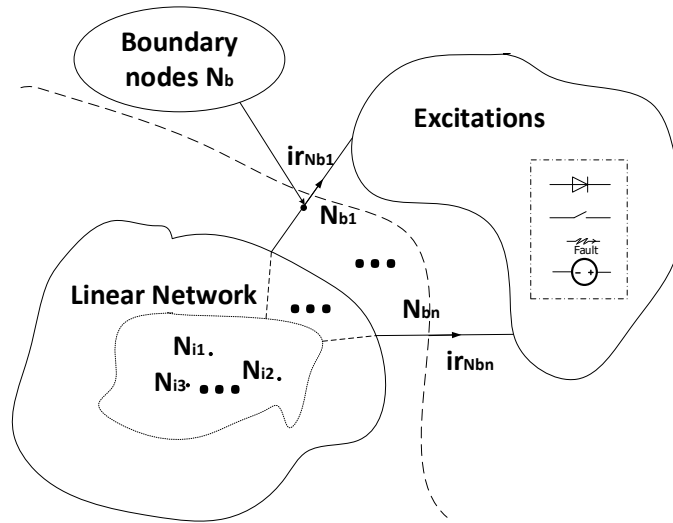


Figure C-1 Network showing boundary and internal buses

The modified nodal analysis formulation of voltage current relationship for  $\mathcal{N}$  can be described as:

$$\begin{pmatrix} \mathbf{I}_i(s) \\ \mathbf{V}_{ex}(s) \end{pmatrix} = \begin{pmatrix} \mathbf{Y}(s) & \mathbf{A} \\ \mathbf{A}^T & \mathbf{0} \end{pmatrix} \cdot \begin{pmatrix} \mathbf{V}_N(s) \\ \mathbf{I}_r(s) \end{pmatrix} \equiv \mathbf{Y}_{\mathcal{N}}(s) \cdot \begin{pmatrix} \mathbf{V}_N(s) \\ \mathbf{I}_r(s) \end{pmatrix} \quad (\text{C.1})$$

where  $\mathbf{V}_N$  is the linear network node voltage vector.  $\mathbf{I}_r$  denotes the current response vector leaving the boundary nodes.  $\mathbf{I}_i$  represents internal currents injections. As all excitation is at external nodes,  $\mathbf{I}_i=0$ . Matrix  $\mathbf{A}$  is incident matrix which denotes the location of excitations.

Letting  $\mathbf{P}_{\mathcal{N}}(s) \equiv (\mathbf{Y}_{\mathcal{N}}(s))^{-1} = \begin{pmatrix} \mathbf{P}_{\mathcal{N}11}(s) & \mathbf{P}_{\mathcal{N}12}(s) \\ \mathbf{P}_{\mathcal{N}21}(s) & \mathbf{P}_{\mathcal{N}22}(s) \end{pmatrix}$ , substituting  $\mathbf{I}_i(s) = 0$  to (C.1) with

simple algebra gives:

$$\begin{pmatrix} \mathbf{V}_N(s) \\ \mathbf{I}_r(s) \end{pmatrix} = \begin{pmatrix} \mathbf{P}_{\mathcal{N}12}(s) \\ \mathbf{P}_{\mathcal{N}22}(s) \end{pmatrix} \cdot \mathbf{V}_{ex}(s) \equiv \mathbf{P}_m(s) \cdot \mathbf{V}_{ex}(s) \quad (\text{C.2})$$

The term  $\begin{pmatrix} \mathbf{P}_{\mathcal{N}12}(s) \\ \mathbf{P}_{\mathcal{N}22}(s) \end{pmatrix}$  will be named as modified admittance and be noted as  $\mathbf{P}_m(s)$ .

As shown in equation (C.2), the output of such transfer includes all the node voltages as well as output currents, which covers most of study interests. A new simulation spectrum could be formed by replacing the  $\mathbf{Y}_b(s)$  in (5.12) with  $\mathbf{P}_m(s)$ .

As a demonstration, by using the new admittance  $\mathbf{P}_m(s)$ , a new simulation spectrum as below could be formed for the circuit as shown in Fig. 5-1:

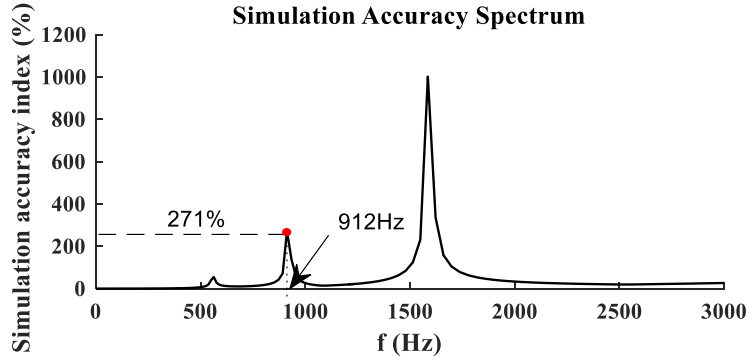


Figure C-2 Simulation Accuracy Spectrum

From the spectrum, we could also see that the accuracy loss around 550 Hz as shown in Fig. 5-3 is predicted. Besides, it also denotes that, with a 912 Hz excitation, the worst term in the simulation result will be 271% different with the original value. By checking the relative error matrix element, we located the worst one is node  $N_{i1}$  voltage. In order to verify this, a corresponding EMT simulation is implemented and the node  $N_{i1}$  voltage is as shown in Fig. C-3. It clearly shows that the magnitude and Phase of simulated  $N_{i1}$  voltage are significantly different with the theoretical solution, which confirms the importance of this method, when internal electric information is the main concern.

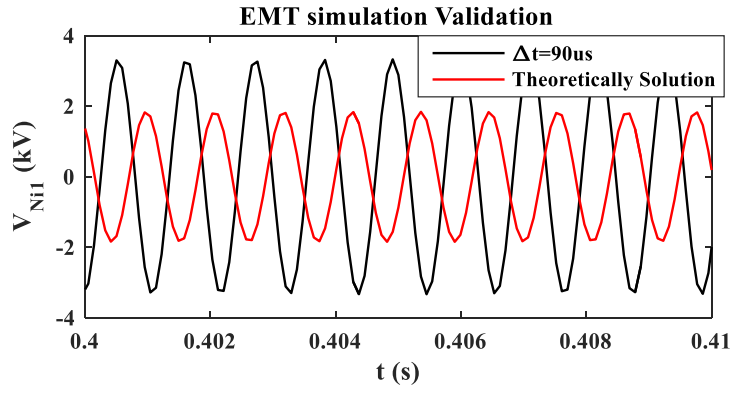


Figure C-3 Simulation of node  $N_{i1}$  voltage with 912 Hz Excitation